ENERGY LOSS FROM NEUTRINO OSCILLATIONS IN MASSIVE STARS

NOR SOFIAH AHMAD

DISSERTATION SUBMITTED IN FULFILMENT OF THE REQUIREMENTS FOR THE DEGREE OF MASTERS OF SCIENCE

DEPARTMENT OF PHYSICS
FACULTY OF SCIENCE
UNIVERSITY OF MALAYA
KUALA LUMPUR

2014

Abstract

When neutrinos propagate through a medium and interact with the electrons, an effective potential energy is produced due to the coherent forward scattering. This potential engenders significant changes in the neutrino masses and their mixing in the medium. Thus electron neutrinos would oscillate into a different mass eigenstate and this is dependent on the energy of the neutrinos. Some of the energy will be lost in the coherent scattering with the electrons by the charged current interaction. We have calculated the energy loss of the neutrinos by using a stopping power equation for both non-rotating and rotating $20M_{\odot}$ and $120M_{\odot}$ stellar models. The total energy loss of the neutrinos depends on the electron number density n_e in the stars and on the survival probability of the electron neutrino $P_{\nu_e \to \nu_e}$. For higher n_e and the survival probability, the energy loss will be significant. These models are generated by using the Geneva code and post-processed to include the oscillation effect. From these models, we obtain the value of the thermal neutrino energy loss, density of matter and n_e used the stopping power equation of matter for neutrinos. We found that the neutrino energy loss of the rotating $20M_{\odot}$ model is the highest by six orders of magnitude than the non-rotating $20M_{\odot}$ model ($\sim 10^{17}$ MeV/cm^3/s) dominated by the bremsstrahlung process. For the $120M_{\odot}$, model the maximum neutrino energy loss is about the same at $\sim 10^{10}$ MeV/cm^3/s and monopolised by the pair-neutrino process. Overall, the neutrino energy loss due to oscillation is $\sim 1\%$ from the neutrino energy loss without oscillations.

Abstrak

Apabila neutrino merambat satu bahantara dan berinteraksi dengan elektron, satu tenaga keupayaan berkesan dihasilkan disebabkan oleh serakan koheren ke depan. Keupayaan ini mengakibatkan perubahan ketara pada jisim-jisim neutrino dan pencampurannya di dalam bahantara. Oleh itu, electron neutrino akan berayun kepada keadaan eigen jisim yang lain dan ini bergantung kepada tenaga neutrino-neutrino tersebut. Sebahagian dari tenaga akan hilang di dalam serakan koheren dengan elektron oleh interaksi cas arus. Kami telah mengira tenaga hilang neutrino dengan menggunakan persamaan kuasa penghenti untuk model-model bintang tidak berputar dan berputar $20M_{\odot}$ dan $120M_{\odot}$. Jumlah tenaga hilang neutrino bergantung kepada ketumpatan nombor elektron n_e di dalam bintang dan juga kebarangkalian kemandirian elektron neutrino $P_{\nu_e \to \nu_e}$. Untuk nilai n_e dan kebarangkalian kemandirian yang tinggi , tenaga hilang adalah ketara. Model-model dijana dari kod Geneva dan pasca-proses dengan memasukkan kesan ayunan. Dari model-model ini, kami memperolehi nilai tenaga terma hilang neutrino, ketumpatan jirim, dan n_e yang akan digunakan di dalam persamaan kuasa penghenti jirim untuk neutrino. Kami mendapati, tenaga hilang untuk model berputar $20M_{\odot}$ adalah tertinggi dengan tertib magnitud enam kali ganda berbanding dengan model tidak berputar $20M_{\odot}$ ($\sim 10^{17}$ MeV/cm^3/s) yang didominasi oleh proses bremsstrahlung. Untuk model $120M_{\odot}$, tenaga hilang maksimum adalah sama ($\sim 10^{10}$ MeV/cm^3/s) dan dimonopili oleh proses neutrino berpasangan. Secara keseluruhannya tenaga hilang netrino yang disebabkan ayunan adalah $\sim 1\%$ dari tenaga hilang neutrino tanpa ayunan.

Acknowledgments

First and foremost, I would like to thank my supervisor, Assoc. Prof. Dr. Hasan Abu Kassim, for his support and confidence in me over the course of my research project. I am fortunate that he occasionally helps me to resolve all the problems that I faced during this research and also give me opportunities to feel the world of researchers. Thank you for all the training and encouragement.

There are many others who have contributed to my research through formal and informal discussions and correspondence. To Norhasliza Yusof, thank you for the help provided towards this research. Many thanks goes to Mrs Azni Abdul Aziz for the cheerful support, advice and motivation during thick and thin, thank you for always being there when needed. I would like to thank Mr. Imran Yusoff for the moral support and the help provided especially in helping me to find some references that are needed for completing this work. To all my friends who made my time in the university a memorable one.

I express my gratitude towards the Department of Physics as well as the University of Malaya for the financial support and space provided.

Special thanks goes to my beloved family; my late father and late grandmother, may Allah bless you, to my mother and grandfather the pillars of my strength now thank you for a lovely support, motivation and trust. Final but not least for the late lecturer Dr. Burhanuddin Kamaluddin, may Allah bless you forever. Thank you for the advice and support.

Special dedication to my beloved family, heart and soul of my life. There is nothing more valuable than to have them in this life.

To the loving memory of my late father, Mr. Ahmad bin Haji Sharif. He was the best father, teacher and friend and always be.
May Allah bless him forever. Al-Fatihah.

To my beloved mother Mrs. Rahmah Haji Ibin. May Allah grant you with love, good health, happiness and always in His blessing.

To my lovely grandfather, Haji Bahari Ibrahim. The pillar and the strength of my life. May Allah protect you and grant you with His blessing, love, good health and happiness forever.

Contents

List of Figures

List of Tables

Chapter 1

Introduction

For half a century, scientists try to understand the properties of the elusive particle known as neutrino that is postulated to exist from the primordial nucleosynthesis in the early universe until now. This elusive particle has no charge and has weak interaction with matter. This particle has a significant effect on the evolution of the universe, galaxies and stars. Results from experiments have open a new perspective that could help solve some questions in astronomy, astrophysics and cosmology.

The neutrinos have significant contribution on the evolution of universe, starting from the few seconds after the Big Bang to the current universe. The Solar Neutrino Problem (SNP) and supernova event SN1987A are the main factors that ignited the scientific interest in neutrinos. From solar neutrinos, scientists had discovered that neutrinos could oscillate from one flavor to another in vacuum and also in matter. Neutrinos are very important for the evolution of massive stars especially in the late stages; during carbon, neon, oxygen and silicon burnings. During these burnings stages, copious number of neutrinos are emitted from the star and this is referred as neutrino-cooled stars [1]. Neutrino emission during the neutrino-cooling is also known as thermal neutrino losses and can be divided into four processes; the photoneutrino process, pair neutrino process, plasma neutrino process and bremsstrahlung neutrino process [2]. These processes do not involve the nuclear reactions, and they are always emitted from the hot and dense plasma [3]. The thermal neutrinos that are determined entirely by the local thermodynamics properties of matter (e.g., temperature T and electron chemical potential μ_e) [4].

The star will loss its energy by neutrino emission during the late stages of the evolution when neutrinos carry away their energy from the star without any obsta-

cle due to the weak interaction with matter. The energy loss of the neutrinos during the late stages has been calculated by Itoh *et. al.* and the effects have been discussed in a series of papers [5] - [16]. In their work, they do not consider the oscillation effect of neutrinos to the energy loss. There is no research that has been made to find the total energy loss of the neutrinos in the massive star by using the stopping power equation [17] through oscillation. Since the oscillation of the neutrinos is now confirmed, we would like to study the total energy loss of the neutrinos through oscillations when they travel from the center of the star to the surface by using the stopping power equation of matter [17]. We would like to see the difference in the total energy loss of neutrinos in a stellar model since different model have different properties that could affect the total energy loss.

The objectives of this work are to evolve two sets of massive stars for both non-rotating and rotating with masses $20M_{\odot}$ and $120M_{\odot}$ and to apply the data to calculate the total energy loss of neutrinos with oscillations. From these models, we can determine their properties such as density of matter ρ, electron number density n_e, radius R, the thermal neutrino energy loss E_ν, etc. As we all know, neutrinos are produced with tremendous amount during the late stages of stellar evolution and with the information on the cross-section between neutrinos and matter, we can calculate the total energy loss of the neutrinos in massive stars by using the stopping power equation of matter for neutrino with the inclusion of oscillation [17]. Finally, we would like to make a comparison between the thermal neutrino energy loss that comes from the stellar models and the total energy loss is being calculated by using the stopping power equation.

In this work, we start our discussion in Chapter 2 on the properties of a neutrino; the interaction of the neutrino with matter where we are focusing on the interaction of the neutrinos with electrons in the stellar matter. Then we will discuss about the neutrino oscillation; the oscillation of active neutrinos. We are focusing on the modified stopping power equation of matter for neutrinos in stellar matter and the ap-

plication of it for the neutrino energy loss through oscillations for both non-rotating and rotating stellar models. We show the application of the stopping power equation to the Big Bang Cosmology where the result of the calculation is comparable with the anisotropy of cosmic microwave background (CMB).

In Chapter 3, we will discuss the details of the evolution of massive stars; $20M_{\odot}$ and $120M_{\odot}$ for both non-rotating and rotating models. We highlight the properties of the stars such as density of matter ρ, chemical abundances X_z, electron density n_e etc that later will be used for the neutrino energy loss calculations. In this chapter, we will give a brief discussion on the energy loss of neutrinos that have been calculated by Itoh *et al* [2].

For Chapter 4, we will discuss the total energy loss of neutrinos for the stellar models that have been chosen and we made some conclusions and suggestions for the future work in Chapter 5.

Chapter 2

Neutrino Oscillations and Stopping Power of Matter

2.1 Introduction

The neutral fermion called neutron emitted from β decays was proposed by Pauli in late 1930s. Later, Enrico Fermi renamed the Pauli particle as neutrino after J. Chadwick discovered the neutron in 1932. Since then, the progress in neutrino physics became significant. The most well known problems arise that lead to rapid progress in neutrino physics and particle astrophysics are the Solar Neutrino Problem (SNP) and the supernova event that occurred in the Large Magellenic Cloud (LMC) in 1987 denoted as SN 1987A. These two remain the only measurements of the astrophysical neutrino sources.

Here, we take the solar neutrino problem as an example that later can be used and extended in order to understand the physics of the evolution of the stars in the astrophysics point of view and particle astrophysics point of view. The Sun and all stars produce their own energy via nuclear reactions that occur at the inner core and produce tremendous number of neutrinos as a product. For the Sun, the neutrino is not the main source of the energy loss compared to the massive stars that later will be discussed in detail in Chapter 3 and Chapter 4. Solar neutrino problem is one of the longest standing problem in astroparticle physics and the most interesting problem that offer a chance to probe neutrino properties at low energy which is not possible by terrestrial means. Solar neutrino also becomes a source motivation for large scale neutrino experiments where over a few decades, several experiments

were designed to investigate the nature of the neutrinos. From SNP, scientists discovered that neutrinos could oscillate into another flavor when the number of electron neutrinos detected from experiments was less than predicted by the Standard Solar Model (SSM) [18] [19].

Up to this time, there are three types of flavors of active neutrinos (ν) and anti-neutrinos ($\overline{\nu}$): electron neutrino (ν_e), muon neutrino (ν_μ) and tau neutrino (ν_τ) that are known. All of these neutrinos have weak interactions with matter and interact through W and Z bosons. For a general discussion on the nuclear reaction in the star, we take the hydrogen fusion as an example:

$$4p \rightarrow^4 He + 2e^+ + 2\nu. \tag{2.1}$$

From this reaction certain amount of energy is released together with the production of neutrinos. Then, the products of the previous burning will be the fuel of the next series of reactions when the sufficient temperature and density are reached. In massive stars ($\geq 8M_\odot$), neutrino energy loss becomes the main cooling process where the energy of neutrinos is lost since the neutrinos easily escape from the stars than the photons. Differ from the Sun, a massive star has different physical properties that allows it to produce neutrinos by thermal processes. Four main processes that are involved in the neutrino energy loss from the star are; pair productions, photoneutrino, plasma neutrino and bremsstrahlung processes. These are known as neutrino-cooling mechanisms [1]. Large number of neutrinos are emitted from the star during the late stages especially in carbon burning onwards. In this chapter, we will discuss the interaction of the neutrino with electrons in stellar matter and the oscillation properties that lead to the total energy loss of neutrino in the stellar matter by using the stopping power equation of matter for the neutrino (SPE) [17].

2.2 Neutrino - Electron Interactions

In a massive star, large number of neutrinos is produced through purely leptonic processes and these neutrinos interact with stellar matter via charged-current interaction (CC) and neutral-current interaction (NC) with the stellar matter on the way out to the surface of the star. The cross section for the interaction of neutrino with matter in the star is very small and it depends on the energy of the neutrino. According to the electroweak theory, neutrino interacts with matter via the charged-current (CC) interaction; exchanging of the $W^{\pm}$ bosons shown in Fig. 2.1 and neutral-current (NC) interaction via the Z bosons given by Fig. 2.2. Normally, at low energy and for the simplicity of our case, we assume that a neutrino and an electron interact through elastic scattering process. Below is the neutrino-electron ($\nu_e - e^-$) interaction which involves both CC and NC interactions.

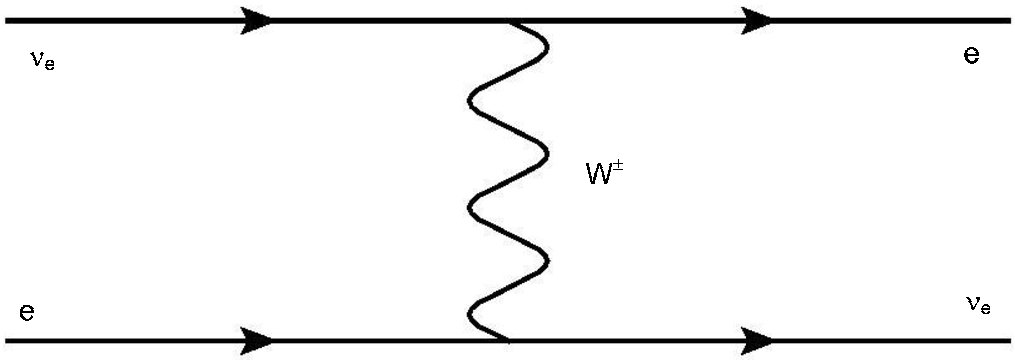

Figure 2.1: Neutrino interacting with electron via charge-current interaction (W exchange).

$$\nu_e + e^- \rightarrow \nu_e + e^-. \tag{2.2}$$

For other types of neutrinos, only NC interaction is involved;

$$\nu_i + e^- \rightarrow \nu_i + e^-. \tag{2.3}$$

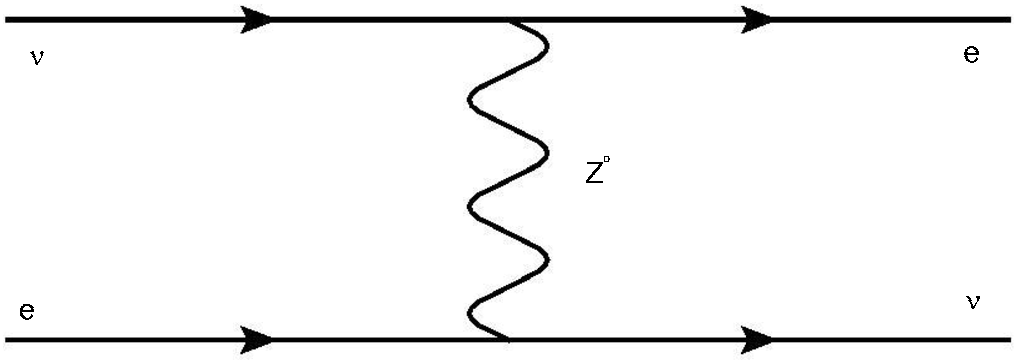

Figure 2.2: Neutrino interacting with electron via neutral-current interaction (Z exchange).

where $i = \mu$ or τ. Guinti and Kim [20] show the low-energy Lagrangian for two level Feynman diagrams is given by

$$\begin{aligned} L_{eff}(\nu_e e^- \to \nu_e e^-) &= -\frac{G_F}{\sqrt{2}}[[\overline{\nu_e}\gamma^\rho(1-\gamma^5)e][\overline{e}\gamma_\rho(1-\gamma^5)\nu_e] \\ &+ [\overline{\nu_e}\gamma^\rho(1-\gamma^5)\nu_e][\overline{e}\gamma_\rho(g_V^l - g_A^l\gamma^5)e]]. \end{aligned} \tag{2.4}$$

where G_F is the weak coupling constant, the coefficients g_V^l and g_A^l both have $1/2$ value [20]. CC contribution is the first term on the right side. NC contribution is shown by the second term of the right side of the equation. In Eq. (2.3), since only NC involves, the effective Lagrangian becomes:

$$L_{eff}(\nu_i e^- \to \nu_i e^-) = -\frac{G_F}{\sqrt{2}}[\overline{\nu_i}\gamma^\rho(1-\gamma^5)\nu_i][\overline{e}\gamma_\rho(g_V^l - g_A^l\gamma^5)e]. \tag{2.5}$$

From Guinti and Kim [20] the differential cross section is

$$\frac{d\sigma}{dQ^2} = \frac{G_F^2}{\pi}\left[g_1^2 - g_2^2\left(1 - \frac{Q^2}{2p_{\nu_i}.p_{e_i}}\right)^2 - g_1 g_2 m_e^2 \frac{Q^2}{2(p_{\nu_i}.p_{e_i})}\right] \tag{2.6}$$

where the values of g_1 and g_2 depend on the flavor of the neutrino, m_e is the mass of

the electron, p is the four-momentum and Q is the energy released. Since neutrino and antineutrino are opposite in chirality, both Q values would be the same. This can be shown as:

$$g_1^{(\nu_e)} = g_2^{(\overline{\nu}_e)} = 1 + \frac{g_V^l + g_A^A}{2} = 1 + g_V^L = \frac{1}{2} + \sin^2\theta_w \backsimeq 0.73, \tag{2.7}$$

$$g_1^{(\nu_e)} = g_2^{(\overline{\nu}_e)} = \frac{g_V^l - g_A^A}{2} = g_R^L = \sin^2\theta_w \backsimeq 0.23, \tag{2.8}$$

$$g_1^{(\nu_{\mu,\tau})} = g_2^{(\overline{\nu}_{\mu,\tau})} = \frac{g_V^l + g_A^A}{2} = 1 + g_L^l = -\frac{1}{2} + \sin^2\theta_w - \backsimeq 0.27, \tag{2.9}$$

$$g_1^{(\nu_{\mu,\tau})} = g_2^{(\overline{\nu}_{\mu,\tau})} = \frac{g_V^l - g_A^A}{2} = g_R^l = \sin^2\theta_w \backsimeq 0.23. \tag{2.10}$$

The four-momentum $\overrightarrow{p}_{e_i} = 0$ in the laboratory frame, then

$$Q^2 = 2m_e T_e \tag{2.11}$$

where T_e is the kinetic energy of the recoiling electron. Then the cross section can be written in terms of T_e

$$\frac{d\sigma}{dT_e}(E_\nu, T_e) = \frac{\sigma_0}{m_e}\left[g_1^2 + g_2^2\left(1 - \frac{T_e}{E_\nu}\right)^2 - g_1 g_2 m_e^2 \frac{m_e T_e}{E_\nu^2}\right] \tag{2.12}$$

which the constants σ_0 is given by:

$$\sigma_0 = \frac{2G_F^2 m_e^2}{\pi}.$$

The energy-momentum conservation in the laboratory frame is then

$$T_e = \frac{2m_e E_\nu^2 \cos^2\theta}{(m_e + E_\nu)^2} - E_\nu^2 \cos^2\theta \tag{2.13}$$

with θ the electron scattering angle which is shown in Fig. 2.3. Then the differentia-

tion of Eq. (2.13) becomes:

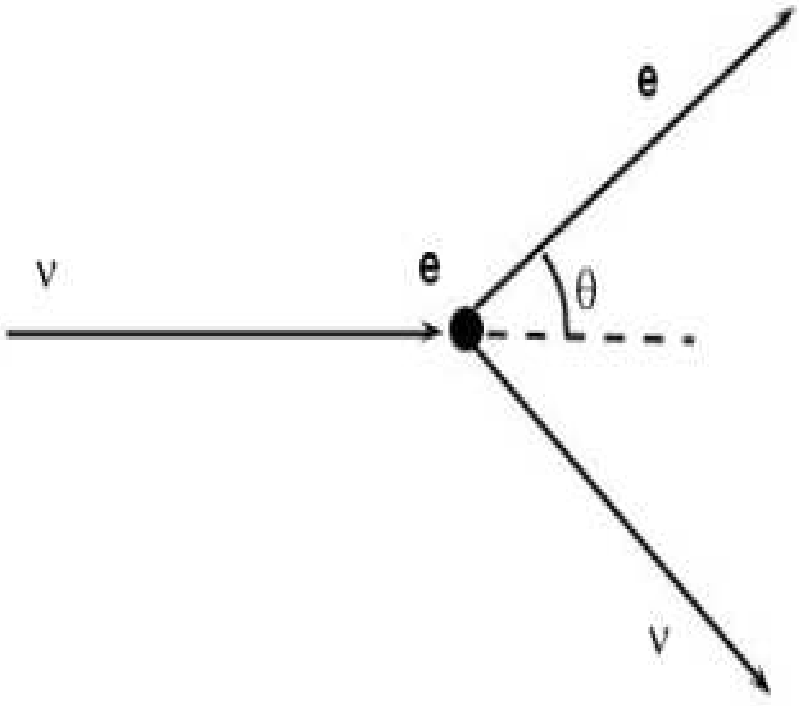

Figure 2.3: Neutrino-electron scattering with angle θ.

$$dT_e = \frac{2m_e E_\nu^2 \cos^2\theta}{(m_e + E_\nu)^2 - E_\nu^2 \cos^2\theta} \cos\theta d\cos\theta. \tag{2.14}$$

We can write the cross section as a function of the scattering angle:

$$\begin{aligned} \frac{d\sigma}{d\cos\theta} &= \sigma_0 \frac{4E_\nu^2 (m_e + E_\nu)^2 \cos\theta}{[(m_e + E_\nu)^2 - E_\nu^2 \cos^2\theta]^2} [g_1^2 + g_2^2 \left(1 - \frac{2m_e E_\nu \cos^2\theta}{(m_e + E_\nu)^2 - E_\nu^2 \cos^2\theta}\right)^2 \\ &\quad - g_1 g_2 \frac{2m_e^2 \cos^2\theta}{(m_e + E_\nu)^2 - E_\nu^2 \cos^2\theta}]. \end{aligned} \tag{2.15}$$

Since the angle $\cos\theta \leqslant 1$, the maximum kinetic energy of the recoil electron can be deduced from a given neutrino energy E_ν:

$$T_e^{\max}(E_\nu) = \frac{2E_\nu^2}{m_e + 2E_\nu} \tag{2.16}$$

leading to the minimum neutrino energy:

$$E_\nu^{\min}(T_e) = \frac{T_e}{2}\left(1+\sqrt{1+\frac{2m_e}{T_e}}\right). \tag{2.17}$$

The minimum energy of the neutrino $E_\nu^{\min} \simeq \sqrt{m_e T_e/2}$ for $T_e \ll m_e$ and $E_\nu^{\min} \simeq T_e + m_e/2$ for $T_e \gg m_e$.

The cross section for the interaction of a neutrino and electron in stellar matter is very small and it is known to depend on the energy of the neutrino. On average, the cross section of the neutrino scattering is around $\sigma \sim 10^{-45}\text{cm}^2$. When a neutrino typically moves through matter and interact with electrons in the star, the volume of the neutrino sweeps V_ν as it moves in the distance l_ν is

$$V_\nu = l_\nu \sigma. \tag{2.18}$$

Suppose we have a cube of matter with density ρ, then the mass of the cube M is density multiple by volume V.

$$M = \rho V. \tag{2.19}$$

Here in our case, we just consider the interaction of the neutrinos with electrons in matter since the interaction of a neutrino with a nucleus is the neutral-current interaction that gives no effect on the energy loss, we just simplify the mass of matter as the mass of electrons and hence the density of matter here is just the density of electrons, ρ_e. Then the number of electrons in this cube is equal to the mass of cube divided by the mass of an electron:

$$N = \frac{M}{m_e} = \frac{\rho_e V}{m_e} \tag{2.20}$$

where V is the volume occupied by the electrons in the cube. From the equation

above, the reciprocal of N is the average volume occupied by each electron and we can write the volume per electron as:

$$V_e = \frac{V}{n} = \frac{m_e}{\rho_e}. \tag{2.21}$$

If the neutrino travels from the center of the star to the surface, it will sweep out a volume equal to the typical volume occupied by one electron and interacts with the electron in that volume. Then we can compute the distance of the neutrino must travel before interacting with an electron L i.e. the mean free path l_ν as

$$V_\nu = V_e$$

$$l_\nu = \frac{m_e}{\rho_e} \tag{2.22}$$

$$l_\nu = \frac{m_e}{\rho_e \sigma}. \tag{2.23}$$

Eq. (2.15) can be integrated over the solid angle to obtain the cross section of the ν_e-e scattering as a function of energy and this is given [20] by

$$\sigma = \int \frac{\sigma_0}{m_e} \left[g_1^2 + g_2^2 \left(1 - \frac{T_e}{E_\nu} \right)^2 - g_1 g_2 m_e^2 \frac{m_e T_e}{E_\nu^2} \right] \tag{2.24}$$

For any given mass of a star, with the density of the electron known form its physical profiles, the mean free path of the neutrino l_ν can always be computed.

2.3 Neutrino Oscillations

From SNP we know that neutrino oscillates from one flavor to another which implies that the neutrino would be massive. There are two types of oscillations; oscillations in vacuum and oscillations in matter. The oscillation of $\nu_e \rightarrow \nu_{\mu,\tau}$ is described in terms of a survival probability which means there is a chance that one flavor of a neutrino oscillates into another or survives as the initial state. In order for the oscil-

lations to occur, neutrino must has mass. There are at least three flavors of known active neutrinos and its respective anti-neutrinos with different masses each.

2.3.1 Neutrino Oscillations in Vacuum

The general equations that describe the oscillations of two neutrino flavors can be shown below:

$$\nu_i = \nu_1 \cos\theta + \nu_2 \sin\theta \tag{2.25}$$

$$\nu_j = -\nu_1 \sin\theta + \nu_2 \cos\theta \tag{2.26}$$

where $i, j = e, \mu$ or τ and ν_1 and ν_2 are the mass eigenstates with θ the mixing angle. For the oscillations of ν_e and ν_μ Eq.(2.25) and Eq. (2.26) become

$$\nu_e = \nu_1 \cos\theta + \nu_2 \sin\theta \tag{2.27}$$

$$\nu_\mu = -\nu_1 \sin\theta + \nu_2 \cos\theta. \tag{2.28}$$

The experiments from all over the world; Homestake, Kamiokande, GALLEX/GNO, SAGE, Super Kamiokande, SNO and many others have prove that neutrinos can oscillate which implies neutrinos have finite mass. The eigenstates of the Hamiltonian of the massive state is $|\nu_k\rangle$

$$H|\nu_k\rangle = E_k|\nu_k\rangle \tag{2.29}$$

where the eigenvalue is

$$E_k = \sqrt{\overrightarrow{p}^2 + m_k^2}. \tag{2.30}$$

When neutrino propagates after time t, the neutrino evolution can be described in

terms of plane waves equation:

$$|\nu_k(t)\rangle = e^{-iE_k t}|\nu_k\rangle. \tag{2.31}$$

For example, at time t, the propagation of $|\nu_e\rangle$ can be described as

$$\begin{aligned}|\nu_e(t)\rangle = &[e^{-iE_1 t}\cos^2\theta + e^{-iE_2 t}\cos^2\theta]|\nu_e(0)\rangle \\ &+ [e^{-iE_2 t}\cos^2\theta + e^{-iE_1 t}]\sin\theta\cos\theta|\nu_e(0)\rangle.\end{aligned} \tag{2.32}$$

Then the probability of the $|\nu_e\rangle$ to oscillate into another flavor for example into $|\nu_\mu\rangle$ is

$$\begin{aligned}P(\nu_e \to \nu_\mu) &= |\langle\nu_\mu|\nu_e(t)\rangle|^2 \\ &= \frac{1}{2}\sin^2 2\theta[1 - \cos(E_2 - E_1)t].\end{aligned} \tag{2.33}$$

For relativistic neutrinos especially in the astrophysical situations where neutrinos are the energy of the neutrinos can be approximated by

$$E_k \simeq E + \frac{m_k^2}{2E} \tag{2.34}$$

where in this case, the difference in energy between these two neutrinos becomes

$$E_2 - E_1 \simeq \frac{\Delta m_{12}^2}{2E}. \tag{2.35}$$

Then the probability equation in Eq. (2.33) becomes

$$P(\nu_e \to \nu_\mu) = \frac{1}{2}\sin^2 2\theta[1 - \cos\frac{\Delta m^2}{2E_\nu}t]. \tag{2.36}$$

After time t, the neutrino travels with some distance that is called the oscillation length L_ν and can be written as:

$$L_\nu = \frac{4\pi E}{\Delta m^2_{12}}. \tag{2.37}$$

The survival probability of ν_e is defined as

$$P(\nu_e \to \nu_e) = 1 - P(\nu_e \to \nu_\mu). \tag{2.38}$$

There are three types of conditions where the survival probability will change depending on the ratio of the distance traveled L to L_ν:

(i) if $L/L_\nu \gg 1$, the oscillations become rapid then the average effect of the survival probability become

$$\langle P(\nu_e \to \nu_e) \rangle = 1 - \frac{1}{2}\sin^2 2\theta. \tag{2.39}$$

(ii) if $L/L_\nu \ll 1$ then oscillation will not occur.

(iii) if $L = \frac{1}{2}L_\nu$ then

$$P(\nu_e \to \nu_e) = 1 - \sin^2 2\theta. \tag{2.40}$$

2.3.2 Neutrino Oscillations in Matter

It was proposed by Wolfenstein in 1978 [21] that if the massless neutrinos propagate through matter, there is a possibility of oscillation to occur when the mixing angle and potential is altered due to the forward elastic scattering of neutrinos in matter. The vacuum mixing angle is replaced by an effective mixing angle in matter which depends on the density of the matter [22]. Mikheyev and Smirnov then discovered that the resonant transition of flavor can occur when a neutrino propagates in a varying density medium [23]. This is later known as Mikheyev-Smirnov-Wolfenstein (MSW) mechanism. This theory explains the flavor transition that occur

in solar neutrinos. We consider only the coherent forward scattering that occur in the medium since the incoherent forward scattering is very small and can be neglected.

The coherent forward elastic scattering can be divided into two types; the charged-current scattering (CC) and neutral-current (NC) scattering. In homogenous and isotropic gas, the potential of CC scattering can be calculated by using the effective CC Hamiltonian:

$$H_{eff}^{(CC)}(x) = \frac{G_F}{\sqrt{2}}[\overline{\nu}_e(x)\gamma^\rho(1-\gamma^5)\nu_e(x)e(x)][\overline{e}(x)\gamma_\rho(1-\gamma^5)\nu_e(x)]. \tag{2.41}$$

The CC potential then given by

$$V_{CC} = \sqrt{2}G_F n_e. \tag{2.42}$$

This coherent neutrino potential is considered if the medium remains unchanged after interaction, and the total Hamiltonian in matter is different from the Hamiltonian in vacuum H_0. This can be shown below, the eigenstate of Hamiltonian H_0 with massive neutrino state $|\nu_k\rangle$ is

$$H_0|\nu_k\rangle \quad = \quad E_k|\nu_k\rangle \tag{2.43}$$

with $E_k = \sqrt{\overrightarrow{p}^2 + m_k^2}$. Then the total Hamiltonian in matter is

$$H = H_0 + H_1 \tag{2.44}$$

with $H_1|\nu_i\rangle = V_i|\nu_\alpha\rangle$. V_m is the potential energy arising from the propagation of a neutrino through a medium.

At low temperature and density in matter that contains nucleons and electrons,

the NC potential for nucleons cancel each other and electrons are the only one that contributes:

$$V_{NC} = -\frac{1}{2}\sqrt{2}G_F n_n \tag{2.45}$$

where n_n is the nuclear density. The effect of NC is very small and we can neglect the effect. The flavor transition amplitude for example between electron neutrino to muon neutrino that propagates from the dense interior of a star is can then be written in the Schrödinger-like equation:

$$i\frac{d}{dx}\begin{pmatrix} \nu_e \\ \nu_\mu \end{pmatrix} = \frac{1}{4E}\begin{pmatrix} -\Delta m^2\cos 2\theta + A_{CC} & -\Delta m^2 \sin 2\theta \\ -\Delta m^2 \sin 2\theta & +\Delta m^2 \cos 2\theta - A_{CC} \end{pmatrix}\begin{pmatrix} \nu_e \\ \nu_\mu \end{pmatrix} \tag{2.46}$$

where $\Delta m^2 = m_2^2 - m_1^2$. The mass squared, A_{CC} acquired from the interactions of CC scattering $\nu_e - e$ in matter is

$$A_{CC} = 2\sqrt{2}G_F N_e E_\nu. \tag{2.47}$$

Then, the effective of mass squared difference in matter is

$$\Delta m_M^2 = \sqrt{(\Delta m^2\cos 2\theta - A_{CC})^2 - (\Delta m^2 \sin 2\theta)^2} \tag{2.48}$$

When neutrinos travel in matter, the mixing angle will change depending on the properties of matter. Below is the relationship between θ and θ_M

$$\sin^2 2\theta_M = \frac{\sin^2 2\theta}{1 - \frac{2A_{CC}\cos 2\theta}{\Delta m^2} + \left(\frac{A_{CC}}{\Delta m^2}\right)}. \tag{2.49}$$

Depending on the matter density, the transition probability will change with time. If the matter density is constant then the transition density is the same as in the oscillation in vacuum with the mixing angle and the squared-mass difference replaced

by their respective values in matter. If ρ is not constant and change with time, we need to consider the adiabatic condition where adiabaticity parameter is involved. The oscillation length in matter is modified:

$$\begin{aligned} L_M^{osc} &= \frac{4\pi E}{\Delta m_M^2} \\ &= \frac{L_\nu}{\left(1 - 2\left(\frac{L_\nu}{L_0}\cos 2\theta\right) + \left(\frac{L_\nu}{L_0}\right)^2\right)^{1/2}} \end{aligned} \tag{2.50}$$

where L_0 is

$$L_0 = \frac{2\pi}{\sqrt{2}G_F n_e}. \tag{2.51}$$

The oscillations length in matter will affect the survival probability $P_{\nu_e \to \nu_e}$. The MSW effect can be described based on the ratio L_ν / L_0. This is valid only for constant density.

(i) If $\frac{L_\nu}{L_0} \ll 1$ the $P_{\nu_e \to \nu_e}$ is the same as in vacuum.

(ii) If $\frac{L_\nu}{L_0} = \cos 2\theta_M$ the maximum mixing happens and is known as MSW resonance.

2.4 Stopping Power of Matter for Neutrinos

In massive stars, copious number of neutrinos are produced and escaped from the star. Since neutrino interact very weakly with matter, we will only concentrate on the weak interaction of neutrinos with electrons. The cross section of neutrino-electron scattering is calculated by Sulaksono and Simanjuntak where the oscillation of the neutrino is taken into account [17]. The stopping power of matter can be determined by the integration of the cross section with respect to the radius of the star. The stopping power of matter can then be shown to be:

$$-\left(\frac{dE_\nu}{dR}\right) = m_e n_e \frac{G_F^2}{2\pi}\left[P_e\left[A_e\frac{Q_{m_e}^2-\eta^2}{2}-B_e\frac{Q_{m_e}^3-\eta^3}{3}-C_e\frac{Q_{m_e}^4-\eta^4}{4}\right]\right] - \left[(P_e-1)\left[A_\mu\frac{Q_{m_\mu}^2-\eta^2}{2}-B_\mu\frac{Q_{m_\mu}^3-\eta^3}{3}-C_\mu\frac{Q_{m_\mu}^4-\eta^4}{4}\right]\right] \quad (2.52)$$

where the constants $A_i, B_i, C_i (i = e, \mu, \tau)$ are given below:

$$A_i = \frac{[E_\nu^2 - \lambda_q E_\nu (E_\nu^2 - M_{\nu_i}^2)^{1/2}]((g_V+g_A)^2+(g_V-g_A)^2) - M_{\nu_i}^2(g_V^2-g_A^2)}{(E_\nu^2 - M_{\nu_i}^2)} \quad (2.53)$$

$$B_i = \frac{\lambda_q}{m_e(E_\nu^2-M_{\nu_i}^2)^{1/2}}\left[\frac{E_\nu(E_\nu+m_e)(E_\nu(g_v-g_A)^2+m_e(g_V^2-g_A^2))}{(E_\nu^2-M_{\nu_i}^2)}\right] + (g_V^2-g_A^2)(m_e-E_\nu) - m_e(g_V^2-g_A^2) - \frac{2E_\nu(g_v-g_A)^2+m_e(g_V^2-g_A^2)}{(E_\nu^2-M_{\nu_i})} \quad (2.54)$$

$$C_i = \frac{[(g_v+g_A)^2+(g_v-g_A)^2]}{(E_\nu^2-M_{\nu_i}^2)} + \frac{\lambda_q((g_v+g_A)^2-(g_v-g_A)^2-(g_v-g_A))^2(m_eE_\nu+M_{\nu_i}^2)}{m_e(E_\nu^2-M_{\nu_i}^2)^{3/2}} \quad (2.55)$$

In Eq. (2.52), m_e is the mass of the electron and n_e is the electron density in the medium. In our calculation, the value of n_e from the massive stars is generated from the Geneva stellar evolution code. Q is the maximum energy transferred to the electron from the neutrino and E_ν is the energy of neutrino that comes from the thermal processes. Here, we use values of the neutrino energy that comes from the photoneutrino, pair neutrino, plasma neutrino and bremsstrahlung processes. Here, η is the plasmon energy of the electrons in the star. Plasmon energy can be

described as the quantization of the electromagnetic field of all three polarization states in a plasma that gives rise to a spin-1 particle with one longitudinal and two transverse spin polarizations. Their dispersion relations depend on the properties of the plasma [25]. Both η and Q_m can be calculated below:

$$\eta = \frac{2n_e e^2}{m_e} \tag{2.56}$$

$$Q_m = 2m_e \frac{(E_\nu^2 - m_{\nu_i}^2)}{(m_{\nu_i}^2 + m_e^2 + 2m_e E_\nu^2)}. \tag{2.57}$$

In our calculations, we consider the oscillations of the electron neutrinos to the muon neutrinos; $\nu_e \rightarrow \nu_\mu$ since the oscillations of $\nu_e \rightarrow \nu_\tau$ is not possible in due to energy consideration. The mass of the ν_τ is very massive compared to the mass of ν_e and this requires sufficiently high energy to make the $\nu_e \rightarrow \nu_\tau$ transition possible.

In Eq. (2.52) we use three survival probabilities of ν_e with $P_{\nu_e \rightarrow \nu_e} = 0.0$, $P_{\nu_e \rightarrow \nu_e} = 0.5$ and $P_{\nu_e \rightarrow \nu_e} = 1.0$. For the $P_{\nu_e \rightarrow \nu_e} = 1.0$, the ν_e will not oscillate into another flavor and they just scatter off the electrons resulting in the full effect of the energy loss mechanism. For $P_{\nu_e \rightarrow \nu_e}$ less than 1, some of the ν_e will be converted into another flavor; $\nu_e \rightarrow \nu_\mu$ and due to these oscillations, the total energy loss of the neutrinos will be less. The reason is that some of the initial energy of the electron neutrinos would be used to convert the lighter electron neutrinos to the more massive muon neutrinos.

We can calculate the energy loss of the neutrinos through oscillations by the integration Eq. (2.52) by using relevant quantities taken directly from the massive stellar models that we evolve from Chapter 3. The integration of respect to the radius of the star R. Given the initial energy of the thermal neutrinos taken from each process of the energy loss in a massive star (photoneutrino, pair neutrino, plasma neutrino and bremsstrahlung processes), the final energy of a neutrino when it emerges from the star is:

$$E_\nu^f = \int_R \left(\frac{dE}{dR}\right) dR. \tag{2.58}$$

The total neutrino energy loss is readily obtained by subtracting the initial energy of the neutrino, E_ν^i from E_ν^f

$$\Delta E_\nu = E_\nu^f - E_\nu^i. \tag{2.59}$$

2.5 Neutrino Energy Loss at Matter-Radiation Decoupling Phase

In this section, we discuss an interesting application in Big Bang Cosmology of the neutrino energy loss mechanism. According to the standard Big Bang cosmology, the early universe is dominated by relativistic particles since the temperature at that epoch is very high [60]. At temperatures in the region of 10^{12}K, the main constituents are photons, muons, neutrino-antineutrino pairs and electron-positron pairs. As the universe expands, the particles that will be at thermal equilibrium at a given time depend on two time scales; the reaction rate of the particles and the expansion rate of the universe. If the reaction rate is slow compared to the expansion rate then the particles will decouple from the rest of the background matter. Neutrinos and antineutrinos ceased to be in equilibrium with radiation when the weak interaction time scale becomes longer than the rate of expansion of the universe. By assuming that the entropy is conserved, the temperature of the photon field T_γ will be higher that the temperature of the neutrinos T_ν by a factor of 1.401 [60]. Recent experiments [61,62] show that neutrinos could oscillate into different flavor through the charged-current interaction with electrons This necessarily means that neutrinos are not massless although in some grand unified theories, neutrinos usually pick up a small mass for instance the seesaw mechanism in the SO(10) model [63]. At the time of the decoupling of neutrinos from matter, the energy loss of the neutrinos is

envisaged to be absorbed by the photons via the annihilation of the $e^{\pm}$ pairs during the matter-radiation phase. This section investigates the changes in the photon temperature at the matter-radiation phase due to the neutrino energy loss through neutrino oscillation.

The ratio of the photon temperature T_γ to neutrino temperature T_ν at the neutrino-matter decoupling phase is given by

$$\frac{T_\gamma}{T_\nu} = \left(\frac{11}{4}\right)^{1/3}. \tag{2.60}$$

The energy loss of a neutrino can be calculated by integrating the stopping power equation with a given initial energy E_ν^i. For every of this initial neutrino energy, the total neutrino energy loss ΔE_ν can be calculated by using the following integration,

$$\Delta E_\nu = \int_{E_\nu^f}^{E_\nu^i} \left(\frac{dE_\nu}{dR}\right) dR \tag{2.61}$$

where E_ν^f is the final neutrino energy after ν - e scattering and R is the radius scale of the expanding universe. Since $R \propto T^{-1}$, then the Eq. 2.61 becomes

$$\Delta E = \int_{E_\nu^f}^{E_\nu^i} \left(\frac{dE_\nu}{dT^{-1}}\right) dT^{-1} \tag{2.62}$$

where T is the temperature of the universe. Let $\tau = \frac{1}{T}$, then Eq.(2.62) is written as

$$\Delta E = \int_{E_\nu^f}^{E_\nu^i} \left(\frac{dE_\nu}{d\tau}\right) d\tau \tag{2.63}$$

Using the notation $T_{12} = 10^{12}T$, the temperature variable is

$$\tau_{12} = \frac{1}{T_{12}}. \tag{2.64}$$

Inserting Eq.(2.64) into Eq.(2.63), we obtain

$$\Delta E = \int_{\tau_\nu^f}^{\tau_\nu^i} \left(\frac{dE_\nu}{d\tau_{12}}\right) d\tau_{12} \tag{2.65}$$

Eq. (2.65) is the total energy loss for a neutrino in units of $10^{12}T$ with initial temperature τ_{12}^{i} and final temperature τ_{12}^{f}. To see the effects of this energy loss towards the photons γ, consider the following interaction $\nu_e + e^- \rightarrow \nu_e + e^-$. During the decoupling of neutrinos matter one can imagine that the energy loss for the neutrinos as a gain in the energy of the electrons. Thus we have the final neutrino energy given by $E_\nu^f = E_e^i - \Delta E_\nu \equiv T_\nu^f = T_\nu^i - \Delta T_\nu^f$. Since an electron takes all of the neutrino energy loss, the final electron energy is $E_\nu^f = E_e^i + \Delta E_\nu \equiv T_e^f = T_e^i + \Delta T_\nu = T_e^i + \Delta T_e$ where $\Delta E_\nu = \Delta E_e$ and thus $\Delta T_\nu = \Delta T_e$ with E_e^i is the initial electron rest mass energy. In the decoupling of electron-radiation $e^+ + e^- \rightarrow \gamma + \gamma$ the extra energy will be transferred to the photons. Since the $e^\pm$ have the same mass, the photon energy increase by ΔE_e i.e for each photon, the energy gain is $\Delta E_\gamma = \frac{1}{2}\Delta E_e$, therefore the final photon temperature is $T_\gamma^f \rightarrow T_\gamma^i + \frac{1}{2}\Delta T_e$ where T_γ^i is the initial photon temperature. Consequently, we could see that this extra energy would increase the photon temperature from $T_\gamma^i \rightarrow T_\gamma^f$ where $T_\gamma^f > T_\gamma^i$. This extra energy can also be associated with the fluctuation of the cosmic microwave background where we divide the extra energy by the initial energy of $10^{12}K$. Since $T_\gamma^f = T_\gamma^i + \Delta T_\nu$ where the increase in the photons temperature $\Delta T_\gamma = \frac{1}{2}\Delta T_e = \frac{1}{2}\Delta T_\nu$ then there should be an increase to the ratio in equation (2.60) given by $\frac{T_\gamma^f}{T_\nu^f} = \left(\frac{11}{4}\right)^{\frac{1}{3}} + \Delta\left(\frac{T_\gamma}{T_\nu}\right)$ or

$$\Delta\left(\frac{T_\gamma}{T_\nu}\right) = \frac{T_\gamma^f}{T_\nu^f} - \left(\frac{11}{4}\right)^{\frac{1}{3}} \tag{2.66}$$

Hence to the first order

$$\frac{T_\gamma^f}{T_\nu^f} = \frac{T_\gamma^i + \Delta T_\nu}{T_\nu^i - \Delta T_\nu} = \frac{T_\gamma^i}{T_\nu^i} + \frac{T_\gamma^i}{T_\nu^i}\left(\frac{\Delta T_\nu}{T_\nu^i}\right) - \frac{\Delta T_\nu}{T_\nu^i}. \tag{2.67}$$

Inserting Eq. (2.65) into Eq. (2.64), we have

$$\Delta\left(\frac{T_\gamma}{T_\nu}\right) = \left[\left(\frac{11}{4}\right)^{\frac{1}{3}} - 1\right]\frac{\Delta T_\nu}{T_\nu^i} = 0.401\frac{\Delta T_\nu}{T_\nu^i} \tag{2.68}$$

Therefore Eq. (2.68) is the extra term that we seek and is shown in Fig 2.4 with

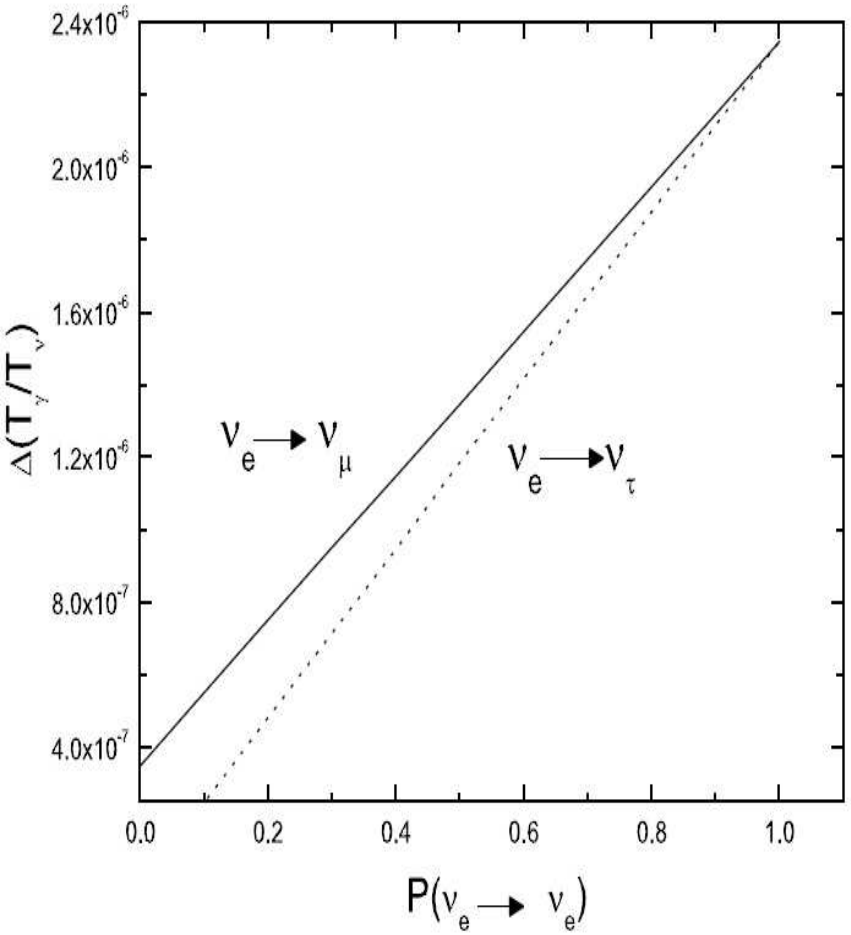

Figure 2.4: $\Delta\left(\frac{T_\nu}{T_\gamma}\right)$ at the decoupling temperature of ν_e.

respect to the oscillation probability. Evidence from the atmospheric and solar neutrinos suggests that neutrinos could oscillate from one flavor to a different flavor. In the MSW mechanism, $\nu_e - e^-$ scattering has charged and neutral currents whereas the other neutrino flavors have only the neutral current interaction. The oscillation is greatly enhanced in a slowly changing electron density.

We have shown that if the energy loss by the electron neutrinos due to the oscillations between active neutrino species, then there is a small correction term $0.401\Delta\left(\frac{T_\nu}{T_\nu^l}\right)$ appears in the canonical value $T_\nu = (4/11)^{1/3}T_\gamma$. In this scenario, this correction term is on average $\sim 10^{-6}$. This value is comparable to the present observational limit of the anisotropy of the CMB. Further work can be done by considering explicit adiabatic and non-adiabatic conversions of the electron neutrinos [26].

Chapter 3

Evolution of Massive Stars

3.1 Introduction

In general, the formation and the evolution of stars are similar for any mass. Stars exist in different sizes, masses and varying amount of chemical composition. Therefore, they will undergo different evolutionary tracks depending on the initial mass m and metalicity Z of the star. Basically, the formation of a star begins with the implosion of interstellar clouds that attain a mixture of elements through the gravitational force towards the center. Once the ball of gasses reaches the equilibrium state where the internal pressure balances the inward gravitational force, it will contain certain values of the radius r, pressure P, density ρ and temperature T. When the temperature is high enough, the first ignition of thermonuclear reactions at the center of the star commences. The thermonuclear reaction rates are usually calculated by using the low energy approximation since the temperature is in the region of keV [27]. For massive stars, we can use a more general formula that can be applied to all energy range [28] [29]. In a nutshell, we can conclude that the evolution of low-mass stars and massive stars in the main sequence of the Herztsprung Russell diagram is quite the same. For low-mass stars, a specific burning process will stop at certain stages depending on the initial mass and metalicity, and for massive stars it will end at silicon burning [1], [3]. How a particular star will end its life is solely depended on the initial mass of the star.

In this chapter, we briefly discuss the evolution of massive stars for both non-rotating and rotating cases. We focus on the evolution stages that produce large number of neutrinos especially in the late stages; viz during carbon burning on-

wards. During these stages, neutrinos are produced copiously and become the dominant process that contributes to the energy loss in the star. This process is also known as neutrino-cooling process [1], [3]. Besides from the importance of neutrino production in stars that contribute to the most effective method of energy loss, we will discuss the role of neutrinos in the nucleosynthesis of elements in the star; during the early stages of the evolution - the hydrogen burning process [30] and the slow neutron capture process (*s*-process) that contributes to the production of the heavy elements in the stars [32], [33].

We have divided this chapter into three sections where in the first section, we will discuss in general the major burning processes that are involved in massive stars starting from the hydrogen (*H*) burning, then follow by the helium (*He*) burning and before proceeding to the advanced burning processes; carbon (*C*) burning, neon (*Ne*) burning, oxygen (*O*) burning and finally the silicon (*Si*) burning. In the second section, we focus on the production of neutrinos in massive stars and the effects to the evolution process. Finally in the third section, we will discuss in detail the models that we have chosen for this work; the non-rotating and the rotating models of $20M_{\odot}$ and $120M_{\odot}$ stars. The $20M_{\odot}$ is the example of a massive star model and the $120M_{\odot}$ is the example of a very massive star.

3.2 Major Nuclear Burning Stages

3.2.1 Hydrogen Burning

After the star reaches hydrostatic equilibrium and the temperature is high enough, the first ignition of the thermonuclear reaction begins at the core of the star. For a low-mass star, the hydrogen burning and the helium burning are the only thermonuclear reactions that are involved. This type of star will end its life as a white dwarf. Massive stars involve more complex series of reactions; hydrogen burning, helium burning, carbon burning, neon burning, oxygen burning and finally silicon

Table 3.1: The *pp* chains.

Reaction	Q value (MeV)	E_ν (MeV)
ppI		
$p + p \rightarrow d + e^+ + \nu$	1.442	≤ 0.420
$d + p \rightarrow {}^3He + \gamma$	5.493	
${}^3He + {}^3He \rightarrow {}^4He + 2p$	12.859	
ppII		
${}^3He + {}^4He \rightarrow {}^7Be + \gamma$	1.586	
${}^7Be + e^- \rightarrow {}^7Li + \nu$	0.861	≤ 0.861
		≤ 0.383
${}^7Li + p \rightarrow {}^4He + {}^4He$	17.347	
ppIII		
${}^7Be + p \rightarrow {}^8B + \gamma$	0.135	
${}^8B \rightarrow 2{}^4He + e^+ + \nu$	18.074	< 15

burning.

The first ignition of the thermonuclear reaction that occurs at the center of the star is the hydrogen burning because it requires the lowest energy for nuclear fusion to occur amongst the chemical abundance. In low mass stars, the main reactions come from the proton-proton (pp) chain in Table 3.1. For massive stars, hydrogen burning stage is dominated by the CNO cycle (Table 3.2).

Table 3.2: The *CNO* cycle.

Reaction	Q value (MeV)	E_ν (MeV)
CN:		
$^{12}C + p \rightarrow ^{13} N + \gamma$	1.944	
$^{13}N \rightarrow ^{13} C + e^+ + \nu$	2.221	≤ 1.199
$^{13}N + p \rightarrow ^{14} N + \gamma$	7.550	
$^{14}N + p \rightarrow ^{15} O + \gamma$	7.293	
$^{15}O \rightarrow ^{15} O + e^+ + \nu$	2.761	1.732
$^{15}N + p \rightarrow ^{12} C + \alpha$	4.965	
$^{15}N + p \rightarrow ^{16} O + \gamma$	12.126	
NO:		
$^{16}O + p \rightarrow ^{17} F + \gamma$	0.601	
$^{17}F \rightarrow ^{17} O + e^+ + \nu$	2.762	≤ 1.740
$^{17}O + p \rightarrow ^{14} N + \alpha$	1.193	
OF:		
$^{17}O + p \rightarrow ^{17} F + \gamma$	5.609	
$^{17}F + e^- \rightarrow ^{18} O + \nu$	1.655	≤ 0.633
$^{17}O + p \rightarrow ^{19} F + \gamma$	7.993	
$^{19}F + p \rightarrow ^{16} O + \alpha$	8.115	

3.2.2 Helium Burning

In the context of massive stars, the continuation of the burning process is totally dependent on the ashes from the previous burning stages. Most massive stars spend about 90% of their life in the hydrogen burning phase. Once the hydrogen is exhausted, the ashes i.e. helium will become the fuel for the next burning stage (helium burning). Once the fuel at the core finishes and the temperature at the core starts to drop, the inward gravitational force towards the center will cause the star to contract. Due to this contraction, density and pressure would increase and eventually causes an increase in the temperature. When the temperature is high enough, the ignition of helium burning starts. The reaction occurs at very high temperature with a shorter time compared to the previous hydrogen burning. There are two principle reactions in helium burning; $3\alpha \rightarrow^{12} C$ and $^{12}C(\alpha,\gamma)^{16}O$. The energy released from the first reaction is 7.275 MeV and for the second reaction is 7.162 MeV [40]. This helium burning process is also known as triple - α process. As we have shown in Table 3.2, there is a small fraction of ^{14}N exists from the hydrogen burning and before the complete energy of triple - α process is released, the fraction of ^{14}N remaining is completely burnt by $^{14}N(\alpha,\gamma)^{18}F(\beta^+,\nu)^{18}O$ and the energy released becomes the initial energy for the helium burning. Towards the end of helium burning, ^{18}O will be converted into ^{22}Ne and provides the neutron source for the s-process [31], [32], [33]. This is the starting point of the s process in massive stars. In this stage, most of the neutrinos are emitted by the hot dense plasma known as plasmon decay as shown in the equation below.

$$\gamma^* \rightarrow \nu_x + \overline{\nu}_x \tag{3.1}$$

where x denotes all neutrino flavors. During this stage, the star is still emitting photons as its main energy source. Thermal neutrinos that are produced are not yet dominant but cannot be neglected [35].

3.3 Advanced Nuclear Burning Stages

Low-mass stars and massive stars undergo different evolutionary tracks and end their lives differently. For low-mass stars there is no more thermonuclear reactions after helium burning due to the low temperature to overcome the Coulomb repulsion. For a massive star, it has a more complex nuclear network that generally will end its life after silicon burning. After helium burning, the star will enter the advanced stages of nuclear burning where the burning will proceed at higher temperature and photons are not longer the dominant energy produced. This is also known as neutrino-cooled stage where energy generation by thermonuclear reactions at the center of the star is balanced by the emission of neutrinos mainly from pair production process [1].

3.3.1 Carbon Burning

Large amount of carbon and energy are produced during helium burning and due to the high temperature, the carbon burning process begins to take place. This reaction occurs at very high temperature $\sim 10^9$ K. During this time, carbon nuclei fuse together to produce the excited state of ^{24}Mg. Due to the instability of the nuclei, ^{24}Mg mostly will disintegrate into ^{20}Ne and α particles. This process is described in Table 3.3.

Large number of ^{20}Ne is produced and the probability of decay to α and proton is the same and the neutron ratio is sensitive to the temperature. The decay of ^{24}Mg to ^{23}Mg is important since it will increase the population of neutrons in the star and will lead into the next series of nuclear reactions. At this stage, neutrino loss has a significant effect on the properties of the core since the photon flux is small and is trapped in the convective zone [36].

Table 3.3: The carbon burning.

Reaction	Q value (MeV)
$^{12}C + ^{12}C \rightarrow ^{24}Mg$	
$^{24}Mg \rightarrow ^{23}Mg + n$	2.62
$^{24}Mg \rightarrow ^{20}Ne + ^{4}He$	4.62
$^{24}Mg \rightarrow ^{23}Na + p$	2.24

3.3.2 Neon Burning

As we have mentioned before, the ashes of the previous burning will be the next fuel for the next set of nuclear burning in the star. Oxygen has a smaller Coulomb barrier compared to neon but before the temperature required for oxygen burning is reached, the reaction of $^{20}Ne(\gamma,\alpha)^{16}O$ occurs by using the high energy photons from the Planck distribution. The separation energy of ^{20}Ne is lower than ^{16}O and allows the production of ^{24}Mg by the fusion of α particles with ^{20}Ne. Most of the energy generation comes from the rearrangement of this $^{20}Ne \rightarrow ^{16}O + ^{4}He + 4.59MeV$ reaction [40].

The secondary reactions that are important for γ - line astronomy which enriches the abundances of magnesium, aluminium, silicon and phosphorus as well as other heavy elements are $^{24}Mg(\alpha,\gamma)^{28}Si$, $^{25}Mg(\alpha,n)^{28}Si$, $^{26}Mg(\alpha,n)^{29}Si$, $^{26}Mg(p,n)^{26}Al$, $^{26}Mg(\alpha,\gamma)^{30}Si$, $^{27}Al(\alpha,p)^{30}Si$ and $^{30}Si(p,\gamma)^{31}P$. Not all of the reactions lead to energy generation. Most of the reactions enrich the nucleosynthesis processes where it generate magnesium isotopes together with other heavy elements. Neon burning is very important in altering the entropy structure of low mass stars and for the next stages of the burning processes. Both carbon and neon burnings share many features and produce many identical nuclei. But in carbon burning, the energy generation is three times higher than in neon burning.

3.3.3 Oxygen Burning

The next nuclear burning that occurs at the center of a massive star is oxygen burning. This reaction is sensitive to the temperature where at temperature around $2T_9$ (T_9 is the temperature in units of 10^9 K), oxygen fusion is dominant but at temperature $\sim 3 - 4T_9$, both photodisintegration and fusion can occur at a comparable rate. This reaction is well described by hydrostatic equilibrium. The fusion of O nuclei produces ^{32}S that may decay into other elements by channels shown in Table 3.4.

Based on Table 3.4, we can see that there are four channels involved; n channel, p channel, deuteron channel and α channel. At lower temperature, the deuteron channel is restrained and three other channels increase in rate. Deuteron is very sensitive to temperature changes; at high temperature, deuteron will disintegrate into a proton and a neutron and this process will balance the whole reactions.

Table 3.4: The oxygen burning.

Reaction	Q value (MeV)
$^{16}O + ^{16}O \rightarrow ^{32}S$	
$^{32}S \rightarrow ^{31}S + n$	1.45
$^{32}S \rightarrow ^{31}P + p$	7.68
$^{32}S \rightarrow ^{30}P + d$	-2.41
$^{32}S \rightarrow ^{28}Si + \alpha$	9.59

As in the neon burning, the secondary burning is important for evolution where the nucleosynthesis produces ^{28}Si, $^{32,33,34}S$, $^{35,37}Cl$, ^{37}Ar, $^{36,38}Ar$, $^{39,41}K$ and $^{40,41,42}Ca$. From these elements, ^{28}Si and ^{32}S are the two most stable and most abundant isotopes. ^{28}Si will be used in the next burning stage which is the final stage in the evolution of massive stars. Elements heavier than nickel will disintegrate back into the iron group because of the instability of the nuclei by photodisintegration process. Only a small amount of heavy elements survive and most of the elements are located in the shell of incomplete oxygen burning further away from the center of

the star.

The most interesting part in this burning is the existence of the weak interactions that leads to the neutron excess in the star. Electron capture process becomes one of the main processes that occur at the center of the star where it will increase the amount of neutron number in the system. This can be described by the reactions of $^{30}P(e^+,\nu)^{30}S$, $^{33}S(e^-,\nu)^{33}P$, $^{35}Cl(e^-,\nu)^{35}S$ and $^{37}Ar(e^-,\nu)^{37}Cl$. The lifetime of the oxygen burning is around several months.

3.3.4 Silicon Burning

The silicon burning is the final stage of the evolution where in this stage, silicon does not undergo normal fusion reaction. This reaction undergoes quasi-equilibrium state where it starts with the photodisintegration of ^{28}Si into n, p and α particles. This can be described by this continuous chain of reactions: $^{28}Si(\gamma,\alpha)^{24}Mg(\gamma,\alpha)^{20}Ne(\gamma,\alpha)^{16}O(\gamma,\alpha)^{12}C(\gamma,2\alpha)\alpha$.

The dynamic of the reactions in the star continues with the equilibrium states between free nucleons and α particles and is maintained by the reactions of $^{28}Si(\alpha,\gamma)^{32}S(\gamma,p)^{31}P(\gamma,p)^{31}Si(\gamma,n)^{29}Si(\gamma,n)^{28}Si$. Each reaction is in equilibrium with its inverse. The product of silicon photodisintegration, α particles and nucleons add onto the quasi-equilibrium group above ^{28}Si and increases its mean atomic weight and finally the fraction of silicon abundances decreases and becomes very small. Bodansky *et al.* [41] shows that the fraction of all nuclei heavier than ^{24}Mg together with the temperature dependency gives the solution to the energy generation for this reaction. The energy release from burning two ^{28}Si nuclei to form ^{56}Ni is less than the oxygen burning. If electron capture is considered at the core of the star, the fuel for the silicon burning is not longer ^{28}Si only but the mixture of other silicon isotopes $^{28,29,30}Si$ and the burning is not governed by the photodisintegration of ^{24}Mg anymore but the other two Mg isotopes $^{25,26}Mg$. This will affect the final product of the burning process where ^{56}Ni is not longer the dominant abundance

but ^{54}Fe or ^{56}Fe.

We must take into account other properties that are involved in the reactions since this is not only affect the nucleosynthesis of the star but also the structure. Implicit coupling of the nuclear burning to the equation of state, the quasi-equilibrium state, the reaction network, and other complex properties are required in order to have a stable model. Other groups have different approaches in calculating this burning. Weaver *et al.* used quasi-equilibrium network coupled to the reaction network below magnesium [42]. Nomoto and Hashimoto used tables to calculate the energy generation [43], Chieffi *et al.* used a different approach where they do not consider the quasi-equilibrium and used a large nuclear network for their calculations [44]. The final result of the silicon burning is ^{56}Ni where this is the most tightly bound nucleus that is allowed to exist in the core of the star.

3.4 Neutrinos in Massive Stars

There are two types of production of the neutrinos in stars i.e. by nuclear reactions and by thermal plasma processes. Neutrinos that are produced from the nuclear reactions i.e. pp chain and CNO cycle have energy in the range of a few MeV reflecting the relevant nuclear energy release. The second source is from the thermal plasma processes. This non-nuclear reaction was recognized in the early 1960's shortly after the V-A theory of weak interactions has been formulated implying the direct interaction between neutrino and electron. These thermal processes do not have a threshold like the solar neutrinos and hence the energy of the neutrinos is dependent on the temperature of the star with the values in the range of the temperature of the star itself. The production of the neutrinos in a massive star begins from the early stage of the star's evolution and continues until the star end its life as core collapse supernova and forms either a neutron star or black hole depending on the final mass. In this work, we are focusing only on the neutrino cooling mechanism through thermal processes during the pre-supernova stages. The other neutrino

cooling mechanism known as the weak nuclear processes is ignored.

Thermal neutrino processes that are involved in the late stages of the evolution of massive stars are the main factor for the energy loss. Neutrinos become crucial in the late stages, starting from the carbon burning onwards where the energy loss of a star is dominated by neutrino-cooling process rather than photon diffusion.

Table 3.5: Thermonuclear burning stages and cooling process.

Fuel	Ashes	Cooling
^{1}H	$^{4}He, ^{14}N$	photons
^{4}He	$^{12}C, ^{16}O, ^{22}Ne$	photons
^{12}C	$^{20}Ne, ^{24}Mg, ^{16}O$	neutrinos
	$^{23}Na, ^{25,26}Mg$	neutrinos
^{20}Ne	$^{16}O, ^{24}Mg, ^{28}Si, ...$	neutrinos
^{28}Si	^{56}Ni	neutrinos

Table 3.5 shows the thermonuclear burning stages and the cooling processes that are involved in the evolution of a star. For massive stars, after helium burning is completed in the core, temperatures and densities are high enough and neutrino emission becomes significant. These neutrinos interact weakly with matter where they are able to carry off their energy instantaneously away from the star. At lowest the densities and temperatures below $\sim 10^9$K, the photoneutrino emission process is the strongest but for temperatures higher than $\sim 10^9$K, the pair-annihilation processes is dominant. Plasmon process is dominant at higher densities. As the star continues to evolve, the temperatures and densities become higher and the emission rate of neutrinos increases. The rate of energy release in the form of neutrinos begins to compete with the rate of convective energy transport and finally becomes dominant. During the silicon burning of a massive star, the energy loss through neutrino emission exceeds the photo luminosity.

From Table 3.5, we can see that neutrinos play an important role in the late evolutionary stages of the stars. A star losses its energy by emitting neutrinos. Since

we know that neutrinos interact very weakly with matter, it carries almost all of the energy out from the star without any obstacle through four processes: pair production, photo disintegration, bremsstrahlung and recombination [5]. In the series of Itoh *et al.* [6] - [16] papers the energy loss of neutrinos during the late stages have been calculated.

3.5 Stellar Models

In the previous section, we give a brief explanation on the general evolution of massive stars. Most massive stars undergo the same evolution where the star begins its life with hydrogen burning and ends with silicon burning. In this section, we present three models that are calculated by using the Geneva evolution code [45]. Geneva code has been used to resolve the most massive star observed to date [46] although it is capable to evolve one solar mass star that is in agreement with the helioseismology data [47]. These models are evolved starting from the zero age main sequence up to silicon burning with mass loss. We choose two models with masses $20M_{\odot}$ and $120M_{\odot}$ for both non-rotating and rotating stars.

For our models, we focus on the stellar properties; the chemical abundances X_z, radius r, density profile ρ for a particular mass m of the star. For different models of stars with initial mass M_{int}, metalicity Z, radius r and rotation, they will undergo different evolutionary tracks. A star with the initial mass M_{int}, metalicity Z and radius r will end its life differently from the star of the same initial mass with rotation even though the stars have the same initial properties. The existence of rotation will cause some of the mass to be sheared to the surroundings by the stellar wind [48] [49] and enhanced the diffusion mixing in the core of the star.

3.5.1 Stellar Structure Equations

Here, we present the general stellar evolution equations that have been used in the models. Consider a static, spherically symmetric with no hydrodynamic motion in the star. We use the following stellar structure equations in the Geneva code:

$$\frac{dP}{dr} = \frac{-GM(r)\rho(r)}{r^2} \tag{3.2}$$

where $M(r)$ is the mass of the star and $\rho(r)$ is the density profile of star. Both of these functions are with respect to the radius r. In the equation above, the pressure P(r) is one of the most important properties in the evolution of the star where the pressure will balance the gravitational force towards the center and prevents the star from collapsing under its own gravity. This is known as hydrostatic equilibrium.

The mass conservation of the star is

$$\frac{dM(r)}{dr} = 4\pi r^2 \rho(r). \tag{3.3}$$

and the energy conservation is given as

$$\frac{dL(r)}{dr} = 4\pi\rho(r)r^2\varepsilon(r). \tag{3.4}$$

where $\varepsilon(r)$ is the nuclear energy production. When thermonuclear reactions occur in the star, star will loss its energy via radiation. Since the energy is conserved, the energy loss via radiation will be balanced by the thermonuclear reactions.

The important properties that are involved in the evolution of a star is the energy transport. Thermonuclear reactions occur at the center of the star and the temperature at the core is higher than at the surface. The heat (energy) will flow out from the center to the surface via three possible ways: conduction, radiation and convection. Most of the stars transfer their energy via radiation where energy is carried by photons and this can be described in terms of the photon flux:

$$\frac{dT(r)}{dr} = -\frac{1}{4\pi r^2 \lambda} L(r). \tag{3.5}$$

where the $T(r)$ is the temperature and the λ is the Stefan Boltzman constant. These four equations are known as the stellar structure equations. We will use the properties of the stars before core collapse to determine the energy loss of the neutrinos through neutrino oscillations.

3.5.2 Evolutionary Models

When a body rotates, it will cause the existence of centrifugal force and angular momentum that act upon the body of the object. When this theory is applied to a ball of gasses that is being held by the gravitational force towards the center, some of the mass of the body will be smeared out. All four stellar structure equations need to be modified [51]. There are two types of rotation that are involved, the critical rotation at the surface and the interior rotation at the core of the star. The interior rotation is more uniform than the surface since there will be centrifugal force and angular momentum involved at the surface. Due to this instability, the mixing of the chemical composition occurs since this is induced by the circulation flow.

The luminosity and the surface temperature of the rotating star are less than the non-rotating star (see Fig. 3.1) and this is due to the fact that, the centrifugal force that exists during the rotation will reduce the effective gravity. This happens at the hydrogen burning stages. When the main sequence evolution of the star starts, the luminosity of the star increases more than the non-rotating star of the same mass because of the mixing of helium at the shell especially at the shell above the core and towards the surface. The increase of mean molecular weight of the star will increase the luminosity of the star and this is described by Eq. (3.4) above. The mixing of the chemical abundances in the rotating star broaden the lifetime on the main sequence. Besides the broadening of Herztsprung-Rusell diagram, rotation also affect the time of the burning process where for example, in the helium burning, the helium core

grows faster due to the depletion in the hydrogen shell in the star and the increase of the mass in the helium core. These two burnings are the main stages that will lead to the next nuclear reactions. Rotation alters the nucleosynthesis processes that occur in the star.

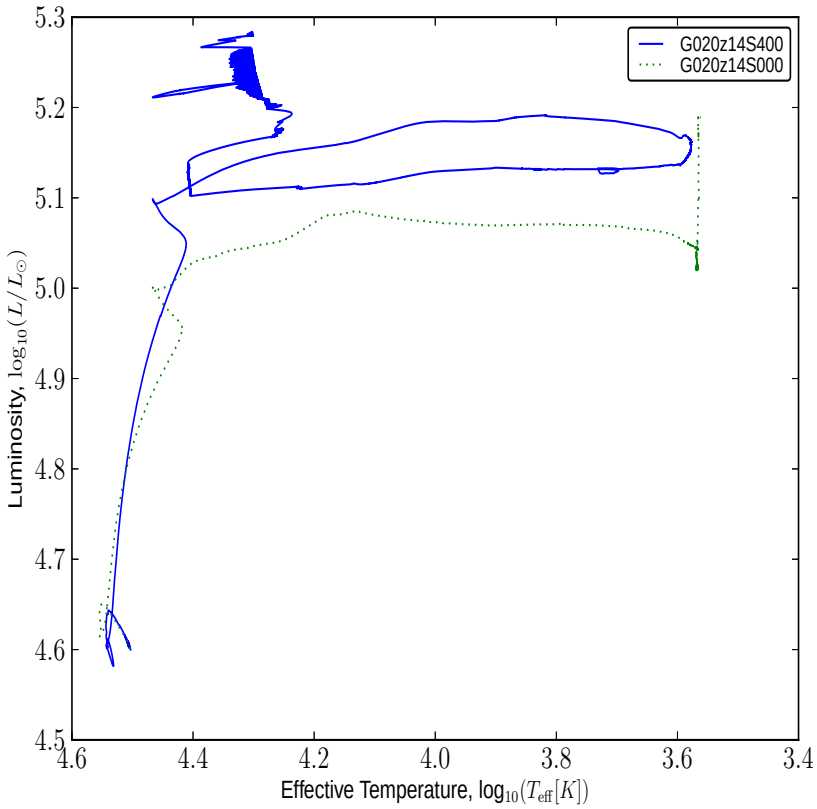

Figure 3.1: The Herztsprung-Rusell diagram of 20 $M_{\odot}$ with rotating and non-rotating models. Solid line represents the rotating model and dotted line represents the non-rotating model.

In this work, we produce stellar models with and without rotation. For the non-rotating models, we treat the models at birth as homogeneous . Two initial masses have been chosen to carried out for this work i.e $20M_{\odot}$ and $120M_{\odot}$. For non-rotating models, they do not suffer much instability compared to the rotating models. Both rotating and non-rotating models undergo all of the burning stages from H-burning up to the Si-burning phase. For mixing, we found that rotation induces mixing in

Table 3.6: End of model burning phase.

M_{ini}	v_{ini}/v_{crit}	End of model burning phase
20	0	O-burning
20	0.4	end of C-burning
60	0	Ne-burning
60	0.4	C-burning
120	0	end of O-burning
120	0.4	end of O-burning

the star during the evolution thus influencing the structure and fate of the star.

All models are evolved from Zero Age Main Sequence up to at least to C-burning stage. For rotating model, we choose the rotation velocity ratio, v_{init}/v_{crit} = 0.4 in order to produce the equatorial velocity of the main sequence (see Ekstrom 2012 for details) [52]. The solar metallicity of these models is $Z = 0.014$ which is taken from Asplund 2005 [53]. Here we list in Table 3.6 the end of the evolution phase of our models. Each model does not end at the burning stage and it depends on how the code successfully converged the model.

In Figs. 3.2 and 3.3, we present the Kippenhahn diagram of all the models with both rotation and no-rotation. These models are enhanced by the new mass loss receipe by Vink (2001) [54] for the O-star and Nugis and Lamers (2000) [55] when the models evolve to the Wolf-Rayet stars. From these figures, we can see rotating models suffer with higher mass loss compared to the non-rotating models.

For 20 $M_\odot$ model, the non-rotating model has convective envelope in its envelope at the end of the main sequence. This is due to the convective process where hydrogen is transported to the surface and continue to burn this excess hydrogen. For the rotating model, no convective envelope is observed in the model. In the rotating model of 20 $M_\odot$, the size of the core is larger since there is no thick envelope around this model. This is due to the strong mass loss in the rotating model which ejects the outer H-rich layer through stellar winds. For the most massive star model which is 120 $M_\odot$, the model undergoes the advanced burning processes up to O-burning. Since it has higher temperature, the nuclei burned more efficiently in the

core and no ashes have been transported to the surface by convection or mixing process induced by rotation. For this particular model, the mass loss plays an extremely important role where these models lose around more than 80% of its original mass during the main sequence. After the main sequence, we observe the mass loss will reach its equilibrium when it reaches the end of He-burning. After the He-burning phase, the thermal neutrino energy loss becomes dominant to cool the star from the extreme mass loss.

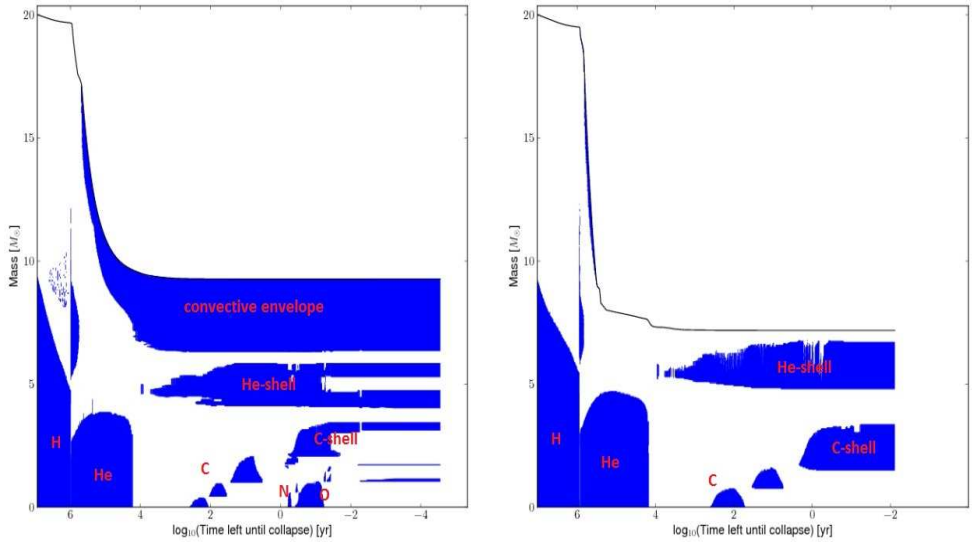

Figure 3.2: The Kippenhahn diagram of rotating and non-rotating 20 $M_\odot$ models.

3.5.3 Abundance profiles of massive stars

Abundance profile is one of the main output from the evolutionary models. From this profile, we can study the properties and the fate of these stars. Comparison of the abundance profile from models and observations will enable us to check the correct nuclear reactions and neutrino cooling mechanisms occurring in the star. Abundance profile of the model is useful in calculating the correct energy loss from the nuclear energy generation and neutrino energy loss from the star.

In Figs. 3.4 and 3.5, we present the chemical abundances of each model at the end of the evolution. All rotating models have longer lifetimes compared to their non-

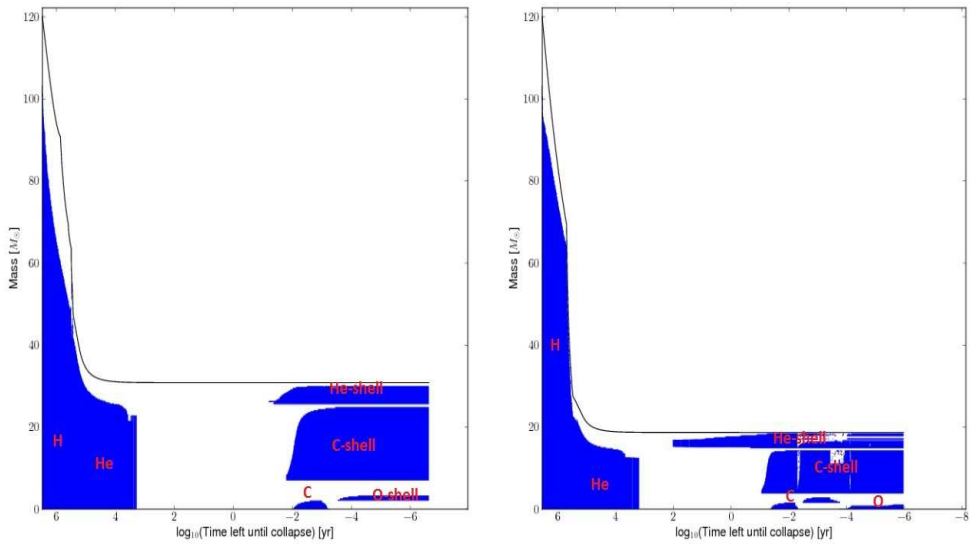

Figure 3.3: The Kippenhahn diagram of rotating and non-rotating 120 $M_\odot$ models.

rotating model. Efficient mixing induced by the rotation will enhance the burning process in the core thus elongating the star lifetime. For the $20M_\odot$ rotating model, the model has high helium content at the surface.

From the figures, all models produce significant amount of oxygen and carbon in the core. Towards the surface of the models, the carbon is more abundant than oxygen except for $20M_\odot$ where the helium is more abundant than the rest of the elements at the surface. This is due to the mixing that transports the helium (and carbon) to the surface. Other elements that actively being produced in the core for massive stars are ^{20}Ne, ^{22}Ne, ^{24}Mg, ^{25}Mg and ^{26}Mg. In the next chapter, we shall demonstrate how the neutrino energy loss due to neutrino oscillation is calculated using the outputs from these models.

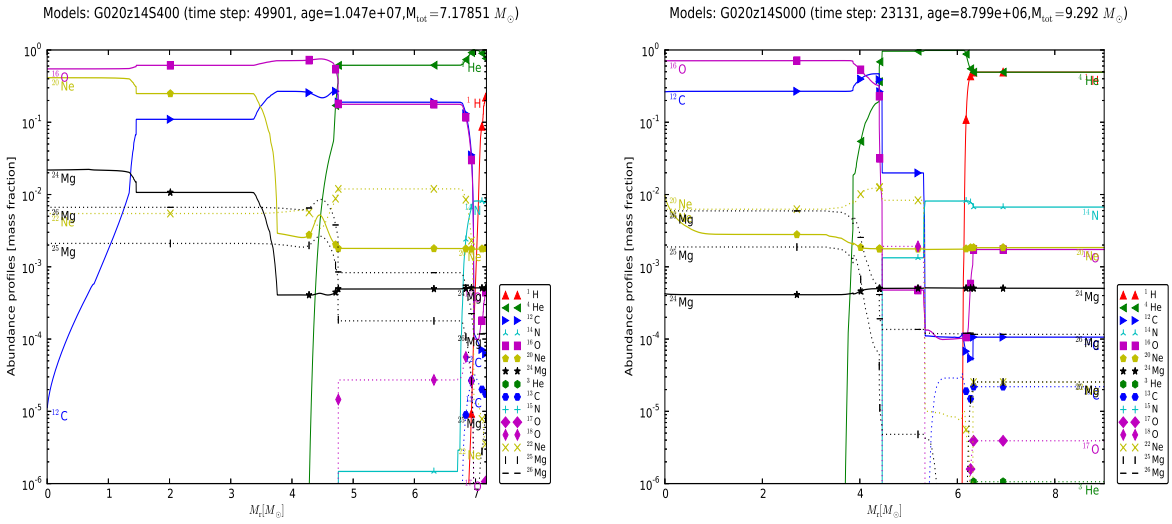

Figure 3.4: The chemical abundance profiles of $20M_{\odot}$ with (left panel) and without rotation (right panel).

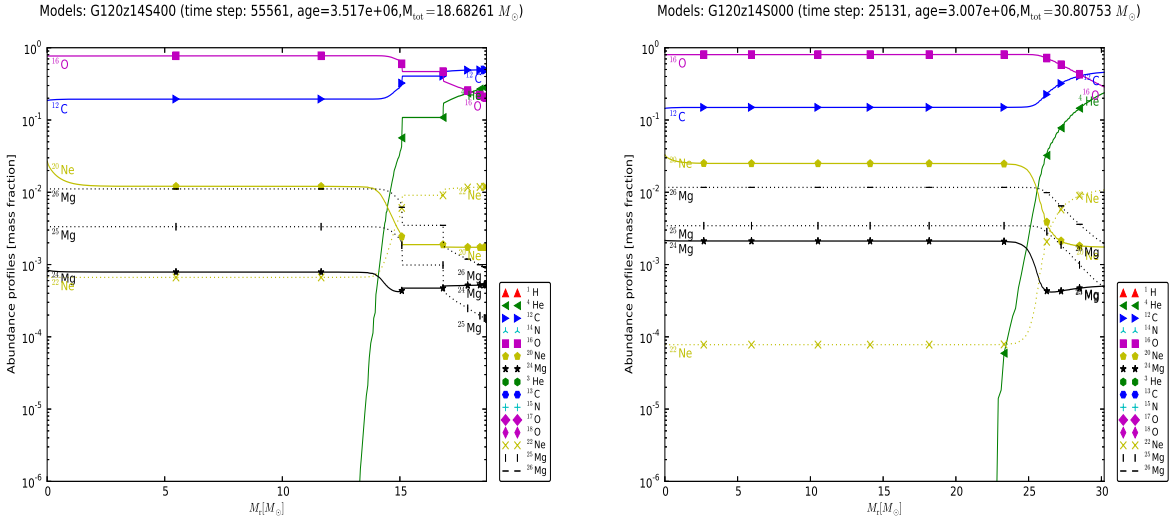

Figure 3.5: The chemical abundance profiles of $120M_{\odot}$ with (left panel) and without rotation (right panel).

3.5.4 Rotational Properties

Due to the mixing that had happened, depleted material from the core of the star will be transferred to the surface and reduces the abundances of the material. This will alter some of the light elements that can be preserved at the outer shell even the percentage of these abundances is very low. This can happen when the most outer layers of the star are sheared away by the stellar wind, the layer below gets closer to the surface and cools down [50].

Normally, the core rotates faster than the envelope because of the angular momentum loss by stellar wind, the expansion in the envelope and also the increasing in the moment of inertia. The initial rotation will affect the lifetime of the star; if the initial rotation of the star is higher then the star will live longer. This is because of the low luminosity at the hydrogen burning. More fuel can be spared since a star spends almost 90% of its life in the hydrogen burning. Due to the large fuel supply and convective core, the effect of high luminosity in the later times in the evolution is not much. The enrichment in helium envelope is weak at the slower rotating model which is $v_{rot} < 200 km/s$. This star will evolve similarly to a non-rotating star.

The rotational velocities of the model will effect the surface evolution and the surface evolution of the star is more important than the core. The rotational velocities are affected by several distributions. Loss of angular momentum due to the stellar wind will slow down the star where its reduces the initial momentum of the star. The expansion of the envelope due to the thermonuclear reactions and also rotation will increase the total moment of inertia. The rotational velocities increase at the end of the hydrogen burning due to the fact that the star will contract after the fuel of the star is exhausted and before the ignition of the shell burning starts.

The hydrogen and helium burning stages are strongly affected by rotation and altered at the early evolution of the star where larger helium core is produced due to this effect. Heger *et al.* [51] suggested that rotation is also important in the late stages of the star especially in sheared instabilities. The ashes from the previous

burning will be the fuel for the next burning stages and since the evolution of the first two major burning stages are already altered causing the whole evolution of the star to be affected. The core of the *CO* contracts and *He* burning continues at the shell. The most outer layer of *He* rich shell cools down due to the decrease in entropy and stellar wind. The existence of protons in the shell of the star will later burn in the *He* burning and leads into new channels of nucleosynthesis. The evolution that occurs at the major burning processes alter the final composition of the chemical abundances.

3.5.5 Neutrino Energy Loss in Stellar Interior

One of the important parameters that strongly effect the evolution of a star is the cooling rate. In the late evolutionary stages of a massive star, the star will lose its energy through the neutrino emission where the rate of emission of the neutrinos exceeds the rate of the photo luminosity. The star will lose its energy through radiation or neutrino emission depending on the evolution of star (mass of the star), for the star that undergoes the advanced burning processes; carbon burning onwards, the neutrinos emission becomes the main cause of energy loss in the star compares to the low-mass star. A star will lose its energy from four processes; photoneutrino, pair annihilation, plasma neutrino and bremsstrahlung process.

There are four leptonic processes that are responsible for the energy loss:

1. pair neutrino: $e^+ + e^- \rightarrow \nu + \overline{\nu}$
2. photoneutrino: $\gamma + e^{\pm} \rightarrow \nu + \overline{\nu}$
3. plasma neutrino: $\gamma^* \rightarrow \nu + \overline{\nu}$
4. bremsstrahlung: $e^{\pm} + Z \rightarrow \nu + \overline{\nu}$

The neutrino energy loss has been studied extensively by Itoh et al [13]. For pair neutrino, the energy loss rate process is expressed as below [13]:

$$Q_{pair} = \frac{1}{2}\left[(C_V^2 + C_A^2) + n(C_V'^2 + C_A'^2)\right] Q_{pair}^{+} + \frac{1}{2}\left[(C_V^2 - C_A^2) + n(C_V'^2 - C_A'^2)\right] Q_{pair}^{-}. \tag{3.6}$$

$$Q_{pair}^{\pm} = \frac{1}{2}\left[(C_V^2 + C_A^2) + n(C_V'^2 + C_A'^2)\right] \times \left[1 + \frac{(C_V^2 - C_A^2) + n(C_V'^2 - C_A'^2)}{(C_V^2 + C_A^2) + n(C_V'^2 + C_A'^2)} q_{pair}\right] \tag{3.7}$$

$$\begin{aligned} q_{pair} &= (10.7480\lambda^2 + 0.3967\lambda^{0.5} + 1.0050)^{-0.1} \\ &\times [1 + (\rho/\mu_e)(7.692e + 7\lambda^3 + 9.715e + 6\lambda^{0.5})^{-1.0}]^{-0.3} \end{aligned} \tag{3.8}$$

where $C_V = \frac{1}{2} + 2\sin^2\theta_w$ with $\theta_w = 0.2319$, $C_A = \frac{1}{2}$, $C_V' = 1 - C_V$ and $C_A' = 1 - C_A$. For high temperature (T$> 10^9$K) with density around $\rho \leq 10^5 \mathrm{gcm}^{-3}$, the pair neutrino process is independent from the density and becomes dominant. In plasma neutrino process, the energy loss rate can be written as:

$$Q_{plasma} = (C_V^2 + nC_A'^2) Q_V. \tag{3.9}$$

Photoneutrino becomes the dominant contribution to the energy loss in the star when the temperature of the core is at the range of $10^8 < T < 10^9$K with density $\rho > 10^5 \mathrm{gcm}^{-3}$ where the lost rate is given by :

$$Q_{photo} = \frac{1}{2}\left[(C_V^2 + C_A^2) + n(C_V'^2 + C_A'^2)\right] Q_{photo}^{+} + \frac{1}{2}\left[(C_V^2 - C_A^2) + n(C_V'^2 - C_A'^2)\right] Q_{photo}^{-}. \tag{3.10}$$

where $C_V = \frac{1}{2} + 2\sin^2\theta_w$ with $\theta_w = 0.2319$, $C_A = \frac{1}{2}$, $C_V' = 1 - C_V$ and $C_A' = 1 - C_A$. Q_L is longitudinal plasmon and Q_T is the transverse plasmon. For the photoneutrino calculations, the range of temperature is $10^7 < T < 10^{11}$K with density range of $1 \leq$

$\rho/\mu_e \leq 10^{11}\text{gcm}^{-3}$.

In bremsstrahlung neutrino process, the density is $\rho > 10^9\text{gcm}^{-3}$ and the temperature is in the range of $10^8 < T < 10^{10}\text{K}$ and this conditions are typically in the white dwarf or in the very massive star region. The equations for the energy loss are found in [13]

Chapter 4

Energy Loss of Neutrinos Through Oscillations

Neutrinos play an important role in both cosmology and astrophysics. In the early universe especially during the big bang nucleosynthesis era, neutrinos have a significant impact on the evolution of the universe starting from the matter-radiation decoupling to the big bang nucleosynthesis. In stars, neutrinos are one of the important cooling agents that contribute significantly during the late stages of evolution of a massive star, starting from carbon burning onwards to the final silicon burning before core collapse. Neutrinos are also important in a supernova event (this is known as supernova neutrinos) and also in a neutron star. In our previous work, we have discussed the effect of the neutrino oscillations during the decoupling phase in the early universe [26] by applying the stopping power equation for a neutrino [17]. In this chapter, we are interested to see the effects of the neutrino oscillations in the evolution of massive stars.

We will be focusing on the results from the evolution of non-rotating and rotating models of $20M_{\odot}$ and $120M_{\odot}$ stars. We choose the $20M_{\odot}$ model as an example of a massive star while the choice of the $120M_{\odot}$ as an example of a very massive star is due to the recent discovery of the most massive star to date i.e. the $320M_{\odot}$ star [46]. We divide this chapter into three sections. The first section focuses on the energy loss of neutrinos from the thermal processes that are involved in a star. In the second section, we show the electron density profile from the stellar evolutionary models for both non-rotating and rotating models where it will then be used in the calculation of the energy loss of neutrinos through oscillations. In the last section,

we discuss about the energy loss of neutrinos through oscillations for non-rotating and rotating models of $20M_{\odot}$ and $120M_{\odot}$ in detail where in this case, the $20M_{\odot}$ model is the example of a massive star and $120M_{\odot}$ model is the example of a very massive star. We investigate the effects of neutrino oscillation towards the energy of the neutrinos when the neutrinos propagate from the core of the star to the surface.

There are two types of processes that are involved in producing neutrinos in a star; the weak processes in the stellar nuclear network and the thermal neutrinos from leptonic processes in stellar plasma. At the end of the evolution of a massive star namely during the silicon burning, there are no more neutrinos produced from the nuclear processes since neutrino-producing hydrogen burning has ceased. Here in this work, we only consider the thermal neutrinos from the purely leptonic processes since the four leptonic processes that are discussed in Chapter 3 are the dominant processes at the temperature-density grids relevant to the models used. Finally, the detail discussion on the neutrino energy loss through oscillations for both non-rotating and rotating models of $20M_{\odot}$ and $120M_{\odot}$ are presented. We choose three survival probabilities of the electron neutrinos $P_{\nu_e \to \nu_e} = 0.0$, $P_{\nu_e \to \nu_e} = 0.5$ and $P_{\nu_e \to \nu_e} = 1.0$ in the energy loss calculation of the neutrinos. For $P_{\nu_e \to \nu_e} = 0.0$, all the electron neutrinos will be converted into another flavor i.e. muon neutrino or tau neutrino and in this work, we choose the oscillation of an electron neutrino to tau neutrino only while for $P_{\nu_e \to \nu_e} = 0.5$, only half of the electron neutrinos will be converted to another flavour. For $P_{\nu_e \to \nu_e} = 1.0$ all of the electron neutrinos will remain as electron neutrinos. We focus on the energy loss from oscillation of the thermal neutrinos with respect to the mass of the star at the final stage of the evolution and not on the energy loss of the neutrinos for each stages in evolutionary track.

In this case, the ν_e will not oscillate into another flavor and they just scatter off the electrons resulting in the full effect of the energy loss mechanism. For the $P_{\nu_e \to \nu_e}$ less than 1, since some of the ν_e will be converted into another flavor; the energy loss of the neutrinos will be less. The reason is that some of the initial energy of the

electron neutrinos would be used to convert the lighter electron neutrinos to more massive neutrinos.

4.1 Thermal Neutrino Energy Loss in Massive Stars

Models of stellar evolution calculate the energy loss of the thermal neutrinos in the star without considering the effects of neutrino oscillations [5]- [16]. There is a scarcity of literature on the effects of the neutrino oscillations towards the neutrino energy loss from stellar evolution since it is believed that the effects are too small to be considered. As we know, enormous number of neutrinos are emitted from a star during the late stages of its evolution and the star will lose most of its energy via neutrino thermal processes since the neutrinos will carry away the energy without any obstacle due to its weak interactions with matter. Since the effects of oscillations are taken to be small, it is usually ignored. Recent results from the Super-Kamiokande experiment have confirmed that the terrestrial matter has effects on solar neutrino oscillations [59] . With this recent development on the neutrino oscillations, we can consider the idea of the effects of oscillations on the energy loss of neutrinos in massive stars since the amount of neutrinos that will be released during the evolution is large and the temperature-density grid is high compared to the solar-like models.

Established stellar evolution codes for example the Geneva Stellar Evolution Code [67] include only the neutrino energy loss from the thermal processes [48] [51]. Details of these processes have been described in [5] where they depend on the temperature and density of the star. Fig. 4.1 shows the temperature and density profiles of the $20M_{\odot}$ and 120 $M_{\odot}$ models. These profiles are important in determining the production of the neutrino flux that will be used later in the calculation of the energy loss of the neutrinos through oscillations.

From Fig. 4.1 , we can see that the temperature and density profiles for the non-rotating and rotating models have similar patterns. The Geneva code produces these

models that ends at different burning stages and hence at different ages due to the different masses. At the center of the star, the value of ρ for each non-rotating and rotating models is higher and decreases towards the surface. When the star evolves, the density ρ of the star starts to deplete due to the changing in the thermodynamics properties inside the star and also from the effect of mass loss. For the temperature of the non-rotating and rotating $20M_{\odot}$ and $120M_{\odot}$ stars, the temperature T is almost in the same order of magnitude where at the center $T_c \sim 10^7$ K and at the surface $T_s \sim 10^9$ K respectively. For the non-rotating $20M_{\odot}$, there is a drop in temperature of $\sim$ two orders of magnitude at the near surface but not seen in the rotating model. This is due to the drop in the density beginning at the 0.155 mass shell.

For the rotating $20M_{\odot}$ model star in Fig. 4.1 (left, solid lines), the value of ρ is a bit higher for the rotating model than the non-rotating model where at the center, the value is around $\rho_c = 10^{6.5}$ gcm $^{-3}$ and slowly decreases towards the surface where the final value is $\rho_s = 10^{-1.5}$ gcm $^{-3}$. For the non-rotating model, at the center of the star, $\rho_c = 10^{5.0}$ gcm $^{-3}$ and at the surface the value is around $\rho_s = 10^{-2.0}$ gcm $^{-3}$. This is due to the lack of mixing of the abundances inside the star and will affect the properties of the star as a whole.

In Fig. 4.1 (right solid lines), the $120M_{\odot}$ rotating model has lower central value of ρ_c compared to the non-rotating model. At the center, the ρ_c is equal to $10^{5.0}$ gcm $^{-3}$ and towards the surface, the value becomes $\rho_s = 10^{-0.5}$ gcm $^{-3}$. The difference in the density profiles is mostly due to the centrifugal force from the rotation which draws the stellar matter away from the center of rotation. When the mass of the star is higher and with the existence of rotation in the body, the probability of the star to lose its surface mass is higher due to the ability of the stellar body to sustain the gravitational force towards the center is disminished. At the surface, the centrifugal force shears off the material to the space surrounding the star. For the non-rotating model, the value of $\rho_c = 10^{4.5}$ gcm $^{-3}$ and at the surface the value is equal to $\rho_s = 10^{1.5}$ gcm $^{-3}$.

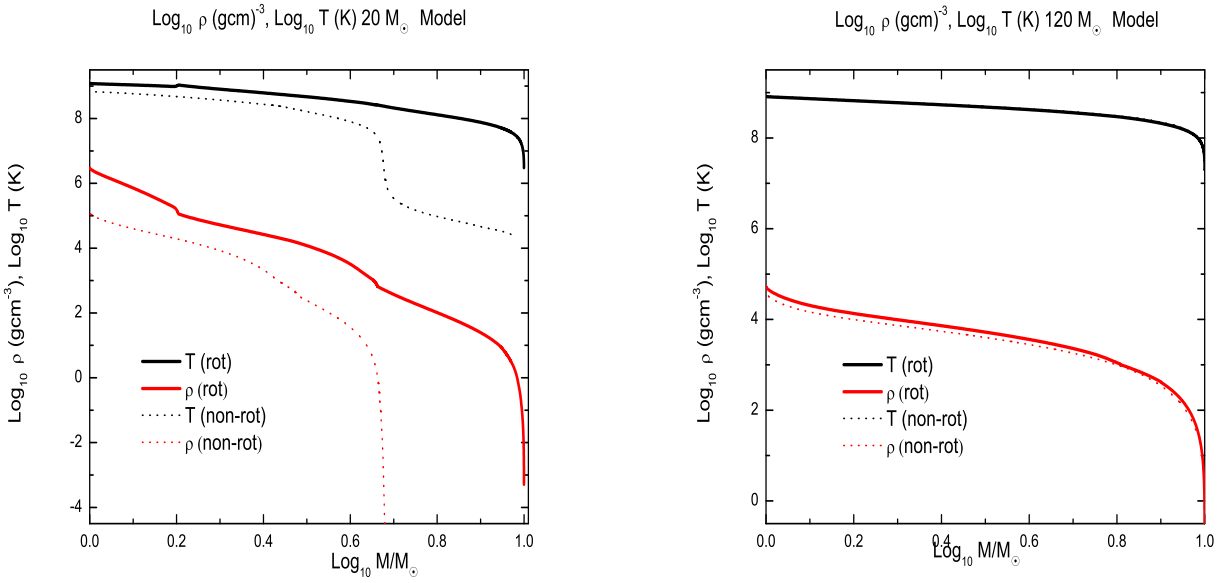

Figure 4.1: The temperature T (K) and density of matter ρ (gcm^{-3}) of 20M$_\odot$ (left) and 120M$_\odot$ (right) models.

The details of the calculation of the neutrino emission are complicated and based on the Weinberg-Salam theory of weak interactions. In this work, details analytical fitting formulas are given by Itoh *et. al* [13]. Different stellar models have different values of the the neutrino energy loss since every star has different thermodynamic properties and this depends on the density of the matter in the star and also on the temperature. Rotation also gives a significant effect on the evolution of the star since the thermodynamic properties are different from the non-rotating models. From Fig. 4.2 we can see that each model has different value of thermal neutrino energy since each model has different evolution track.

For the 20M$_\odot$ non-rotating models in Fig. 4.2 (left, dotted lines), plasma neutrino has lowest value of the neutrino energy loss Q$_\nu$ as compared to the other three processes. For the pair annihilation, at the higher T $\sim 10^{8.8}$ K, Q$_\nu$ becomes the highest. The other two neutrino energy loss mechanisms that have the high values of Q$_\nu$ at lower T are the photo neutrino and bremsstrahlung processes. Almost the same conclusions can be made for the 20M$_\odot$ rotating model. A small difference in Q$_\nu$ value

for photo neutrino, plasma and bremsstrahlung processes. The major difference occurs in the pair annihilation process where at lower T, Q_ν is very low and as the temperature increases, the value of Q_ν increases rapidly and becomes the highest energy which is around 15 MeV/g/s.

For the non-rotating model $120M_\odot$ in Fig. 4.2 (right, dotted lines), two major processes that contribute to the highest neutrino energy loss Q_ν are the photo neutrino and the bremsstrahlung processes. For plasma neutrino, the energy loss of Q_ν is the lowest even when T is high. The pair annihilation has the lowest Q_ν at low T and becomes the highest Q_ν at the highest T.

For the $120M_\odot$ rotating model; the processes that are involved are quite the same as in the non-rotating models; the only difference is on the values of Q_ν at different values of T in the star. For the photo and bremsstrahlung processes, the values of Q_ν are lower than the non-rotating model and the same goes to the plasma neutrino. For pair annihilation process, the value of Q_ν along the whole range of T is the same as in non-rotating model.

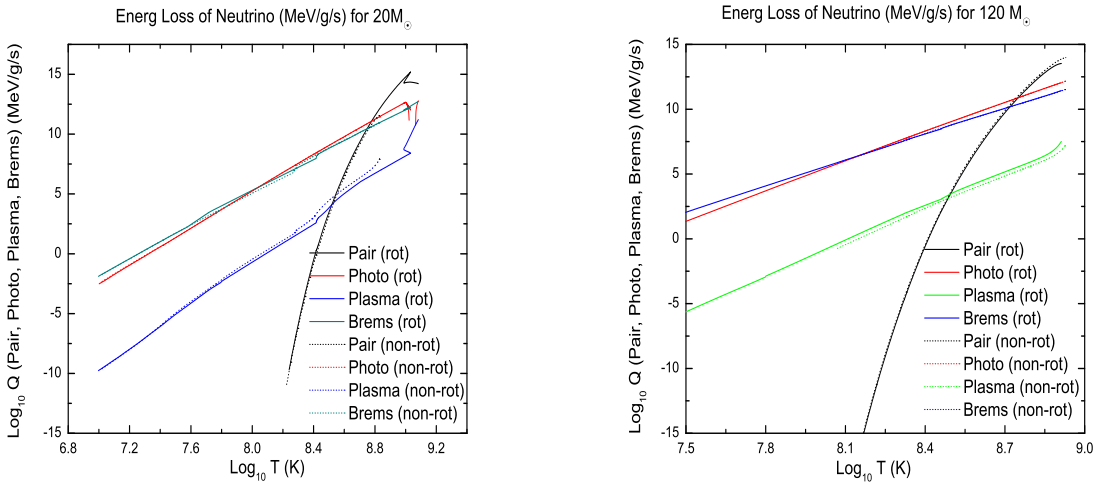

Figure 4.2: The neutrino energy loss from pair production, photo neutrino, plasma neutrino and bremsstrahlung processes log Q_ν (MeV/g/s) of $20M_\odot$ model (left) and $120M_\odot$ (right).

4.2 Electron Density Profile From The Evolutionary Models

In Chapter 3, we have discussed the evolutionary models and the chemical abundance profiles at the end of the evolution of rotating and non-rotating models of massive stars. In order to calculate the neutrino energy loss through oscillations, we need to calculate the electron number density, n_e by using the chemical abundance profile. The electron number density can be calculated by using following equation:

$$n_e = \rho N_A \sum \frac{X_Z Z}{A_Z} \tag{4.1}$$

where X_Z is the fraction of the gas by weight of element Z and A_Z is the mass number of element Z. Fig. 4.3 shows the electron number density as a function of the radius of the star. The density of matter is included as comparison. Since rotation influences the mixing and mass loss during the evolution of massive star, it will cause different values of ρ and n_e. The 20$M_\odot$ rotating model has lower values of ρ and n_e at the inner core than in the non-rotating model. In the 120$M_\odot$ models, the values of ρ and n_e in the inner core for the rotating model are higher than the non-rotating model. Different models have different type of evolution and this will affect the final product of the star.

As we can see in Eq. (4.1), the value of n_e is dependent on the value of ρ. The value of n_e will not be the same due to the different value of ρ for each model. The values of n_e and ρ in 120$M_\odot$ are lower than the 20$M_\odot$ due to the higher diffusion rate of the elements.

4.3 Energy Loss of Neutrinos in Massive Stars

In the previous section, we have discussed about the values of ρ and n_e and in this section, we will use that values to calculate the energy loss of neutrinos through os-

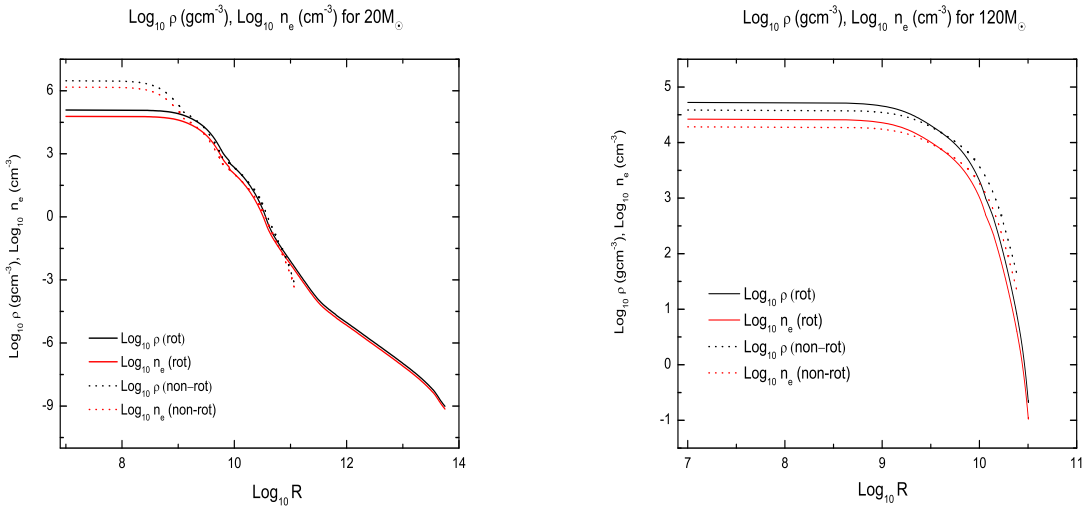

Figure 4.3: The graphs of density of matter, electron number density vs. radius of $20M_\odot$ (left) and $120M_\odot$ (right) model.

cillations by using the stopping power equation of matter for neutrinos. The quantity n_e has a significant effect on the total energy loss because for higher value of n_e, the energy loss will be higher. We can see in Eq. (2.52) that the value of the stopping power equation is proportionally dependent on the values of n_e. The integration of Eq. (2.52) with respect to the normalized radius of each star will give the total value of the energy loss of the neutrinos in the star. Below we will show the value of each energy loss of the neutrinos for both non-rotating and rotating of $20M_\odot$ and $120M_\odot$ models.

We will investigate the effect of the survival probability of the neutrinos $P_{\nu_e \to \nu_e}$ on ΔE_ν (defined in Eq. (2.52)). We choose three values of $P_{\nu_e \to \nu_e}$; $P_{\nu_e \to \nu_e} = 0.0$, $P_{\nu_e \to \nu_e} = 0.5$ and $P_{\nu_e \to \nu_e} = 1.0$. For $P_{\nu_e \to \nu_e} = 1.0$, this means that the ν_e does not oscillate into another flavor and remains as ν_e only. For $P_{\nu_e \to \nu_e} = 0.5$, half of the initial electron neutrinos will remain as electron neutrinos and another half will be converted into another flavor. For $P_{\nu_e \to \nu_e} = 0.0$, all of the electron neutrinos will oscillate into another flavor.

Since the neutrino energy loss originating from the thermal processes is the en-

ergy carried away by the neutrinos from the star, it will be used as the initial energy of the neutrinos in our calculation of the energy loss of the neutrinos due to the neutrino-electron scattering. This will be used in the integration of Eq. (2.58) as E_ν^i.

According to the standard model, neutrinos interact only by the weak force. They are also massless due to the absence of the right-handed neutrinos and thus Yukawa-type coupling would not be possible. In the case of electron neutrinos, the elastic scattering with electrons is mediated by the $W^\pm$ and Z° bosons. For other types of neutrinos, the scattering from electrons can only proceed by the neutral boson. This brings about the differences in the total cross sections of the scatterings. For purely leptonic reactions of the neutrino-electron scatterings, the tree-level Feynman diagrams given in Figs. (2.1) and (2.2) which contribute to the elastic scattering of electron neutrinos on electrons produce a cross section described in Chapter 2:

$$\sigma_{\nu_e - e} \approx 10^{-48} \left(\frac{E_\nu}{MeV} \right)^2 m^2. \tag{4.2}$$

The cross sections of $\nu_{\mu,\tau}$ scatterings with electrons are smaller by a factor of ~ 2.

In thermal conditions of stellar interiors the energy of neutrino, $E_\nu \sim 1$ MeV with the mean free path of the neutrinos $\ell_\nu \sim 10^9$ $R_\odot$ and this is much larger than the size of massive stars. Thus neutrinos are able to escape from the stars with the result that a star loses much of its internal energy to the neutrinos leading to the neutrino cooling process. The neutrino cooling process is an important phase in the evolution of a massive star as it causes the star to contract, rising its internal temperature and sets about the next set of nuclear reactions. This continues to the pre-supernova stage.

In the thermal processes, the neutrino emission competes with the production of photons, for example in the plasma neutrino process. The probability to emit a $\nu_e - \overline{\nu}_e$ pair, P_ν with respect to the emission of a photon, P_γ is given as

$$\frac{P_\nu}{P_\gamma} \sim \left(\frac{E_\nu}{m_e c^2}\right)^4. \tag{4.3}$$

We can then calculate the energy loss of a neutrino by knowing the rate of the neutrinos produced in a thermal process.

In order to calculate the energy loss by the neutrinos through oscillations, we need to consider the reaction rate of the thermal processes that produce the neutrinos. We use the methodology from nuclear astrophysics to derive the equation describing the reaction rate. Consider the general reaction $a + X$. The reaction rate per unit volume between two particles, the projectile a and target X that produces a neutrino is given as

$$r_\nu = n_a n_X \int_0^\infty v\sigma(v)\phi(v)dv \tag{4.4}$$

where $n_{a,x}$ are the number densities of particle a and X respectively, v is the relative velocity, σ is the cross section that depends on v and $\phi(v)$ is the velocity distribution of the particles that is normalized i.e. $\int_0^\infty \phi(v)dv = 1$. In stellar astrophysics the reaction rate is usually expressed in units $\mathrm{cm}^{-3}\mathrm{s}^{-1}$ which we will adopt in our calculations. The reaction rate is averaged over the velocity distribution of the particles and thus the integral in Eq. (4.4) is written in a compact form as $< \sigma v >_{aX}$ which describes the reaction rate per pair of particles. The probability of producing a neutrino has to be folded with the reaction rate leading to Eq. (4.4) written as

$$r_\nu = n_a n_X < \sigma v >_{aX} \left(\frac{P_\nu}{P_\gamma}\right). \tag{4.5}$$

One of the quantities we are able to compute using the stellar evolution code is the rate of energy loss of the neutrinos per unit volume, ε_ν. Dividing this energy loss rate by the rate of the production of the neutrinos gives the energy loss per neutrino,

$$E_\nu = \frac{\varepsilon_\nu}{r_\nu}. \tag{4.6}$$

Inserting Eq. (4.6), the final form of the energy loss through a neutrino is described by

$$E_\nu \sim \left(\frac{\varepsilon_\nu (m_e c^2)^4}{n_a n_X < \sigma v >_{aX}} \right)^{0.2}. \tag{4.7}$$

Using Eq. (4.7), we can now derive the equations necessary to calculate the energy loss per neutrino for the thermal processes described in Chapter 3.

(i) Pair Annihilation Neutrinos

In the ionized gas of the stellar environment at high temperature and density, the $e^+ + e^-$ scattering is well described by the Thompson cross section, σ_T:

$$\sigma = \pi r_e^2 = \frac{3}{8}\sigma_T \tag{4.8}$$

where r_e is the classical electron radius and the value of $\sigma_T = 0.665$ barn [70]. For all thermal processes that we consider, the electrons are weakly degenerate. This means that, for simplicity, we can apply the Maxwell-Boltzmann distribution to describe the velocity distribution of the electrons and positrons. The reaction rate per pair when integrating over the velocity space which depends only on the energy, with the cross section given by Eq. (4.8), is written as

$$< \sigma v >= \left(\frac{16 k T \sigma^2}{\pi m_e} \right)^2. \tag{4.9}$$

Another simplification that we adopt is that the total chemical potential is zero in the Fermi statistics ($\mu_{e^-} + \mu_{e^+} = 0$) and with this we can impose the following condition:

$$n_{e^-} = n_{e^+} = \frac{2(m_e k/2\pi)^{3/2}}{\hbar^3} T^{3/2} e^{-m_e c^2/kT}. \tag{4.10}$$

Thus inserting Eq. (4.9) and Eq. (4.10) into Eq. (4.7), the energy loss of a pair production neutrino is given as

$$E_\nu^{\text{pair}} = \left(\frac{\varepsilon_\nu (m_e c^2)^4}{n_{e^-} n_{e^+} \frac{16kT\sigma^2}{\pi m_e}} \right)^{1/5} \tag{4.11}$$

where E_ν^{pair} will be in MeV if ε_ν is in MeVcm^{-3}s^{-1}, $\sigma\nu$ in cm^{-3} s^{-1} , n_{e^-} and n_{e^+} are both in cm^{-3}.

(ii) Photo-Neutrinos

Assuming that the $\gamma + e^-$ scattering happens at thermodynamic equilibrium, the cross section of this reaction is given by the Thomson scattering, σ_T and the relative velocity is taken to be the velocity of light, c. Photons are bosons and thus the distribution for a gas of photons in equilibrium is given by the Bose-Einstein distribution. To obtain the number density of photons, n_γ one must integrate the distribution over energy and obtain,

$$n_\gamma = 20.2T^2(\text{cm}^{-3}). \tag{4.12}$$

Thus inserting Eq. (4.12) into Eq. (4.7), the energy loss of a photo-neutrino is given as

$$E_\nu^{\text{photo}} \sim \left[\frac{\varepsilon_\nu (m_e c^2)^4}{n_{e^-} n_\gamma \sigma_T c} \right]^{1/5}. \tag{4.13}$$

(iii) Plasma Neutrino

For a longitudinal neutrino, assuming a non-realativistic and non-degenerate plasma, the average neutrino energy is given by

$$< \varepsilon_L >= \frac{1}{2}\omega_o \tag{4.14}$$

where the plasma frequency is

$$\omega_o = \sqrt{\frac{4\pi n_e e^2}{m_e}} \tag{4.15}$$

$$E_F = \frac{(3\pi^2 c^3 \hbar^3 n_e)^{2/3}}{2m_e}. \tag{4.16}$$

We need to check the degeneracy of the plasma by using the degeneracy parameter θ:

$$\theta = \begin{cases} \leq 1 & \text{plasma is strongly degenerate,} \\ = 1 & \text{plasma is moderately degenerate,} \\ = 0 & \text{classical plasma.} \end{cases} \tag{4.17}$$

where θ is defined as

$$\theta = \frac{\text{thermal energy}}{\text{Fermi energy}} = \frac{kT}{E_F}. \tag{4.18}$$

The average neutrino energy for the transverse neutrino spectrum is given by

$$< \varepsilon_T > kT. \tag{4.19}$$

Thus the total (average) plasma energy is

$$E_\nu^{\text{plasma}} = < \varepsilon_L > + < \varepsilon_T > \tag{4.20}$$

$$= \frac{1}{2}\omega_o + kT. \tag{4.21}$$

(iv) Bremsstrahlung Neutrinos

The reaction rate of electrons with nuclei in the stellar plasma according to Eq. (3.11) is given by

$$r_{eZ} = \sum_{Z} n_e n_Z < \sigma v >_{eZ} \left(\frac{P_{\nu_e}}{P_\gamma} \right) \tag{4.22}$$

for all nuclei with Z as the atomic number. Assuming the electrons bombarding bare nuclei, the cross section is determined by the impact parameter b_Z:

$$\sigma_{ez} \sim \pi b_z^2 \tag{4.23}$$

The energy loss of the neutrinos is proportional to the thermal energy of the neutrinos and assuming the nuclei are at rest, the reaction rate per pair can be approximated by the thermal velocity, v_{th} i.e.

$$\sigma_{eZ} \sim \pi b_Z^2 v_{th} \tag{4.24}$$

In this present scenario, the density of the nuclei in the fully ionized plasma is described by

$$n_Z = \rho \frac{X_Z}{A_z} N_A \tag{4.25}$$

where X_Z is the mass fraction of nucleus with atomic mass A_Z while N_A is the Avogadro's number.

4.3.1 Energy Loss of Neutrinos in 20M$_\odot$ Model

In this section, we will discuss the result of ΔE_ν for both non-rotating and rotating 20M$_\odot$ models. The method to calculate the energy per neutrino arising from the thermal processes has been discussed above from Eq. (4.2) to Eq. (4.25). We have calculated the energy loss per neutrino (MeV) and the total energy loss ΔE_ν (MeV/cm^3/s) due to the $\nu_e - e^-$ scattering with the survival probabilities of $P_{\nu_e \to \nu_e} = 0.0$, $P_{\nu_e \to \nu_e} = 0.5$ and $P_{\nu_e \to \nu_e} = 1.0$.

Nonrotating:

The energy loss per neutrino for each $P_{\nu_e \to \nu_e}$ is shown in Figs. 4.4 - 4.6. For $20M_\odot$ nonrotating model with $P_{\nu_e \to \nu_e} = 0.0$, the maximum energy loss per neutrino in Fig. 4.4 is bremsstrahlung process with a value of 2.25×10^{-8}MeV. The lowest energy loss per neutrino is from plasma neutrino which is 7.5×10^{-12}MeV. This can be explained by referring to Fig. 4.2. The bremsstrahlung has the highest value of Q_ν during the thermal processes. The higher the energy of the neutrinos produced during the thermal processes, the higher is the value of the energy loss through the oscillations. For the lowest energy loss which comes from the plasma neutrino, the neutrino energy from this thermal process is the lowest amongst the neutrino producing processes. The small increment in the value of the energy loss per neutrino for $P_{\nu_e \to \nu_e} = 0.5$ can be seen in Fig. 4.5. The highest value is $\sim 2.0 \times 10^{-8}$ MeV and the lowest value is around 1.0×10^{-11} MeV. For $P_{\nu_e \to \nu_e} = 1.0$, the maximum energy loss per neutrino is 6.0×10^{-8} MeV and the lowest energy loss per neutrino is 9.5×10^{-12} MeV. As a summary, for all of these three survival probabilities, the highest energy loss per neutrino comes from the bremsstrahlung process and the lowest energy loss per neutrino comes from the plasma neutrino process. This can be described by referring to Fig. 4.2. In Fig. 4.2, the plasma neutrino has the lowest energy in the thermal processes while the bremsstrahlung process has the highest energy compared to the three other processes.

After calculating the energy per neutrino for each process, the total energy loss of the neutrinos through oscillations can be determined by using Eq. (2.58) by integrating the energy loss with respect to the normalized radius of the star. The total energy loss for each $P_{\nu_e \to \nu_e}$ is shown in Figs 4.7-4.9.

For $P_{\nu_e \to \nu_e} = 0.0$ in Fig. 4.7, the maximum total energy loss through oscillations is due to the bremsstrahlung process where the value is 1.0×10^{11} MeV/cm^3/s and the lowest total energy loss is 800 MeV/cm^3/s from the oscillations of the plasma neutrinos. In Fig. 4.8 with $P_{\nu_e \to \nu_e} = 0.5$, the maximum total energy loss is 9.0×10^{10} MeV/cm^3/s from the bremsstrahlung and the lowest from plasma process at $9.0 \times$

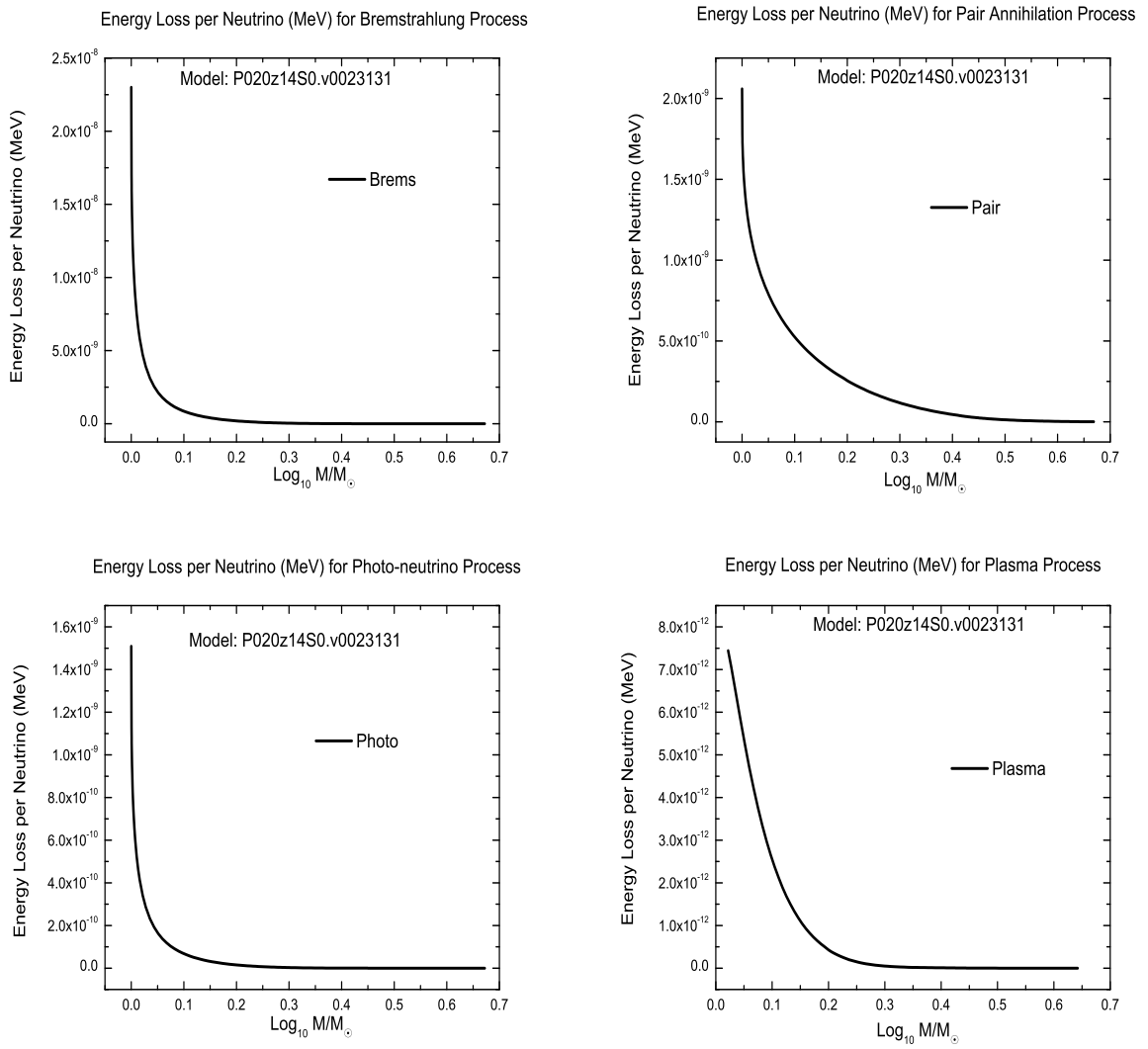

Figure 4.4: The graphs of energy loss per neutrino for bremsstrahlung, pair annihilation, photo-neutrino and plasma processes of non-rotating $20M_{\odot}$ model with $P_{\nu_e \to \nu_e} = 0.0$. Bremsstrahlung has the maximum value of energy loss per neutrino and plasma neutrino has the lowest energy loss per neutrino.

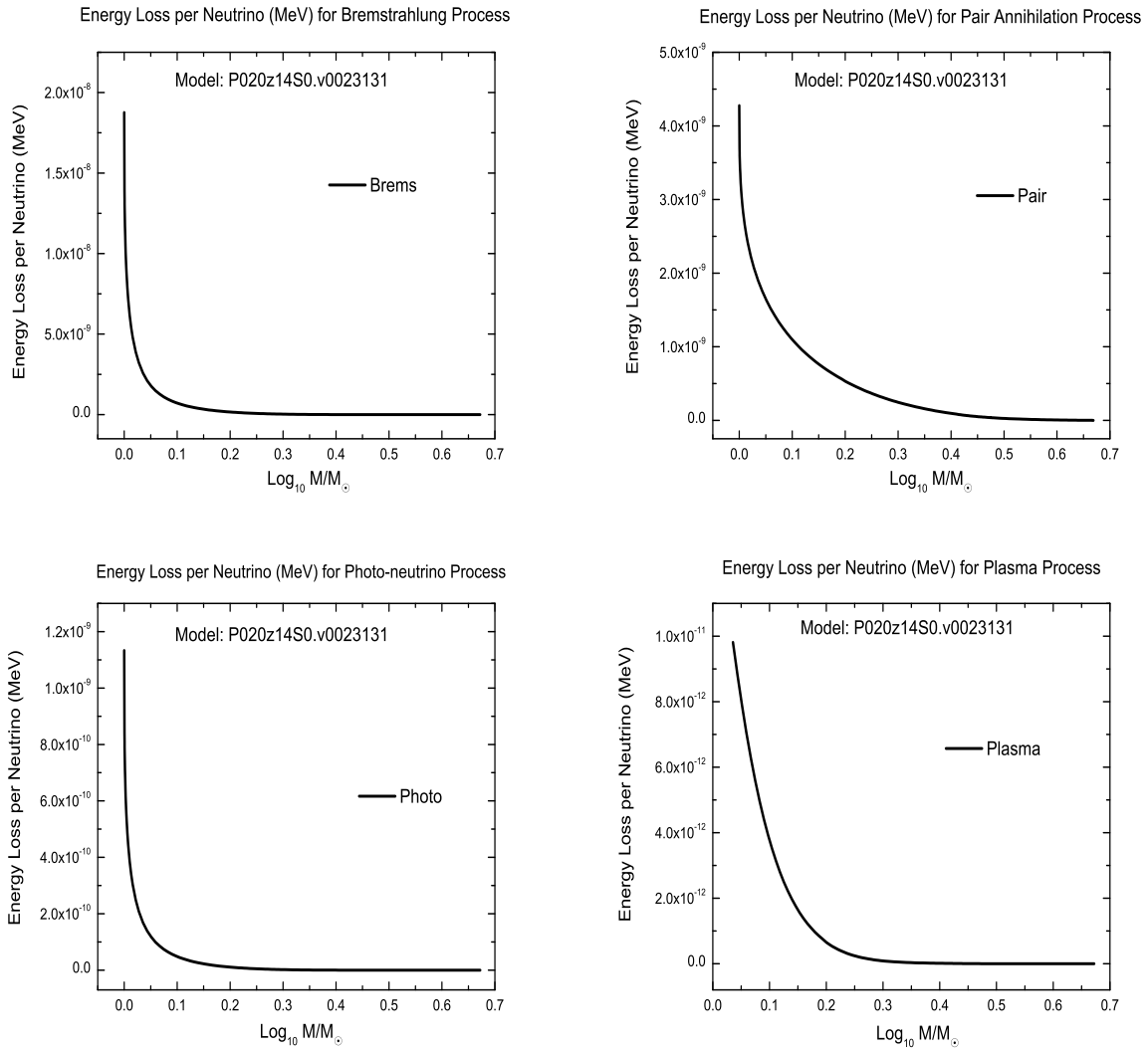

Figure 4.5: The graphs of energy loss per neutrino for bremsstrahlung, pair annihilation, photo-neutrino and plasma processes of non-rotating $20M_{\odot}$ model with $P_{\nu_e \to \nu_e} = 0.5$. Bremsstrahlung has the maximum value of energy loss per neutrino and plasma neutrino has the lowest energy loss per neutrino. The value of energy loss per neutrino for this survival probability is slightly higher than $P_{\nu_e \to \nu_e} = 0.0$.

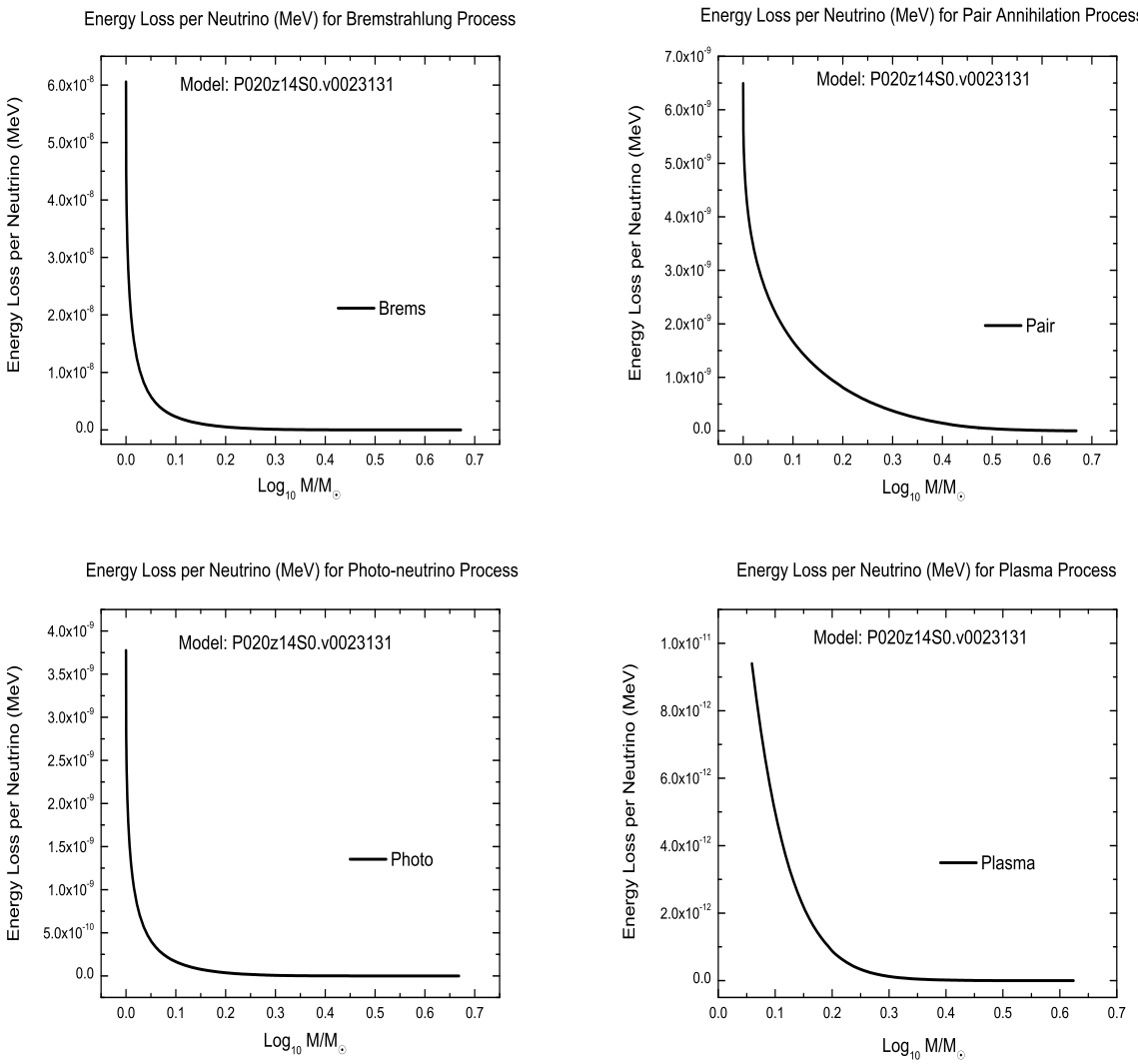

Figure 4.6: The graphs of energy loss per neutrino for bremsstrahlung, pair annihilation, photo-neutrino and plasma processes of non-rotating $20M_{\odot}$ model with $P_{\nu_e \to \nu_e} = 1.0$. Bremsstrahlung has the maximum value of energy loss per neutrino and plasma neutrino has the lowest energy loss per neutrino. The value of energy loss per neutrino for this survival probability is higher than $P_{\nu_e \to \nu_e} = 0.0$ and $P_{\nu_e \to \nu_e} = 0.5$.

10^{-10} MeV/cm^3/s. For $P_{\nu_e \to \nu_e} = 1.0$ in Fig. 4.9, the maximum total energy loss is 2.5×10^{11} MeV/cm^3/s and the lowest total energy loss is 2.25×10^3 MeV/cm^3/s. As we can see, the maximum total energy loss is from the bremsstrahlung process and the lowest total energy loss is from the plasma neutrino process for all cases. The total energy loss depends on $P_{\nu_e \to \nu_e}$. For $P_{\nu_e \to \nu_e} = 0.0$, the energy from the neutrinos will be used to convert all the electron neutrinos to another flavor and this will effect the total energy loss of the neutrinos. The $P_{\nu_e \to \nu_e} = 1.0$ has the highest value of the energy loss compared to the other two survival probabilities since in this probability, all of the electron neutrinos will remain as electron neutrinos and this allows all of the energy to be lost when interacting with the electrons in the star. This senario is equivalent to the case of the scattering of $\nu_e - e$ without oscillations. For $P_{\nu_e \to \nu_e} = 0.5$, part of the initial energy from the neutrinos will be converted into the creation of a massive neutrino and the rest will become the total energy loss of neutrinos through oscillations.

Rotating:

The effects of rotation on the evolution of massive stars have been discussed widely [69], [68]. In general, the rotation gives a significant impact on the evolution of a massive star through the changes in effective temperature, luminosity, chemical properties, etc. Due to the changes that occur in the stellar structure, the basic properties of one star will be altered and this will definitely change the whole evolution of a massive star. The rotation also induces mixing that eventually causes the enrichment at the convective core and also at the surface of the star and will finally alter the production of the neutrinos in the star. The energy loss per neutrino due to stellar rotation and also the total energy loss of neutrinos in massive stars will be discussed in this section. The neutrino energy loss per neutrino for each $P_{\nu_e \to \nu_e}$ is shown in Figs. 4.10-4.12.

In the Fig. 4.10, the energy loss per neutrino for the four thermal processes for $P_{\nu_e \to \nu_e} = 0.0$ is shown. Bremsstrahlung has the highest energy loss per neutrino

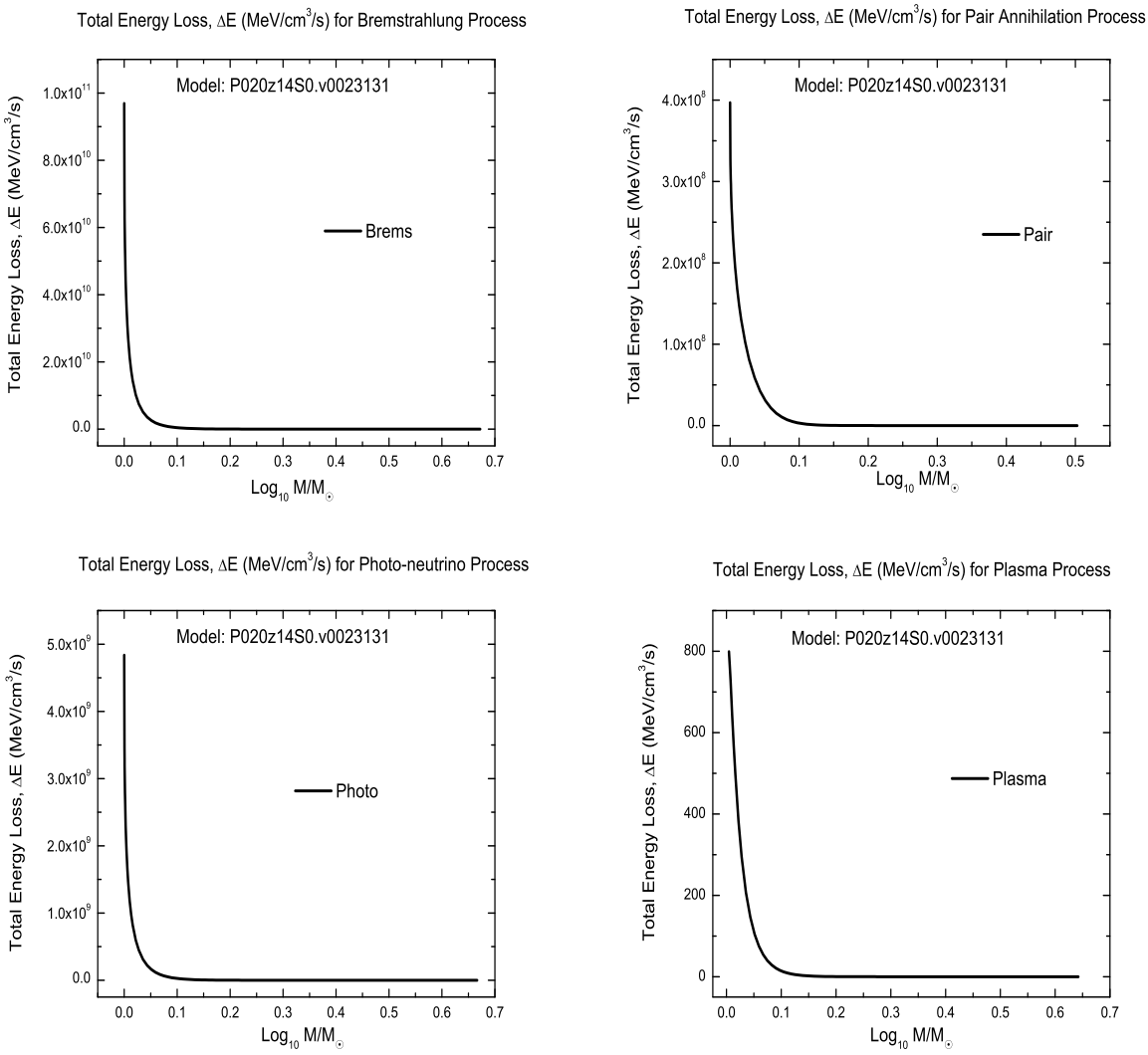

Figure 4.7: The graphs of total energy loss (MeV/cm^3/s) for bremsstrahlung, pair annihilation, photo-neutrino and plasma processes of non-rotating 20M$_\odot$ model with $P_{\nu_e \to \nu_e} = 0.0$.

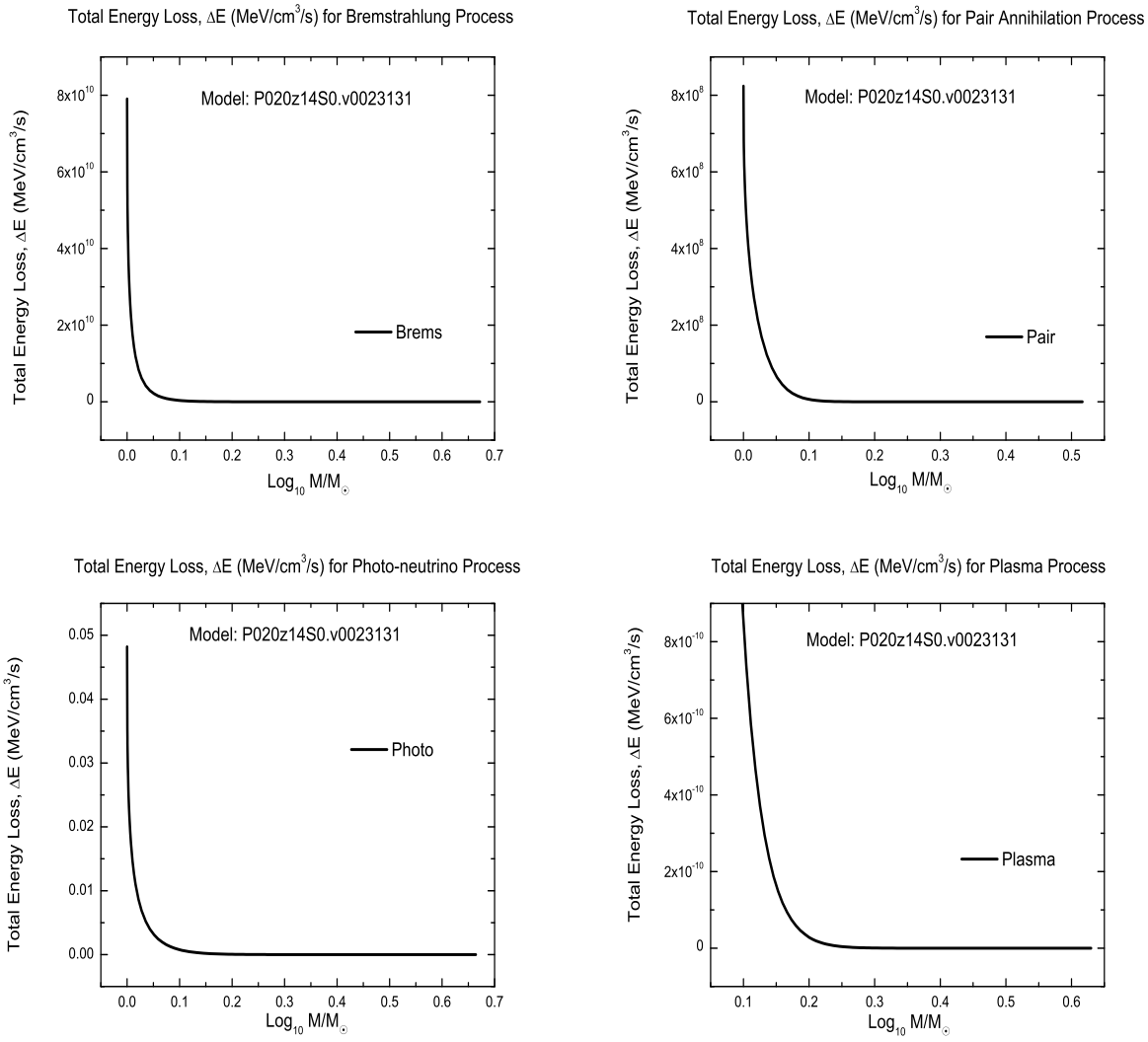

Figure 4.8: The graphs of total energy loss (MeV/cm^3/s) for bremsstrahlung, pair annihilation, photo-neutrino and plasma processes of non-rotating 20M$_\odot$ model with $P_{\nu_e \to \nu_e} = 0.5$.

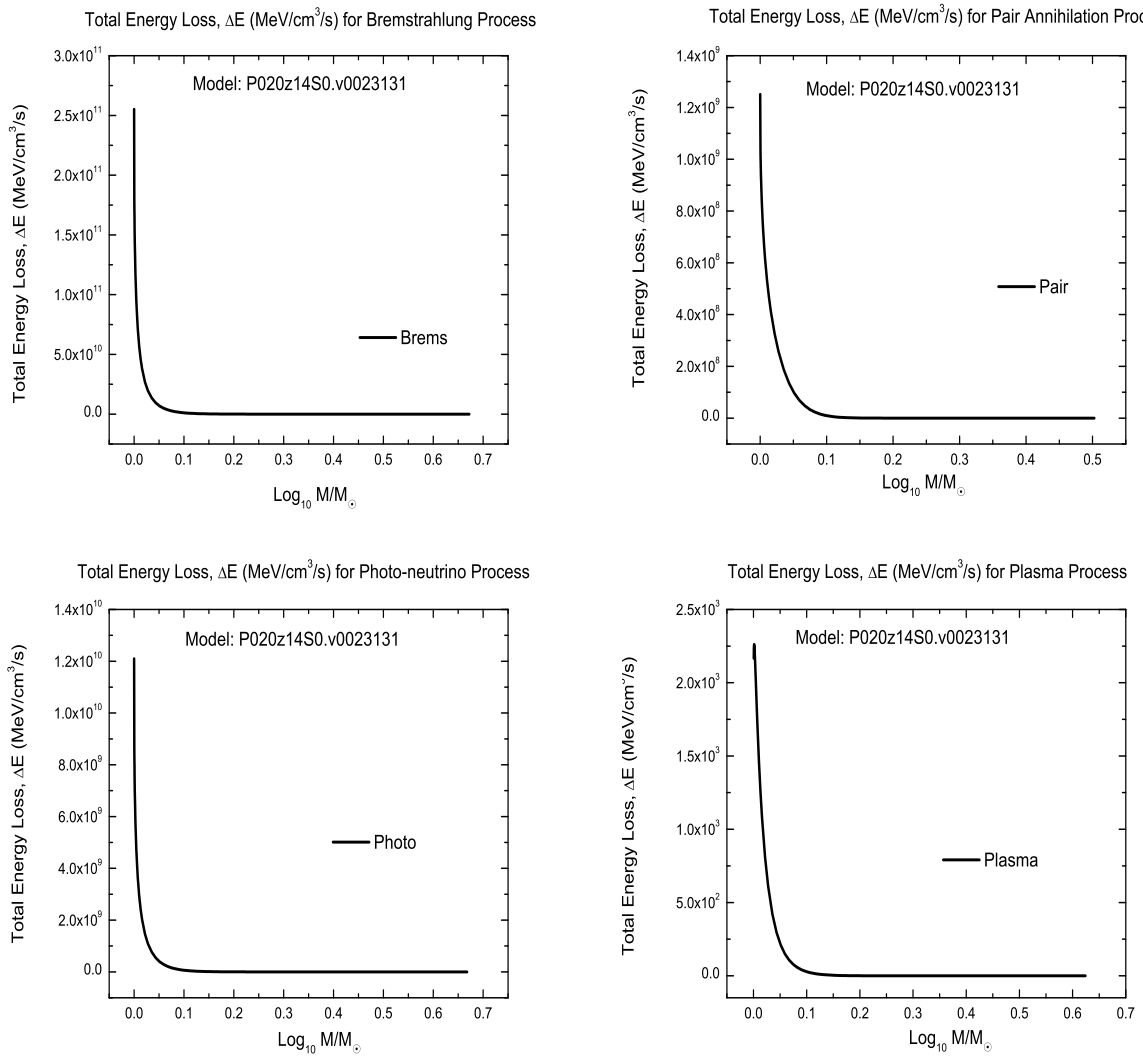

Figure 4.9: The graphs of total energy loss (MeV/cm^3/s) for bremsstrahlung, pair annihilation, photo-neutrino and plasma processes of non-rotating for 20M$_\odot$ model with $P_{\nu_e \to \nu_e} = 1.0$.

where the value is around 1.2×10^{-5} MeV and the lowest energy loss per neutrino belongs to plasma neutrino at 1.0×10^{-9} MeV. In Fig. 4.11 with $P_{\nu_e\to\nu_e} = 0.5$, the maximum energy loss per neutrino is 8.0×10^{-6} MeV and the lowest is 2.5×10^{-9} MeV. For $P_{\nu_e\to\nu_e} = 1.0$ in Fig. 4.12, the maximum value of energy loss per neutrino is 3.0×10^{-5} MeV and the lowest value is 3.5×10^{-9} MeV. The maximum energy loss per neutrino is from bremsstrahlung process and the lowest energy loss per neutrino comes from the plasma neutrinos. We can conclude that the energy loss per neutrino is higher in the rotating models than in the non-rotating models and the difference is of three orders of magnitude.

We now discuss the total energy loss of the neutrinos for the thermal processes. The total energy loss of the neutrinos for each $P_{\nu_e\to\nu_e}$ is shown in Figs. 4.13-4.15. For $P_{\nu_e\to\nu_e} = 0.0$, the total energy loss of the neutrinos from the bremsstrahlung process is 5.0×10^{16} MeV/cm^3/s and for plasma neutrinos has the lowest total energy loss of 2.0×10^{9} MeV/cm^3/s (Fig 4.13). The $P_{\nu_e\to\nu_e} = 0.5$ gives the maximum total energy loss of 3.5×10^{16}MeV/cm^3/s and the lowest value of 4.0×10^{9} MeV/cm^3/s (Fig 4.12). The maximum total energy loss for $P_{\nu_e\to\nu_e} = 1.0$ is 1.2×10^{17} MeV/cm^3/s and the lowest total energy loss is 7.0×10^{9} MeV/cm^3/s (Fig 4.13). For all of these three survival probabilities, the maximum total energy loss comes from the bremsstrahlung process and the lowest total energy loss goes to the plasma neutrinos. As we can see here, the value of the total energy loss is very high compared to the non-rotating models.

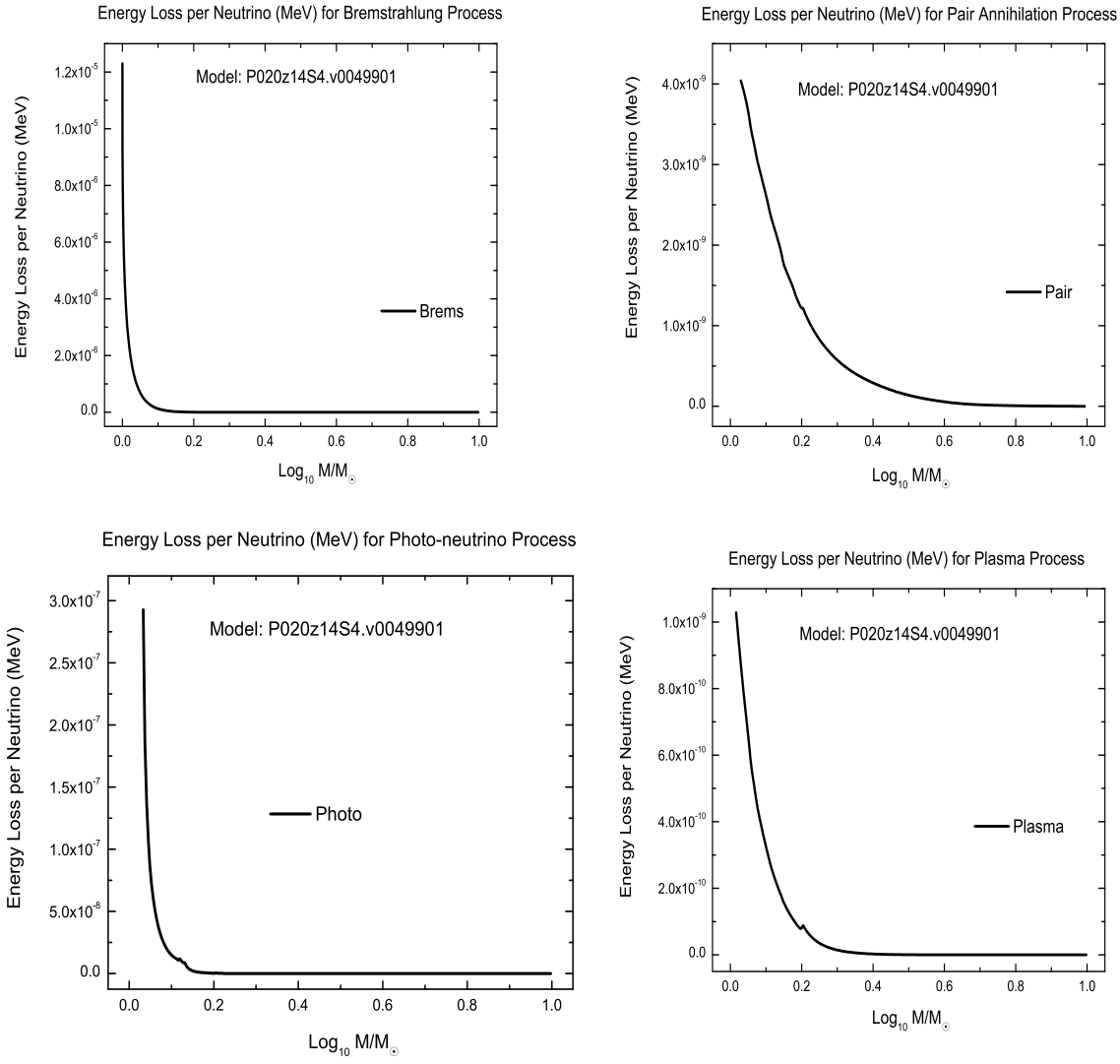

Figure 4.10: The graphs of energy loss per neutrino (MeV) for bremsstrahlung, pair annihilation, photo-neutrino and plasma processes of rotating of $20M_{\odot}$ model with $P_{\nu_e \to \nu_e} = 0.0$.

.

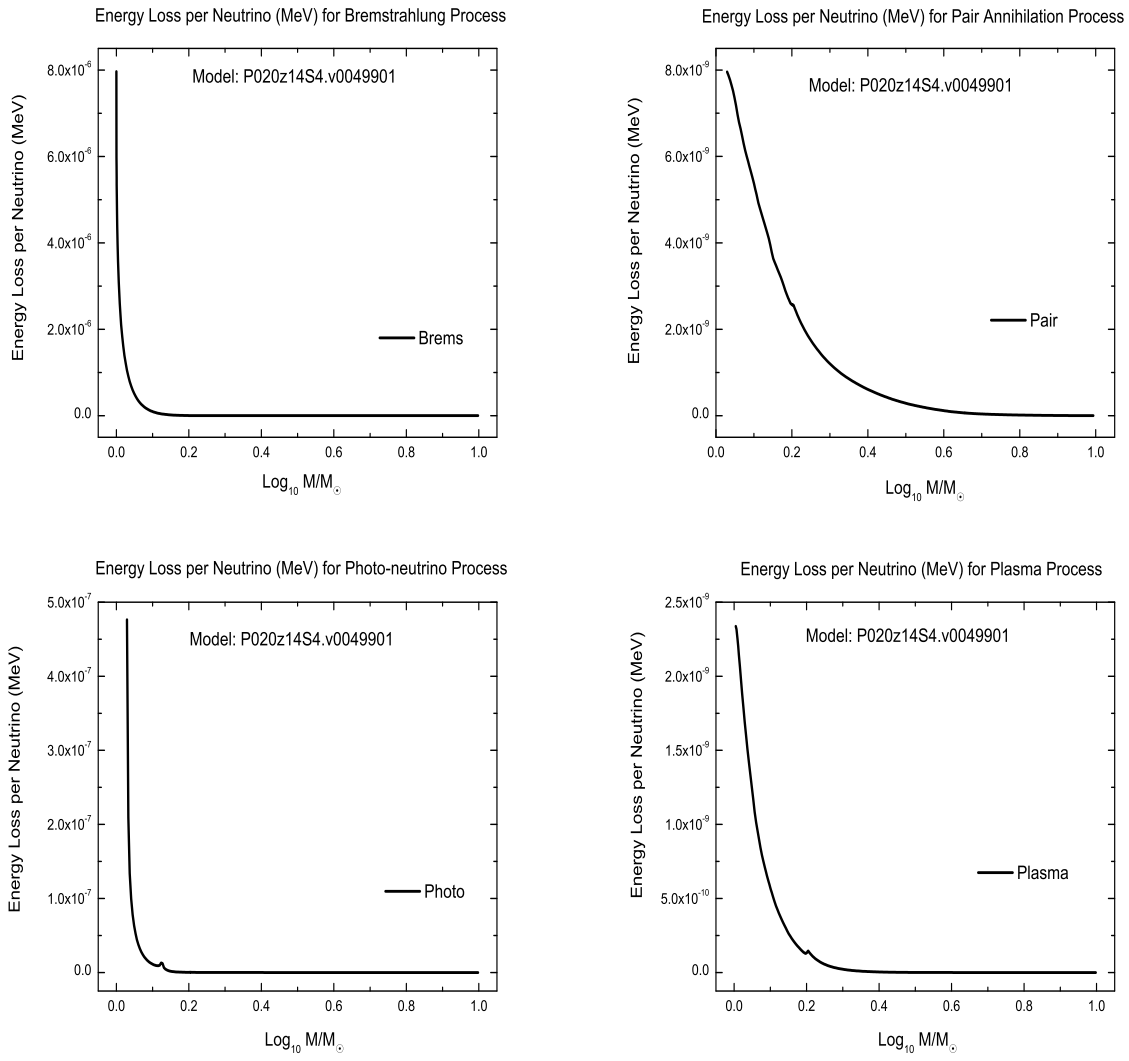

Figure 4.11: The graphs of energy loss per neutrino (MeV) for bremsstrahlung, pair annihilation, photo-neutrino and plasma processes of rotating of $20M_{\odot}$ models with $P_{\nu_e \to \nu_e} = 0.5$.

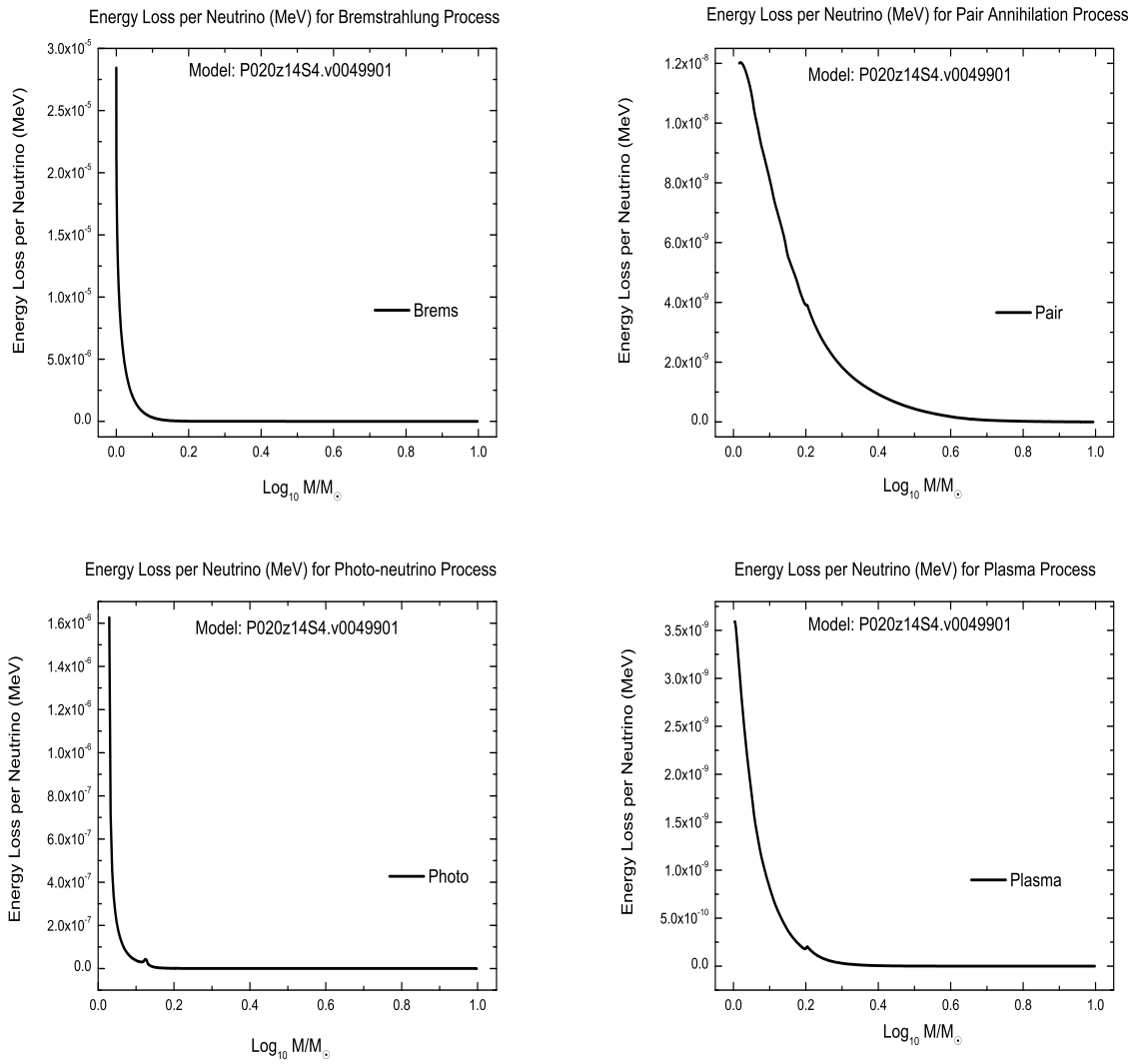

Figure 4.12: The graphs of energy loss per neutrino (MeV) for bremsstrahlung, pair annihilation, photo-neutrino and plasma processes of rotating of $20M_{\odot}$ model with $P_{\nu_e \to \nu_e} = 1.0$.

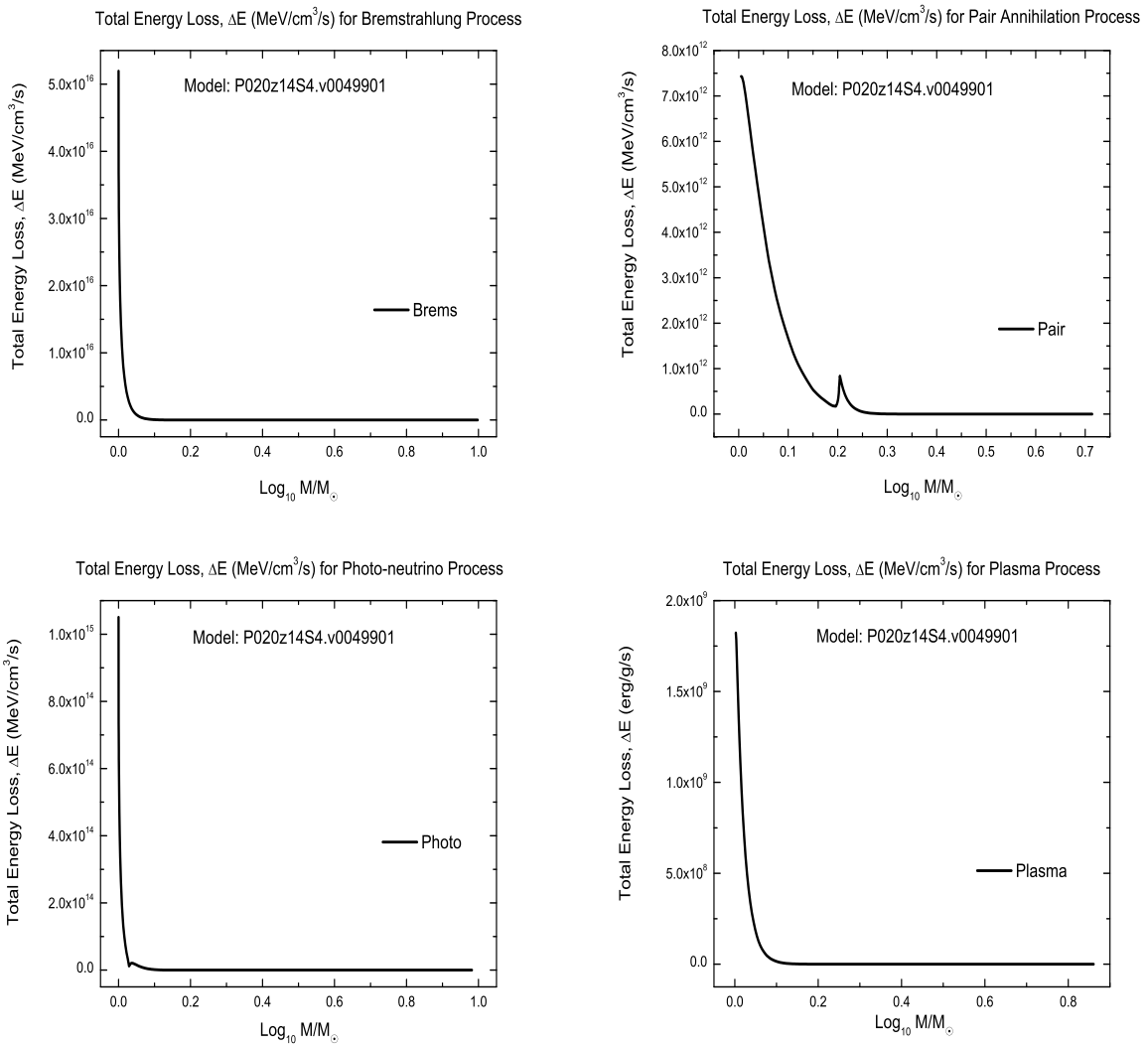

Figure 4.13: The graphs of total energy loss (MeV/cm^3/s) for bremsstrahlung, pair annihilation, photo-neutrino and plasma processes of rotating of 20M$_\odot$ models with $P_{\nu_e \to \nu_e} = 0.0$.

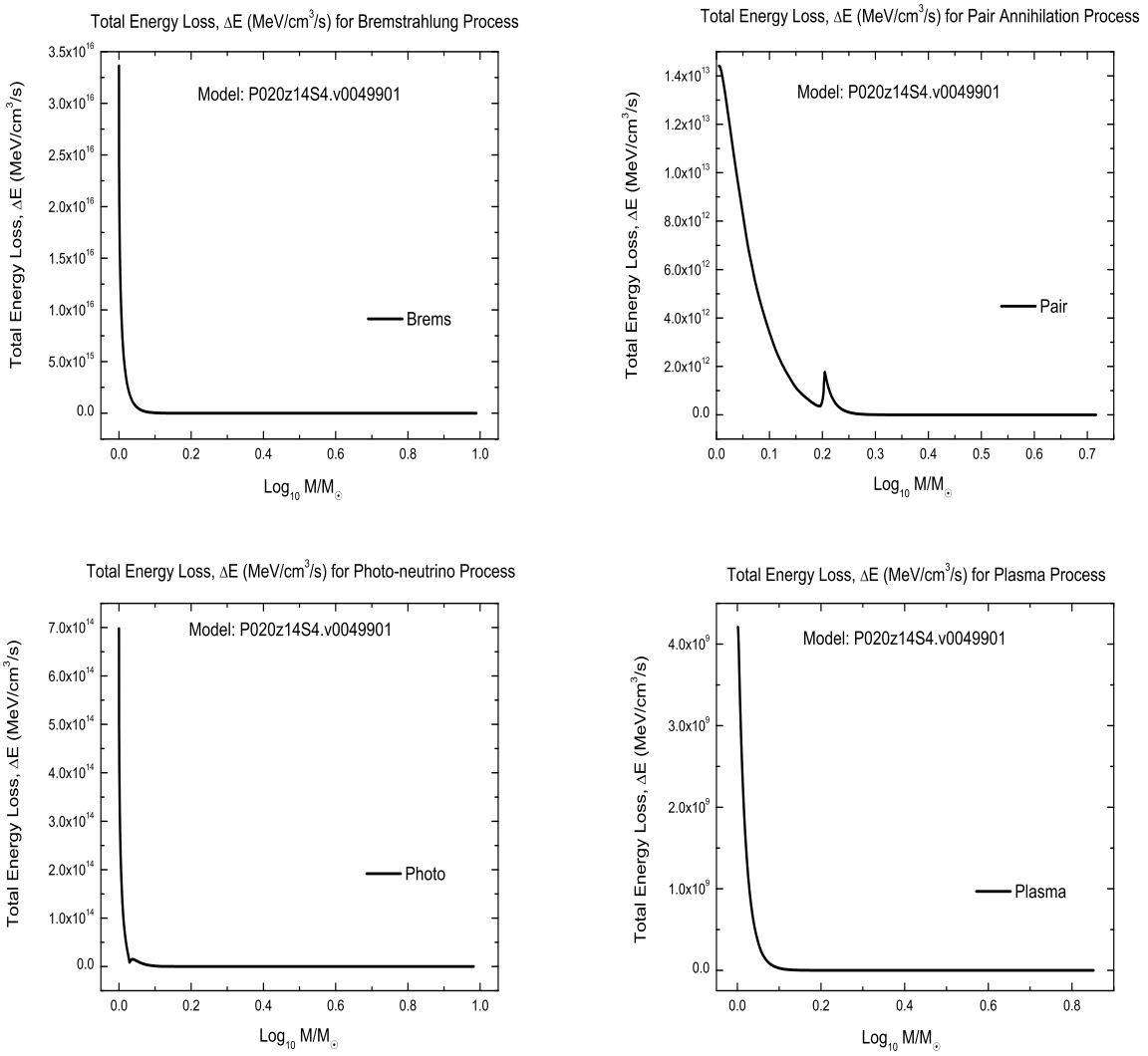

Figure 4.14: The graphs of total energy loss (MeV/cm^3/s) for bremsstrahlung, pair annihilation, photo-neutrino and plasma processes of rotating of 20M$_\odot$ models with $P_{\nu_e \to \nu_e} = 0.5$.

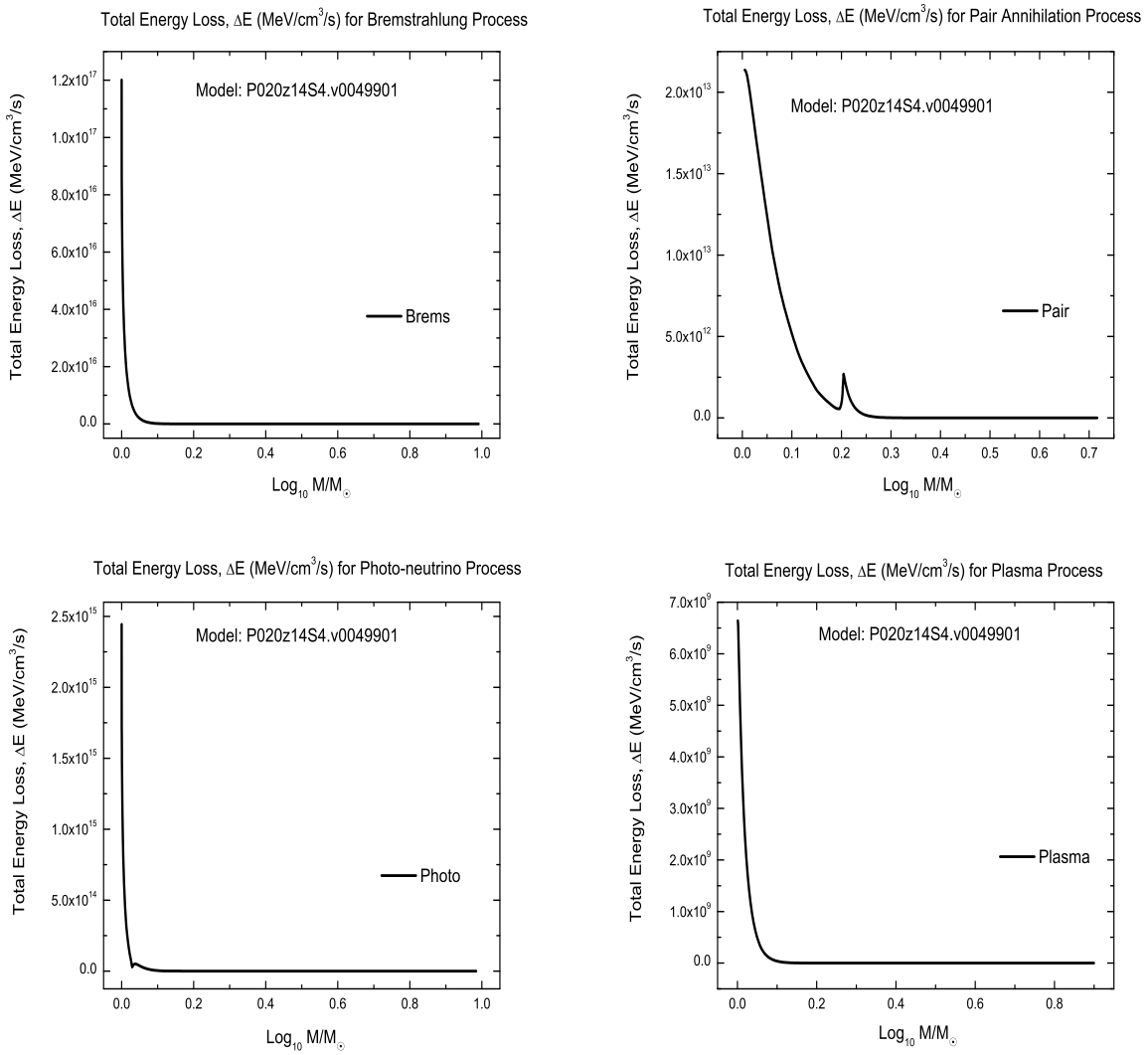

Figure 4.15: The graphs of total energy loss (MeV/cm^3/s) for bremsstrahlung, pair annihilation, photo-neutrino and plasma processes of rotating of 20M$_\odot$ models with $P_{\nu_e \to \nu_e} = 1.0$.

4.3.2 Energy Loss of Neutrinos in 120M$_\odot$ Model

The 120M$_\odot$ non-rotating and rotating models are examples of very massive stars that are used in our calculations. Energy loss per neutrino and the total energy loss of the neutrinos for both models will be discussed below.

Nonrotating:

The energy loss per neutrino for each $P_{\nu_e \to \nu_e}$ is shown in Figs 4.16-4.18. For non-rotating model of 120M$_\odot$ star, the maximum energy loss per neutrino for $P_{\nu_e \to \nu_e} = 0.0$ is 1.0×10^{-9}MeV/cm^3/s for the pair annihilation process and the minimum energy loss is 5.5×10^{-11}MeV/cm^3/s for the plasma neutrino process (see Fig 4.16). For $P_{\nu_e \to \nu_e} = 0.5$ the maximum energy loss per neutrino is 4.0×10^{-9}MeV/cm^3/s for the pair annihilation and the minimum energy loss per neutrino due to the photo-neutrino process (see Fig 4.17). With the $P_{\nu_e \to \nu_e} = 1.0$, the maximum energy loss per neutrino is due to the pair annihilation process with a value of 6.0×10^{-9}MeV/cm^3/s and for the lowest energy loss per neutrino is 1.0×10^{-11}MeV/cm^3/s that is due to the plasma neutrino process (Fig 4.18).

In this model, we can see that the pair annihilation is the major contributor to the energy loss per neutrino. This can be explained based on Fig. 4.2 (left panel) where the main process that has the highest energy loss through thermal process is pair annihilation. This shows that the dependence of energy loss per neutrino on the thermal process type.

The total energy loss for $P_{\nu_e \to \nu_e}$ shown in Fig.4.19 - 4.21. For $P_{\nu_e \to \nu_e} = 0.0$, the maximum total energy loss is due to the pair annihilation with the value of 3.0×10^{10}MeV/cm^3/s and the lowest total energy loss of the neutrinos for plasma neutrino process is 450MeV/cm^3/s only (Fig 4.19). The maximum total energy loss of neutrinos for $P_{\nu_e \to \nu_e} = 0.5$ is 6.0×10^{10}MeV/cm^3/s from the pair annihilation process. The minimum total energy loss of neutrinos has value of 700MeV/cm^3/s for the plasma neutrino process (Fig 4.20). Bremsstrahlung process becomes the major

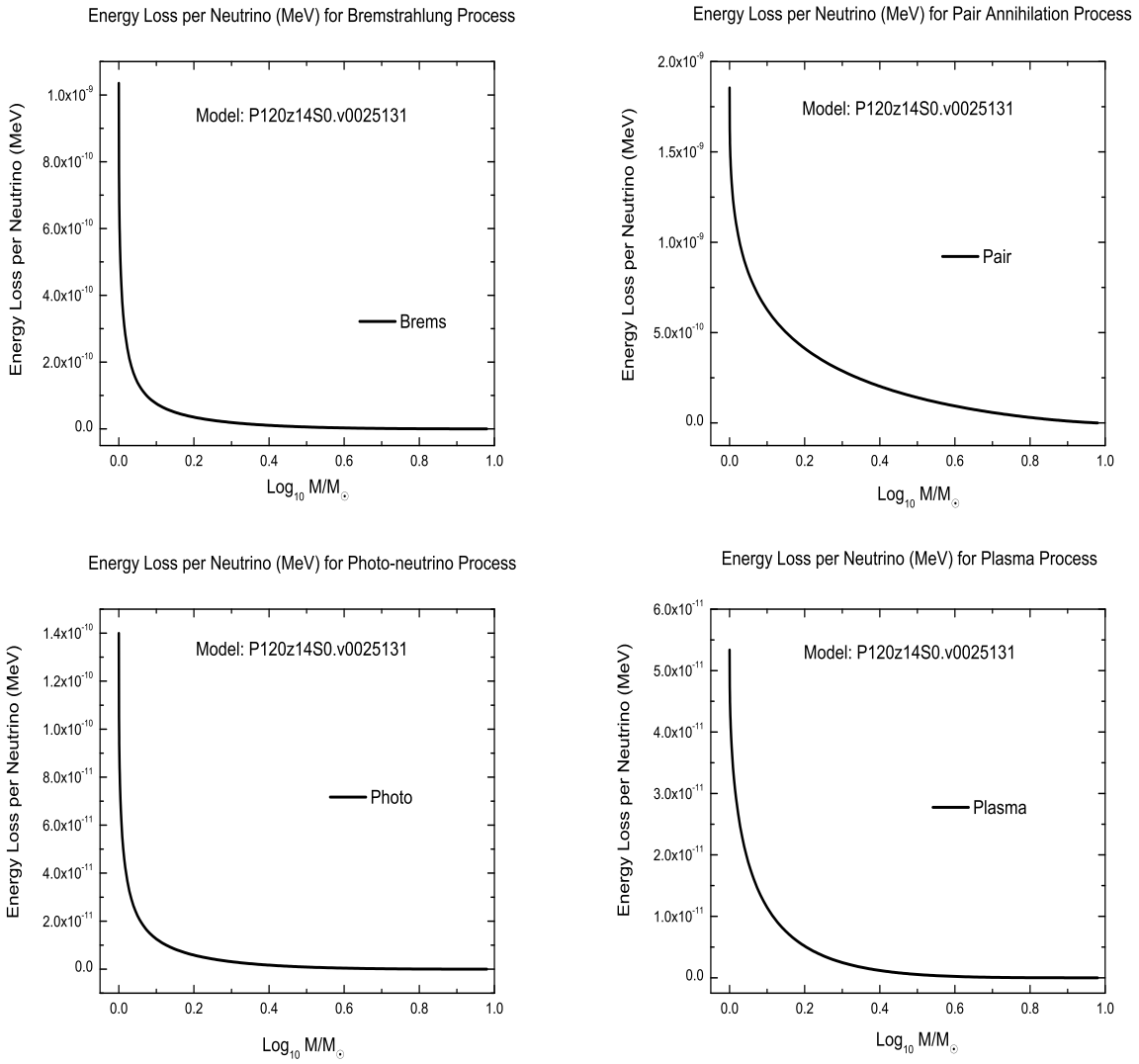

Figure 4.16: The graphs of energy loss per neutrino for bremsstrahlung, pair annihilation, photo-neutrino and plasma processes of non-rotating of $120M_{\odot}$ models with $P_{\nu_e \to \nu_e} = 0.0$.

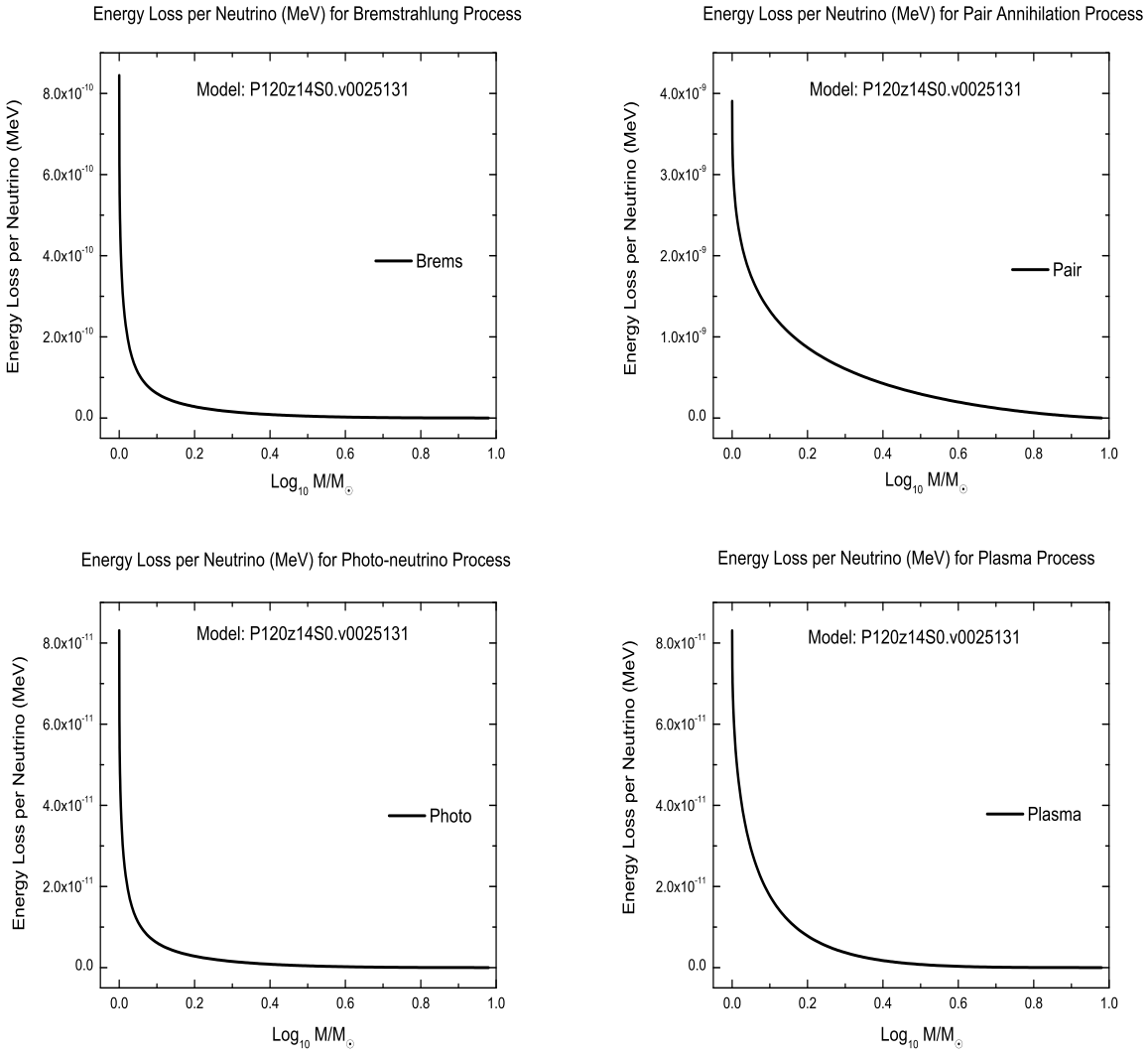

Figure 4.17: The graphs of energy loss per neutrino for bremsstrahlung, pair annihilation, photo-neutrino and plasma processes of non-rotating of $120M_{\odot}$ models with $P_{\nu_e \to \nu_e} = 0.5$.

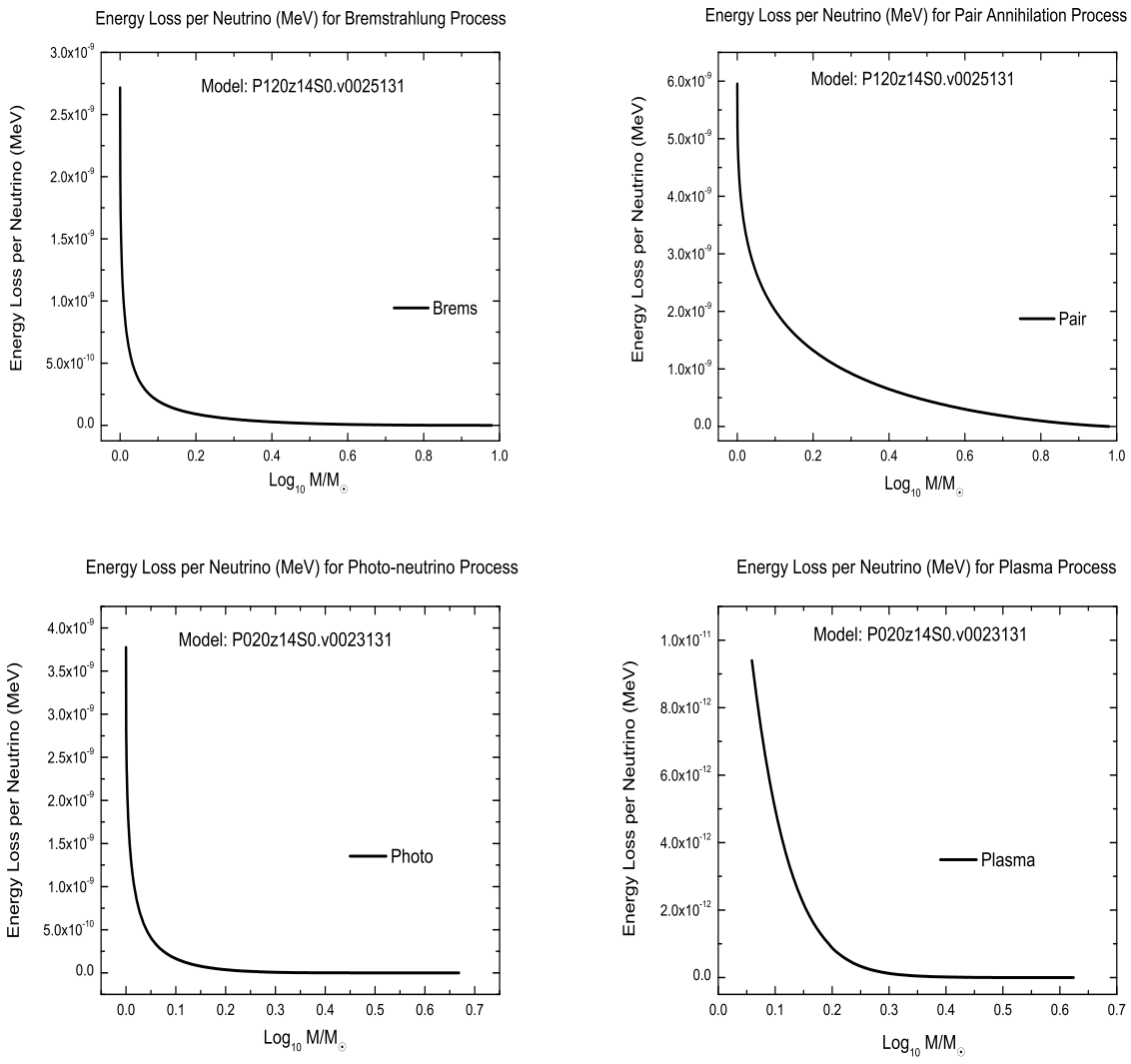

Figure 4.18: The graphs of energy loss per neutrino for bremsstrahlung, pair annihilation, photo-neutrino and plasma processes of non-rotating of $120M_{\odot}$ models with $P_{\nu_e \to \nu_e} = 1.0$.

contributor for the total energy loss of the neutrinos for $P_{\nu_e \to \nu_e} = 1.0$ with a value of $7.5 \times 10^9 \mathrm{MeV/cm^3/s}$ and plasma neutrino has the lowest total energy loss of the neutrinos of $1000 \mathrm{MeV/cm^3/s}$ (Fig 4.21).

For total energy loss of neutrinos, the maximum value of energy loss varies, for $P_{\nu_e \to \nu_e} = 0.0$ and $P_{\nu_e \to \nu_e} = 0.5$ pair annihilation becomes the biggest contributor and for $P_{\nu_e \to \nu_e} = 1.0$, the Bremsstrahlung becomes the major one.

Rotating:

In the last part of this chapter, we will see the effect of $P_{\nu_e \to \nu_e}$ on the energy loss per neutrino and also the total energy loss of neutrinos for the $120 \mathrm{M}_\odot$ rotating star. The energy loss per neutrino for each $P_{\nu_e \to \nu_e}$ is shown in Figs 4.22 - 4.24. We begin our discussion with the $P_{\nu_e \to \nu_e} = 0.0$ in Fig. 4.22. The maximum energy loss per neutrino has a value of $2.00 \times 10^{-9} \mathrm{MeV}$ that comes from the pair annihilation process and the minimum energy loss of neutrino is from the plasma neutrino process with value of $5.00 \times 10^{-11} \mathrm{MeV}$. For $P_{\nu_e \to \nu_e} = 0.5$, the maximum energy loss per neutrino comes from the photo-neutrino process with $5.00 \times 10^{-7} \mathrm{MeV}$ and the minimum is from the bremsstrahlung process with $2.00 \times 10^{-19} \mathrm{MeV}$ (Fig 4.23). The maximum energy loss per neutrino for $P_{\nu_e \to \nu_e} = 1.0$ is from the pair annihilation and the minimum energy loss per neutrino comes from the photo-neutrino with $6.00 \times 10^{-10} \mathrm{MeV}$ (Fig 4.24).

This paragraph describes the total energy loss of the neutrinos from the $120 \mathrm{M}_\odot$ rotating model. The total energy loss for each $P_{\nu_e \to \nu_e}$ is shown in Figs 4.25 - 4.27. The maximum total energy loss comes from the pair annihilation process for $P_{\nu_e \to \nu_e} = 0.0$ to $P_{\nu_e \to \nu_e} = 1.0$. For $P_{\nu_e \to \nu_e} = 0.0$, the maximum total energy loss is $1.4 \times 10^{10} \mathrm{MeV/cm^3/s}$ (Fig 4.25), for $P_{\nu_e \to \nu_e} = 0.5$ the value is $3.0 \times 10^{10} \mathrm{MeV/cm^3/s}$ (Fig 4.26) and for $P_{\nu_e \to \nu_e} = 1.0$, $4.0 \times 10^{10} \mathrm{MeV/cm^3/s}$ (Fig 4.27). The minimum value of total energy loss for all survival probabilities comes from the plasma neutrino process. For $P_{\nu_e \to \nu_e} = 0.0$, the minimum energy loss is $1.0 \times 10^3 \mathrm{MeV/cm^3/s}$, for $P_{\nu_e \to \nu_e} = 0.5$, $1.5 \times 10^3 \mathrm{MeV/cm^3/s}$ and for $P_{\nu_e \to \nu_e} = 1.0$ is $2.0 \times 10^3 \mathrm{MeV/cm^3/s}$.

We can conclude that for the 120$M_\odot$ rotating star, the maximum total energy loss comes from the pair annihilation process where it is the major contributor to the energy loss of neutrinos through oscillations.

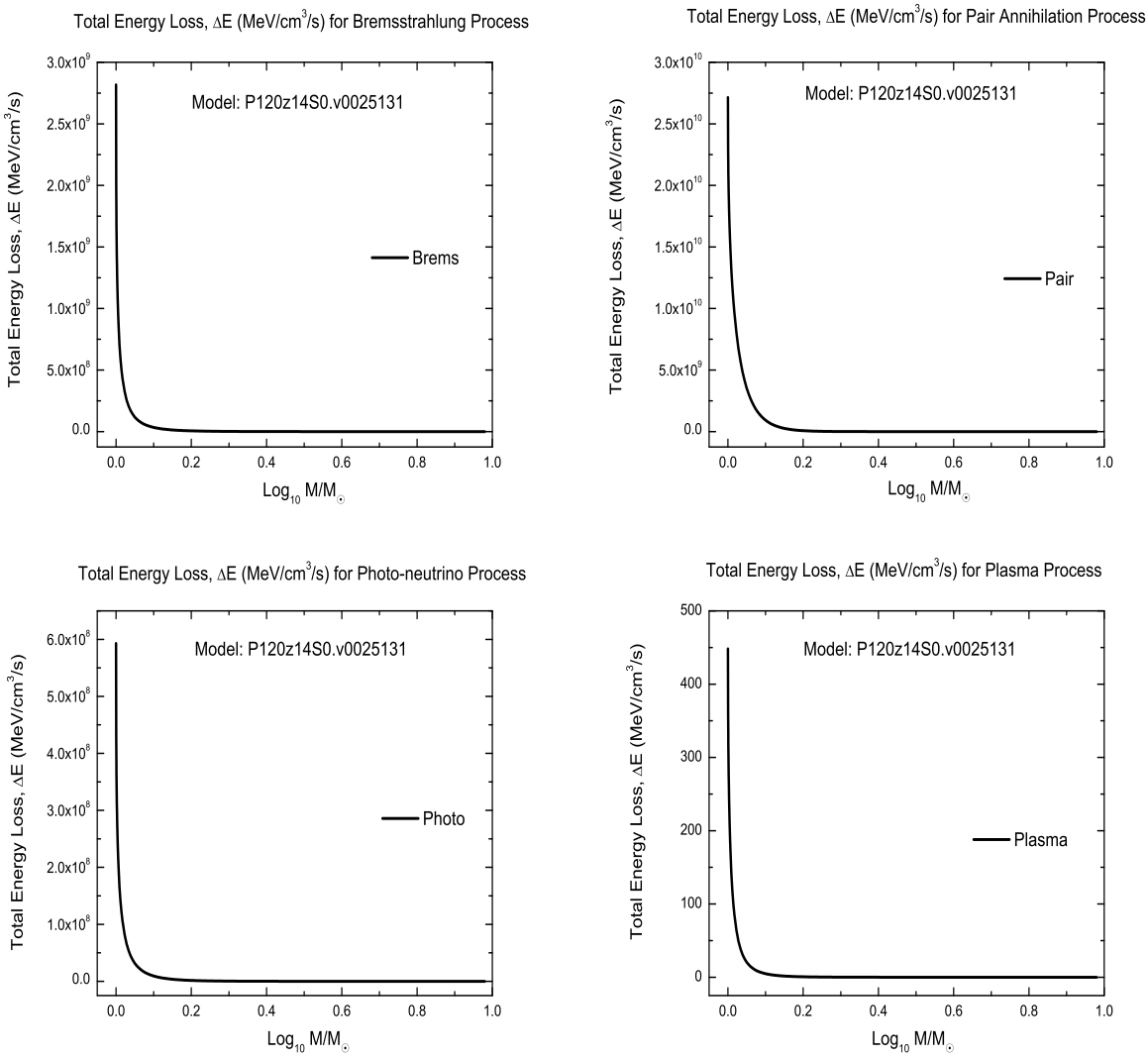

Figure 4.19: The graphs of total energy loss (MeV/cm^3/s) for bremsstrahlung, pair annihilation, photo-neutrino and plasma processes of non-rotating of 120$M_\odot$ models with $P_{\nu_e \to \nu_e} = 0.0$.

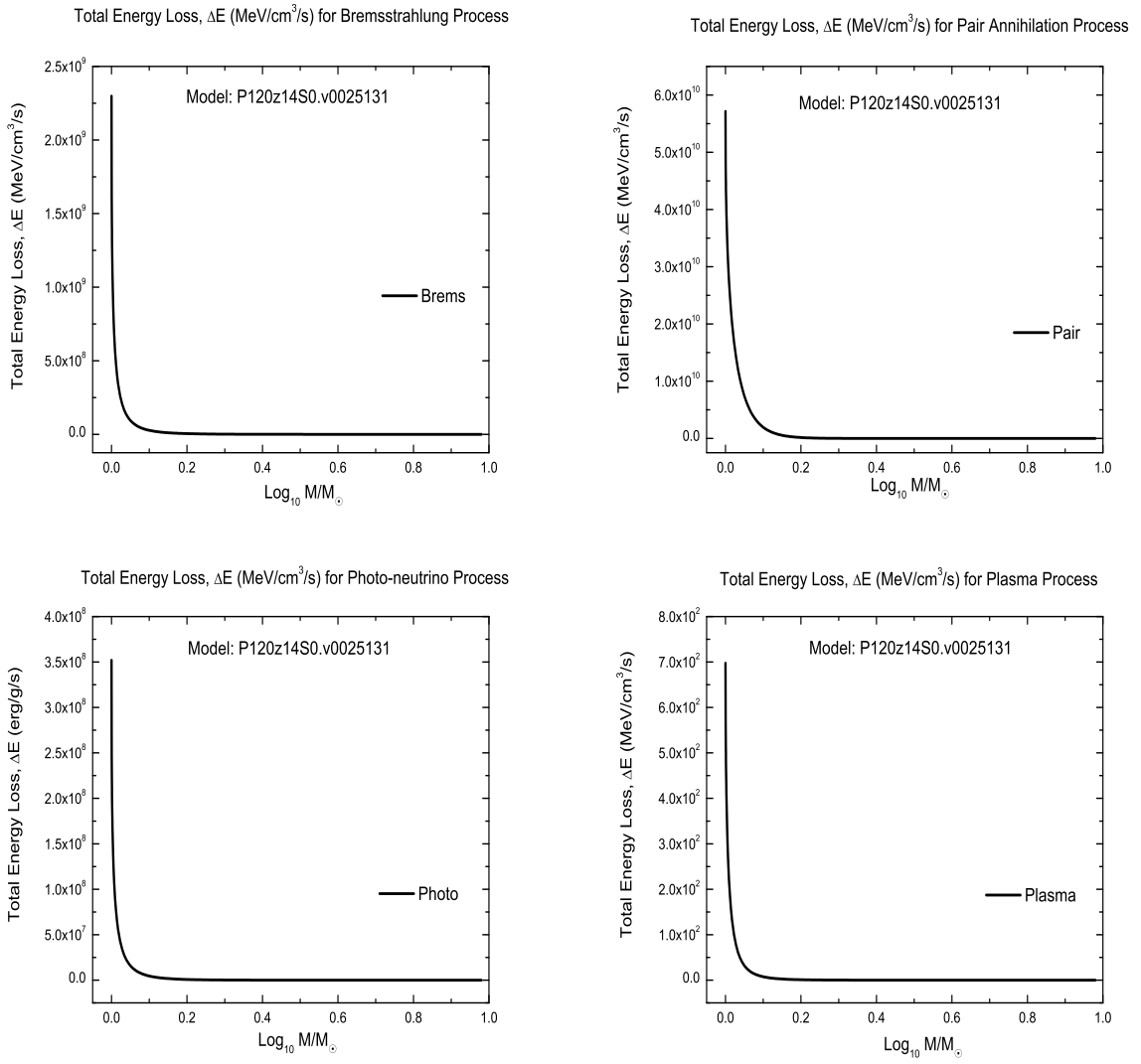

Figure 4.20: The graphs of total energy loss (MeV/cm^3/s) for bremsstrahlung, pair annihilation, photo-neutrino and plasma processes of non-rotating of 120M$_\odot$ models with $P_{\nu_e \to \nu_e} = 0.5$.

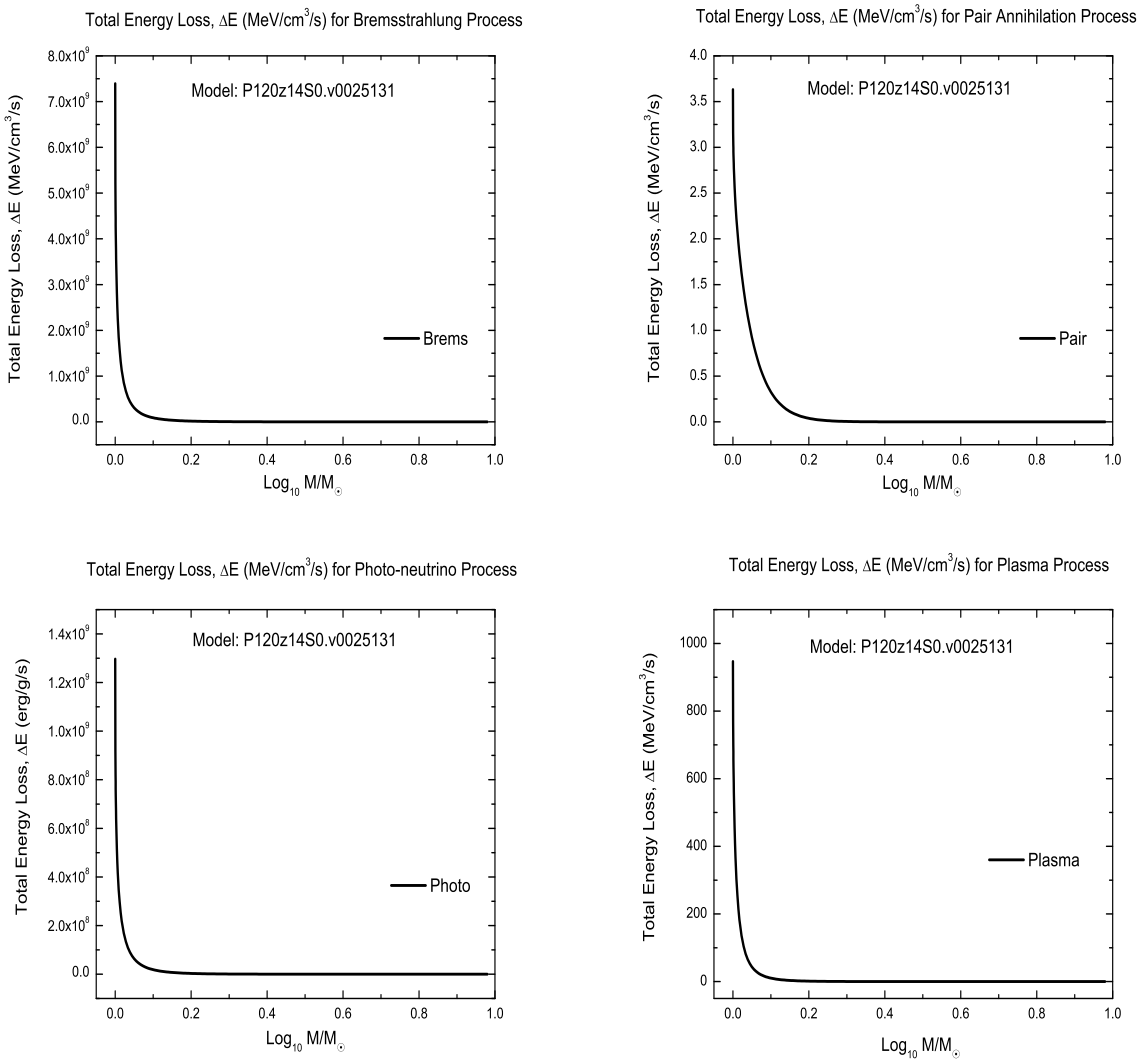

Figure 4.21: The graphs of total energy loss (MeV/cm^3/s) for bremsstrahlung, pair annihilation, photo-neutrino and plasma processes of non-rotating of 120M$_\odot$ models with $P_{\nu_e \to \nu_e} = 1.0$.

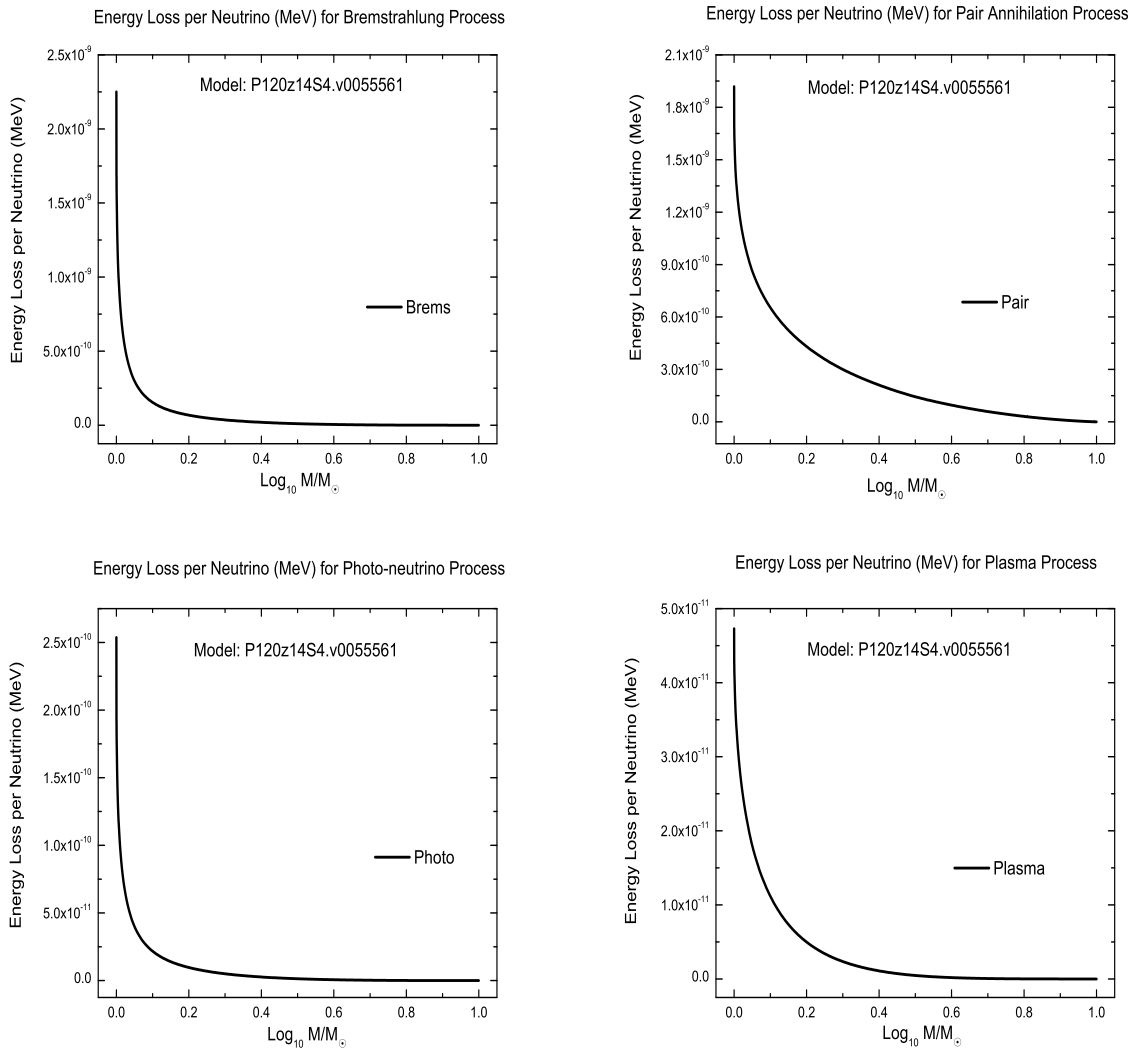

Figure 4.22: The graphs of total energy loss (MeV/cm^3/s) for bremsstrahlung, pair annihilation, photo-neutrino and plasma processes of rotating of 120M$_\odot$ models with $P_{\nu_e \to \nu_e} = 0.0$.

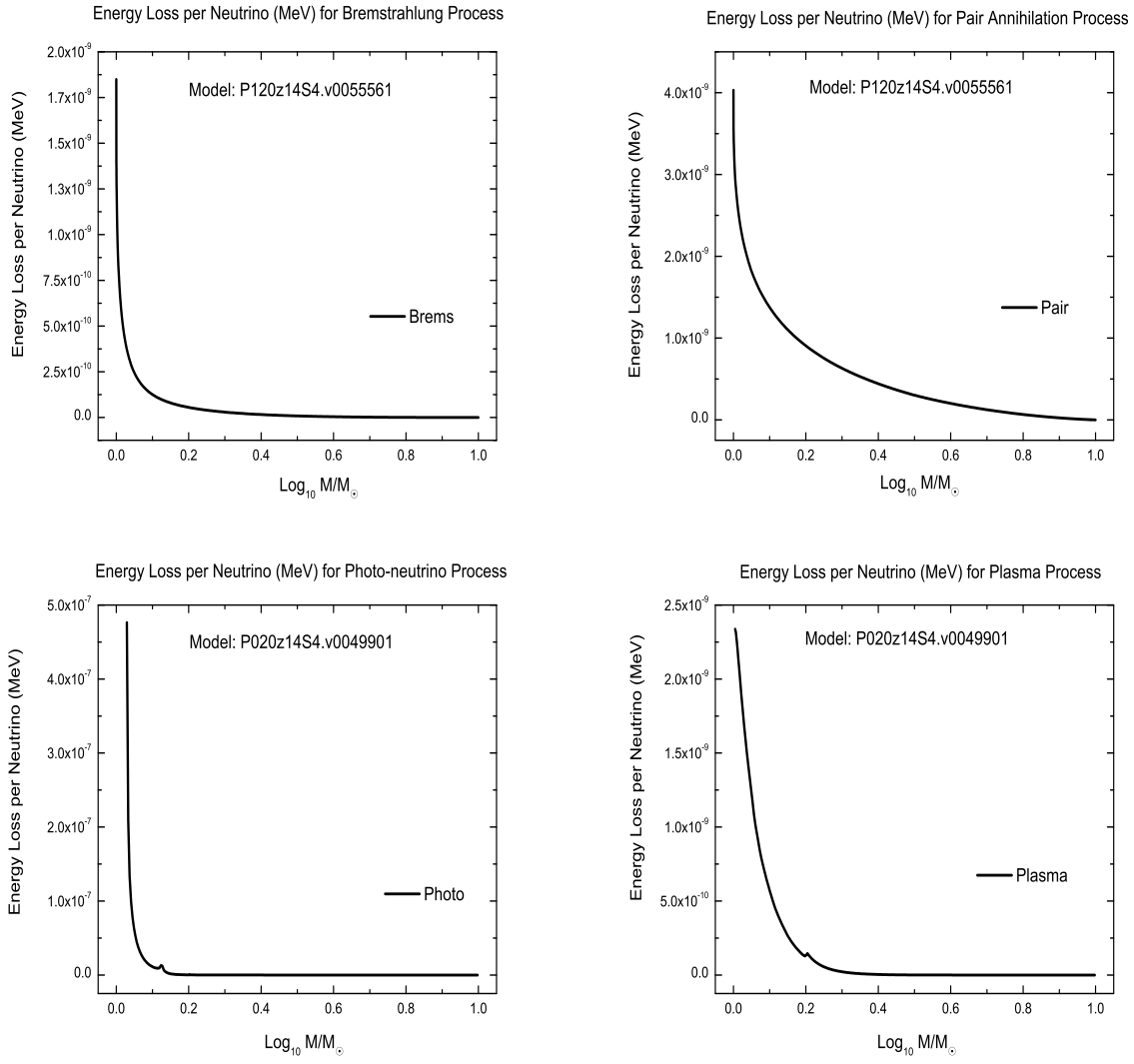

Figure 4.23: The graphs of total energy loss (MeV/cm^3/s) for bremsstrahlung, pair annihilation, photo-neutrino and plasma processes of rotating of 120M$_\odot$ models with $P_{\nu_e \to \nu_e} = 0.5$.

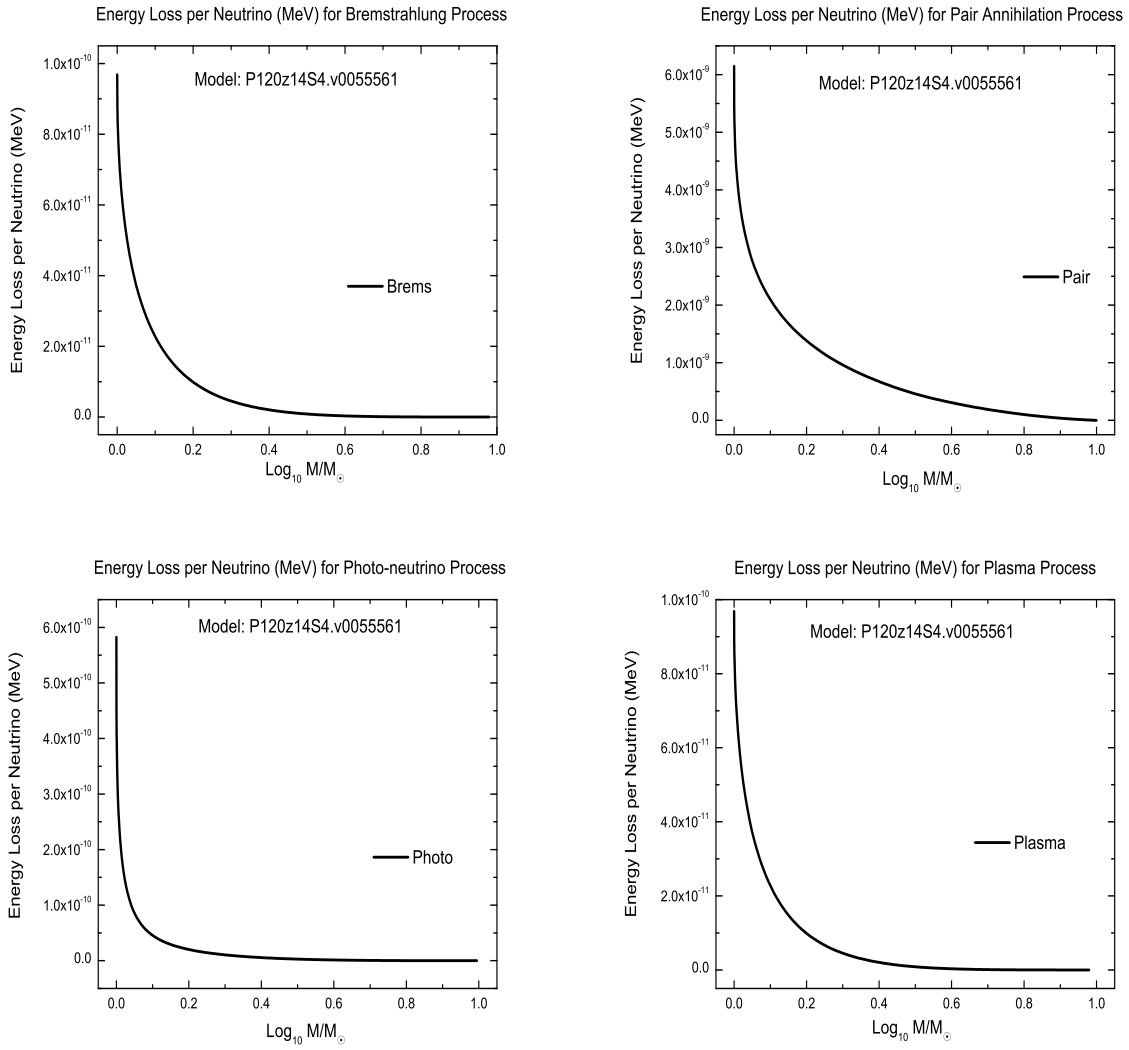

Figure 4.24: The graphs of total energy loss (MeV/cm^3/s) for bremsstrahlung, pair annihilation, photo-neutrino and plasma processes of rotating of $120M_\odot$ models with $P_{\nu_e \to \nu_e} = 1.0$.

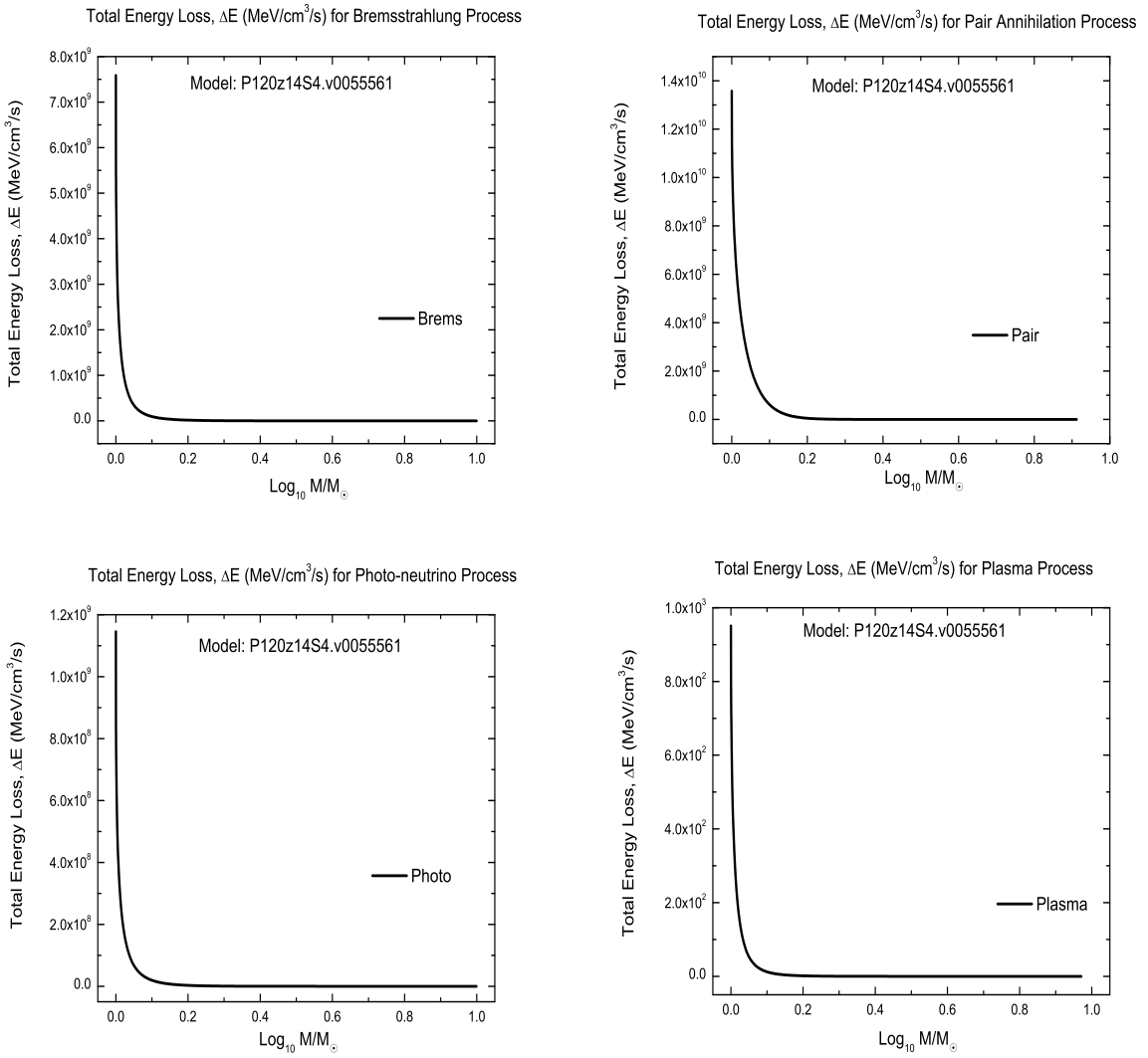

Figure 4.25: The graphs of total energy loss (MeV/cm^3/s) for bremsstrahlung, pair annihilation, p hoto-neutrino and plasma processes of rotating of $120M_{\odot}$ models with $P_{\nu_e \to \nu_e} = 0.0$.

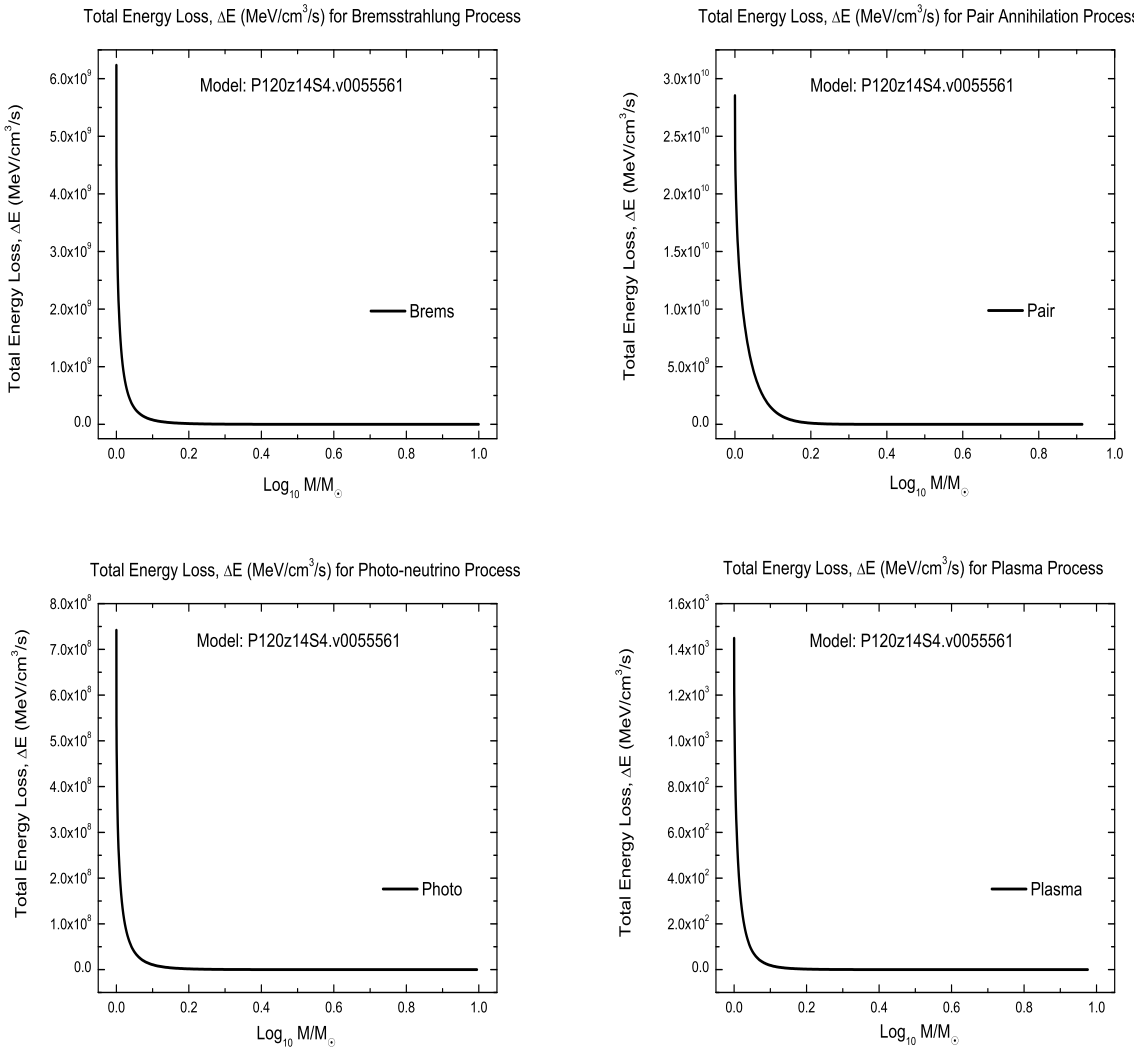

Figure 4.26: The graphs of total energy loss (MeV/cm^3/s) for bremsstrahlung, pair annihilation, photo-neutrino and plasma processes of rotating of $120M_\odot$ models with $P_{\nu_e \to \nu_e} = 0.5$.

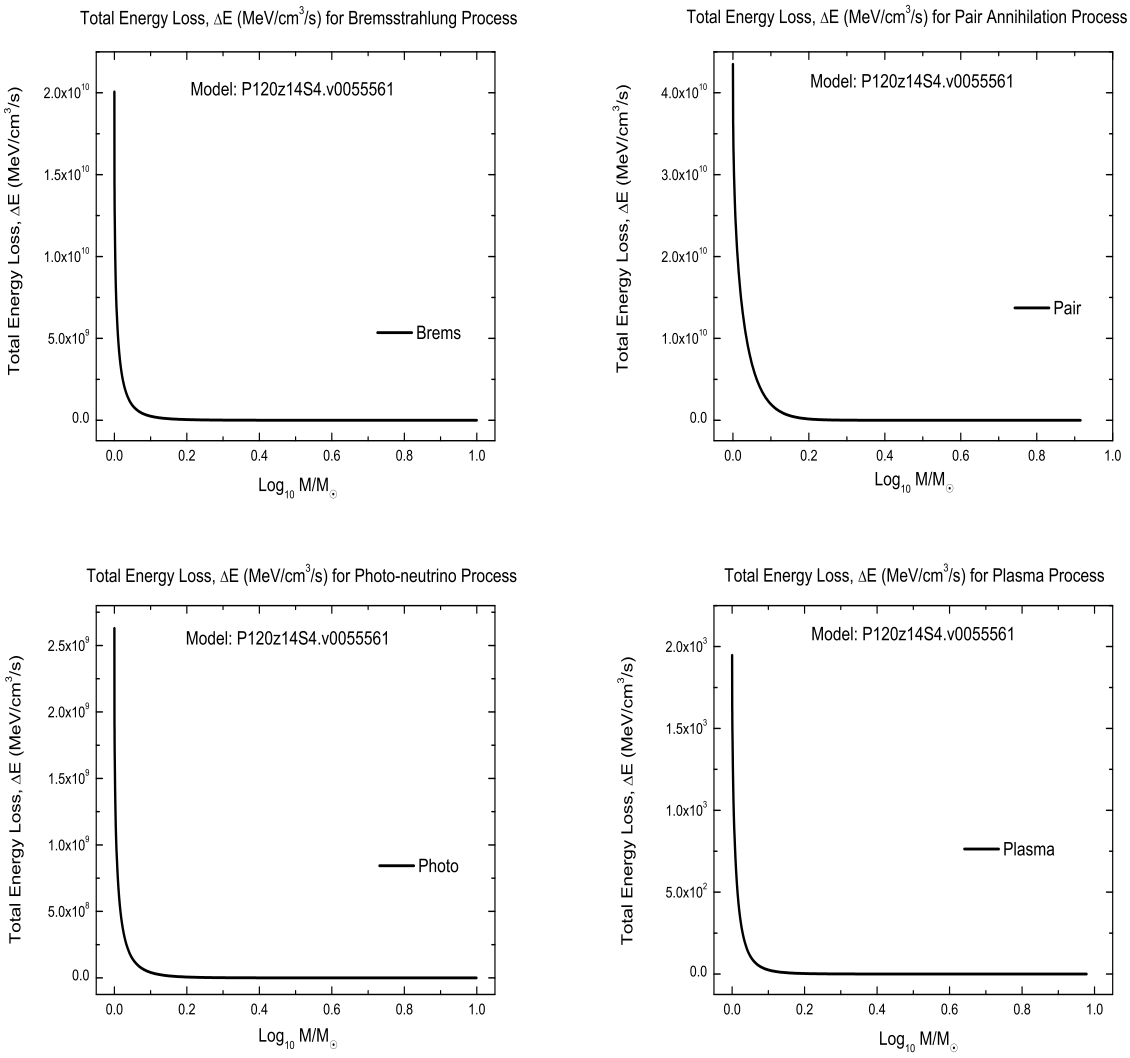

Figure 4.27: The graphs of total energy loss (MeV/cm^3/s) for bremsstrahlung, pair annihilation, photo-neutrino and plasma processes of rotating of $120M_{\odot}$ models with $P_{\nu_e \to \nu_e} = 1.0$.

Chapter 5

Conclusions

In this work we have investigated the effects of neutrino oscillations on the neutrino energy loss ΔE_ν of two stellar models namely a $20M_\odot$ and a $120M_\odot$ massive star. The values of ΔE_ν are dependent on ρ and n_e . For a model with large n_e, ΔE_ν will be higher since the stopping power equation of matter for neutrinos is proportional to n_e. Besides the dependence on n_e, ΔE_ν will be affected by $P_{\nu_e \to \nu_e}$. We have selected in this work representative values of the neutrino survival probability, at 0.0, 0.5 and 1.0. For lower values of $P_{\nu_e \to \nu_e}$, ΔE_ν is lower. For high values of $P_{\nu_e \to \nu_e}$, the value of ΔE_ν is higher. For $P_{\nu_e \to \nu_e} = 1.0$, the ν_e will remain as ν_e and will give the highest value of ΔE_ν for a particular value of initial energy of the neutrinos. For $P_{\nu_e \to \nu_e}$ less than one, this is means that the ν_e can oscillate into another flavor (i.e ν_μ or ν_τ) depending on the initial energy of the neutrinos. Tables 5.1 and 5.2 summarise the energy loss for the stellar models. A neutrino can oscillate into another flavor (massive neutrinos) if it has enough energy to transform from one flavor to another. For $P_{\nu_e \to \nu_e} = 0.0$, all neutrinos will oscillate into another flavor (i.e ν_μ or ν_τ). Comparison with the neutrino energy loss without oscillation from the stellar models yield a difference of at most $\sim 1\%$. This means the oscillation effect is not significant to the neutrino cooling process.

For stellar matter with high density, the value of ΔE_ν can be higher due to the high value of n_e. For further work, a new calculation of total energy loss of neutrinos in the star can be made that include both thermal neutrino and effects of oscillations. Since neutrinos are produced copiously in the star, we can determine the total flux of the neutrinos. Then, we can integrate the stopping power equation of matter for neutrino with the total flux of neutrinos in the star with respect to the radius of the

star.

Bear in mind that we have not consider oscillation resonance regions in the stellar models. Due to the various mass shells dominated by certain elements the survival probability would necessary change along the neutrino passage from the center of the star to the surface.

This work can also be extended to very massive stars for example R136a [29] and supernovae. Other than that, we can try to include the value of ΔE_ν to the evolution code and see the effect of ΔE_ν to the evolution as a whole.

A precise determination of neutrino emission rates is therefore a crucial issue in any study of stellar evolutionary tracks. Changes during the cooling rates at the very last stages of a massive star evolution may sensibly affect the evolutionary time scale and the iron core configuration at the onset of the supernova explosion, whose triggering mechanism is still lacking a full theoretical understanding.

Table 5.1: The energy loss per neutrino (MeV) for non-rotating and rotating model of $20M_\odot$ and $120M_\odot$ stars

		Lowest			Highest		
		Process	$P_{\nu_e \to \nu_e}$	ΔE_ν	Process	$P_{\nu_e \to \nu_e}$	ΔE_ν
Non-rotating	$20M_\odot$	Plasma	0.0	7.5×10^{-12}	Brems	1.0	6.0×10^{-8}
	$120M_\odot$	Plasma	0.5	1.0×10^{-11}	Pair	1.0	6.0×10^{-9}
Rotating	$20M_\odot$	Pair	0.5	8.0×10^{-9}	Brems	1.0	3.0×10^{-5}
	$120M_\odot$	Plasma	0.0	5.0×10^{-11}	Photo	0.5	5.1×10^{-7}

Table 5.2: The total energy loss of neutrinos (MeV/cm^3/s) for non-rotating and rotating model of $20M_\odot$ and $120M_\odot$ stars

		Lowest			Highest		
		Process	$P_{\nu_e \to \nu_e}$	ΔE_ν	Process	$P_{\nu_e \to \nu_e}$	ΔE_ν
Non-rotating	$20M_\odot$	Plasma	0.5	9.0×10^{-10}	Brems	1.0	2.5×10^{11}
	$120M_\odot$	Pair	1.0	3.7	Pair	0.5	6.0×10^{10}
Rotating	$20M_\odot$	Plasma	0.0	2.0×10^{9}	Brems	1.0	1.2×10^{17}
	$120M_\odot$	Plasma	0.5	1.5×10^{3}	Pair	1.0	4.0×10^{10}

Appendix A

List of Publications

1. Ungku Ferwani Salwa Ungku Ibrahim,Nor Sofiah Ahmad, Norhasliza Yusof, Hasan Abu Kassim (2009). Neutrino Energy Loss at Matter-Radiation Decoupling Phase, Modern Physics Letters A **11-13**, pp. 1051-1054. (ISI)

2. Nor Sofiah Ahmad, Norhasliza Yusof, Hasan Abu Kassim (2010). Energy Loss of Neutrinos in $20M_{\odot}$ Star, The 10^{th} International Symposium On Origin Of Matter Aand Evolution Of Galaxies (OMEG2010), 8Ű10 March 2010, *AIP Conf. Proc.* **1269**, pp. 357-359 (2010). (ISI)

3. Nor Sofiah Ahmad, Norhasliza Yusof, Hasan Abu Kassim (2010). Energy Loss of Neutrinos in $20M_{\odot}$ and $40M_{\odot}$ in Massive Stars, MALAYSIA ANNUAL PHYSICS CONFERENCE 2010 (PERFIK-2010), 8Ű10 March 2010, *AIP Conf. Proc.* **1328**, pp. 59-61 (2011). (ISI)

Bibliography

[1] D. Arnett, "Neutrino-Cooled Star" in *Supernovae and Nucleosynthesis : An Investigation of the History of Matter, From the Big bang to the Present*, Princeton University Press, 1996, pp. 284-311.

[2] N. Itoh *et al. ApJ* **339**, 354-364 (1989).

[3] A. Odrzywolek, M. Misiaszek and M. Kutschera *Astropart. Phys.* **21**, 303-313 (2004).

[4] A. Odrzywolek *Phys. Rev. C* **80**, 0458011-04580111 (2009).

[5] H. Munakata, Y. Kohyama and N. Itoh, *ApJ* **296**, 197- 203 (1985).

[6] N. Itoh *et al. ApJ* **279**, 413-418 (1984).

[7] N. Itoh *et al. ApJ* **280**, 787-791 (1984).

[8] N. Itoh *et al. ApJ* **310**, 815-819 (1986).

[9] N. Itoh *et al. ApJ* **316**, 708-715 (1987).

[10] N. Itoh *et al. ApJ* **362**, 620-623 (1990).

[11] N. Itoh *et al. ApJ* **415**, 267-277 (1993).

[12] N. Itoh *et al. ApJ* **431**, 761-766 (1994).

[13] N. Itoh *et al. ApJ* **470**, 1015-1017 (1996).

[14] N. Itoh *et al. ApJ Suppl. Ser.* **102**, 411-424 (1996).

[15] N. Itoh *et al. ApJ* **579**, 580-585 (2002).

[16] N. Itoh *et al. ApJ* **611**, 1041-1044 (2004).

[17] A. Sulaksono and P. Simanjuntak, *Solar Phys.* **151**, 205-212 (1994).

[18] J. Bahcall, *Solar Phys.* **151**, 205-212 (1994).

[19] K. Zuber "Solar Neutrinos" in *Neutrino Physics*, Taylor&Francis, 2004.

[20] C. Guinti and C. W. Kim, "Neutrino Interactions" in *Fundamental of Neutrino Physics and Astrophysics*,Oxford University Press, 2007.

[21] L. Wolfenstein *Phys. Rev. D* **17**, 2369Ű2374 (1978).

[22] L. Wolfenstein *Phys. Rev. D* **27**, 1228â-1242 (1983).

[23] S. P. Mikheyev and A. Yu. Smirnov *Il. Nouvo Cimento* **Vol. 9**, 17-26 (1986).

[24] A. Odrzywolek, and A. Heger *Acta Physica Polonica B* **41**, 1611-1627 (2010).

[25] E. Braaten and Daniel Segel, *Phys. Rev. D*, **48**, 1478-1491 (1993).

[26] U. F. S. U. Ibrahim, N. S. Ahmad, N. Yusof and H. A. Kassim, *Mod. Phys. Lett. A*, **24**, Nos. 11-13 1051-1054 (2009)

[27] D. D. Clayton, *Principles of Stellar Evolution and Nucleosynthesis* The University of Chocago Press, United State of America, 1984.

[28] N. Yusof and H. A. Kassim, *Mod. Phys. Lett. A* **24**, 1071-1075 (2009).

[29] N. Yusof and H. A. Kassim, *Astrophys. Space Sci.* **328**, 157-161 (2010).

[30] C.H. Kishimoto and G. M. Fuller *Astrophys. J.* **656**, 7, 1104-1108 (2007).

[31] M. Pignatari, R. Gallino,G. Meynet, R. Hirschi, F. Herwig, and M. Wiescher *Astrophys. J.* **687**, L95ï£¡L98 (2008).

[32] C. Tur, A. Heger, and S. M. Austin *Astrophys. J.* **702**, 1068ï£¡1077 (2009).

[33] M. L. Pumo*arXiv:1202.6577v2 [astro-ph.SR]* (2012).

[34] A. M. Serenelli and M. Fukugita *Astrophys. J.* **632**, L33-L36 (2005).

[35] M. Haft, G. Raffelt and A. Weiss *Astrophys. J.* **425**, 222-230 (1994).

[36] S. A. Lamb, I. Iben Jr. and W. M. Howard *Astrophys. J.* **207**, 209-232 (1976).

[37] Y. Abe et al, *arXiv:1112.6353v2 [hep-ex]*(2012).

[38] G. M. Fuller and X. Shi *Astrophys. J.*, **487**, 7, L25-L28 (1997).

[39] W. D. Arnett *ApJ* **176**, 681-698 (1972).
W. D. Arnett *ApJ* **176**, 699-710 (1972).
W. D. Arnett *ApJ* **179**, 249-256 (1973).
R. G. Couch and W. D. Arnett *ApJ* **178**, 771-777 (1972).
W. D. Arnett *ApJ* **193**, 169-176 (1974).
W. D. Arnett *ApJ* **194**, 373-383 (1974).
W. D. Arnett *ApJ. Suppl. Series* **35**, 145-159 (1977).

[40] S. E. Woosley and A. Heger, *Rev. Mod. Phys.* **74**, 1015-1071 (2002)

[41] D. Bodansky, D. D. Clayton, and W. A. Fowler, 1968, *Astrophys. J., Suppl. Ser.* **16**, 299 (1968)

[42] T. A.Weaver, G. B. Zimmerman, and S. E. Woosley, *Astrophys. J.* **225**, 1021 (1978)

[43] K. Nomoto, and M. Hashimoto,*Phys. Rep.* **163**, 13 (1988).

[44] A. Chieffi, M. Limongi, and O. Straniero , *Astrophys. J.* **502**, 737 (1998)

[45] P. Eggenberger et. al., *Astrophys. Space Sci.* **316**, 43-54 (2008).

[46] P. A. Crowther et al., *MNRAS* (2010). doi:10.1111/j.365-2966.2010.16386.x.

[47] H. A. Kassim, N. Yusof, R. Hirschi and P. Eggenberger, *Astrophys. Space Sci.* **328**, 163-166 (2010).

[48] G. Meynet and A. Maeder *A& A* **361**, 101-120 (2000).

[49] A. Heger, S. E. Woosley and H. C. Spruit *ApJ* **626**, 350-363 (2005).

[50] A. Heger, and N. Langer *ApJ* **544**, 1016-1035 (2000).

[51] A. Heger, N. Langer and S. E. Woosley *ApJ* **528**, 368-396 (2000).

[52] S. Ekstrom et. al. *Astron. Astrophys.* **537**, A416 (2012).

[53] M. Asplund et. al. *Cosmic Abundances as Records of Stellar Evolution and Nucleosynthesis* **336**,25 (2005).

[54] J. S. Vink, A. de Koter, H. J. G. L. M. Lamers *Astron. Astrophys.* **369**, 574 (2001).

[55] T. Nugis, H. J. G. L. M. Lamers *Astron. Astrophys.* **360**, 227 (2000).

[56] B. T. Cleveland et al. *ApJ* **496**, 505-526 (1998).

[57] J. N. Abdurashitov et al., *Astropart. Phys.* **25**, 349-354 (2006).

[58] J. Hosaka et al., *Phys. Rev. D* **73**, 112001 (2006).

[59] A.Renshaw et al. *Phys. Rev. Lett.* **112**, 091805 (2014).

[60] E. W. Kolb and M. S. Turner, *The Early Universe*, (Addison Wesley, 1990).

[61] J. Hosaka *et al.*, *Phys. Rev. D* **73**, 112001 (2006).

[62] S. N. Ahmed *et al.*, *Phys. Rev. Lett.* **92**, 18101 (2004).

[63] M. Gell-Mann, P. Ramond and R. Slansky *Supergravity*, (North Holland, (1979)

[64] A. Sulaksono and H. P. Simanjuntak, *Solar Phys.* **151**, 205 (1994).

[65] U. F. S. U. Ibrahim, M.Sc. thesis, University of Malaya, 2000.

[66] W. M. Yao *et al.*, *J. Phys. G* **33**, 1 (2006)

[67] R. Hirschi, G. Meynet, and A. Maeder, *Astro. Astrophys.* **425**, 649Ű670 (2004).

[68] N.Langer, *Ann. Rev. of Astro. and Astrophys.* **50**, 107-164 (2012).

[69] P.Eggenberger, *EPJ Web of Conf.* **43**, 01005 (2013).

[70] J. Beringer et al. (Particle Data Group) *Phys. Rev. D* **86**, 010001 (2012).